POLITECNICO DI TORINO

Corso di Laurea Magistrale

in Ingegneria Biomedica

Tesi di Laurea Magistrale

Biointerfaces based on conductive polymer/nanoceria composites

Relatori

Prof.ssa Valentina Alice Cauda

Correlatori

Prof. Gianni Ciofani

Dr. Francesco Greco

Dr.ssa Giada Graziana Genchi

Candidata

Valeria Serino

Anno Accademico 2019/2020

Sei più forte di quello che credi.

A papà, mamma e Roberta.

Abstract

This thesis project focuses on the investigation of inkjet printing of redox active nanoceria and conducting polymer composites for cell cultures. The aims were: to create a multifunctional neuronal interface combining electroconductivity with antioxidant/radical scavenging ability, to evaluate the antoxidant action of hybrid substrates in contact with neuronal cells.. To this end, the experimental work has been divided into two parts: the fabrication and surface and electrical characterisation of antioxidant substrates have been carried out at the Institute of Solid State Physics of the TUGraz (Austria). The subsequent biological characterisation and the response of the antioxidant capacity of composites substrates was implemented at the Italian Institute of Technology (IIT) of Pontedera (Italy).

The first section of the thesis reviews concepts and recent advancements in neural tissue engineering through the strategies for repairing and regenerating peripheral nervous tissue, highlighting its solution in neural interface systems. A general presentation of rapid prototyping techniques is shown with particular attention to the inkjet printing, which is the used process for producing hybrid samples. Then employed materials of the project such as cerium oxide nanoparticles (nanoceria) and the conductive polymer and their use in the foreseen field of application are described.

The second section presents an overview of the devices used and the operating principles behind the characterization techniques used. Information is provided on the materials and the various experimental methods. The preparation of the inks and the printing process is also illustrated.

The third section includes the characterisations of antioxidant substrates. The first chapter is focused on the surface and structural characterisation of materials, obtained usingprofilometry and optical microscopy. Functional characterization of printed hybrid substrates included assessment of electroconductivity and electrochemical behaviour. Ultimately, the combination of living cells and conducting nanofilms is an important study tool for the development of innovative biomedical devices. For this reason, in this chapter is also present the biological characterisation, aimed at assessing through immunofluorescence techniques the proliferative and differentiating capacity of cells on the substrates. The cytocompatibility of cells in terms of cell proliferation was performed by Pico Green Assay. Through flow cytometry, the response of the cells to an oxidative stress insult was also investigated, in order to verify protection by the cerium oxide nanoparticles.

Finally, the last part of the thesis concerns the analysis and discussion of the results obtained from the different characterisations, comparing the several images taken from the tests. The work was concluded with the assessment of the best hybrid substrate in terms of viability and cell cytocompatibility.

Contents

List of figures

List of tables

Acronyms

CCD charge coupled device

CIJ continous inkjet printing

CV cyclic voltammetry

DMEM Dulbecco's Modified Eagle's Medium

DoD drop-on-demand

DPBS Dulbecco's phosphate-buffered saline

ECM extracellular matrix

FBS fetal bovine serum

ICC immunocytochemistry

PET-ITO Indium Tin Oxide coated PET

NC nanoceria

PDMS polydimethylsiloxane

PEDOT:PSS Poly(3,4-ethylenedioxythiophene):polystyrene sulfonate

PJet 700 PEDOT:PSS ink formulation for ink-jet printing

PNS peripheral nervous system

P/S penicillin/streptomycin

ROS reactive oxygen species

SCE saturated calomel electrode

Part I
Introduction and fundamentals

1. Introduction

1.1. Peripheral Nervous System

One of the most complex biological systems is certainly the nervous one. Shown in Figure 1, the nervous system is distinguished into the central nervous system (CNS), contained within bone casings, and the peripheral nervous system (PNS), consisting of all the nervous elements that ensure its connection (afferent and efferent) with the rest of the organism. The central nervous system and the peripheral nervous system, interacting with each other, have the function of transmitting and analyzing the stimuli coming from the external environment and from the internal organs and therefore to elaborate a response that can be voluntary or involuntary. The role of the central nervous system (CNS) is to process the afferent sensitive information, integrating it with the information already acquired and therefore to propose the specific responses. The peripheral nervous system (PNS), placed outside the bone envelopes, consists of those formations (spinal nerves and brain nerves with related ganglia) that transmit impulses to and from extranervous organs. The spinal and encephalic nerves, which connect the center with the periphery, consist of both sensitive fibers that carry information from the periphery to the center (*afferent fibers*), and effector fibers directed to the skeletal muscles, the myocardium, the smooth muscle and the glands exocrine and endocrine (*efferent fibers*) (1).

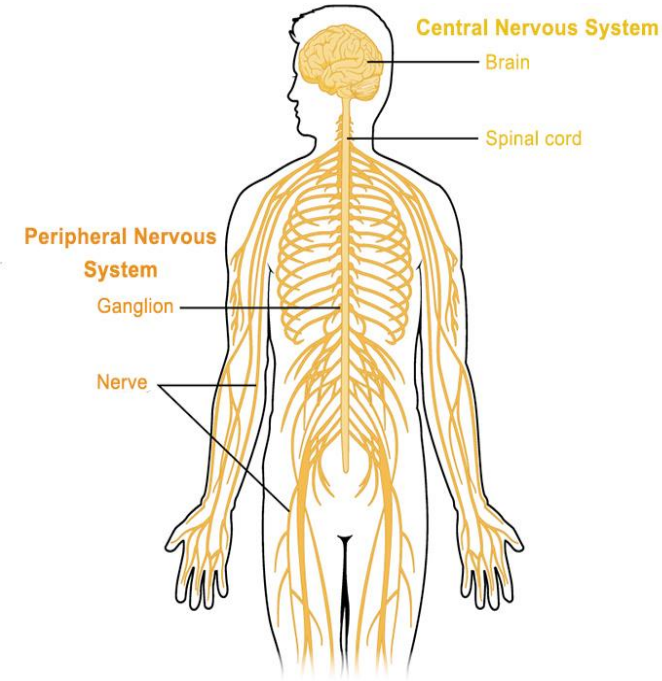

Figure 1-Illustration of the central nervous system (CNS) and the peripheral nervous system (PNS) (2).

The PNS is composed by 43 pairs of sensory and motor peripheral nerves that are responsible for transporting information from all parts of the body to and from the CNS (3). In the peripheral nervous system, a somatic part is distinguished which has the function of conducting stimuli specific to the life of relationship, the *somatic peripheral nervous system*, and a part which is used for the innervation of the viscera, vessels and glands, the *visceral nervous system or autonomic*. The somatic nerves emerge directly from the central nervous system and are distributed to the superficial and skeletal districts of

the body. On their course there are intercalating *somatic ganglia*, aggregates of sensory neurons. The nerves of the sympathetic system have the function of conducting visceral stimuli and are also called *visceral nerves*. In the course of these nerves there are intercalating *visceral nerves*.
The afferent impulses of somatic and visceral sensitivity are collected by cells of the *encephalospinal ganglia*. Peripheral reception and conduction at the center of the sensory stimulus always take place by a single neuron. Effector impulses are transmitted to peripheral organs differently in the somatic and visceral peripheral nervous systems. In the first, the effector impulse is transmitted to the periphery by a single neuron, while in the second, the stimulus reaches the periphery through a series of two neurons (1).
A peripheral nerve is formed by a cellular body with extensions, called axons, which are coated with membranes of myelin sheath, formed by Schwann cells, and are enclosed in bundles called fascicles. The motor and sensory axons are held together by supporting tissues in an anatomically defined trunk. As shown in Figure 2, the peripheral nerve consists of several layers: endoneurium, perineurium and epineurium. The first layer, formed by oriented collagen fibres, envelops the individual axons and their Schwann cell sheaths. Perineurium consists of fibroblasts and collagen, surrounding groups of axons to create fascicles. The last layer, the epineurium, is given by an outer sheath of loose fibrocollagenous tissue, which fuses the individual nerve bundles into a nerve trunk. The peripheral nerves are well vascularized thanks to the capillaries inside the supporting tissue of the nerve trunk or the vessels that come into the nerve from the surrounding arteries and veins (4).

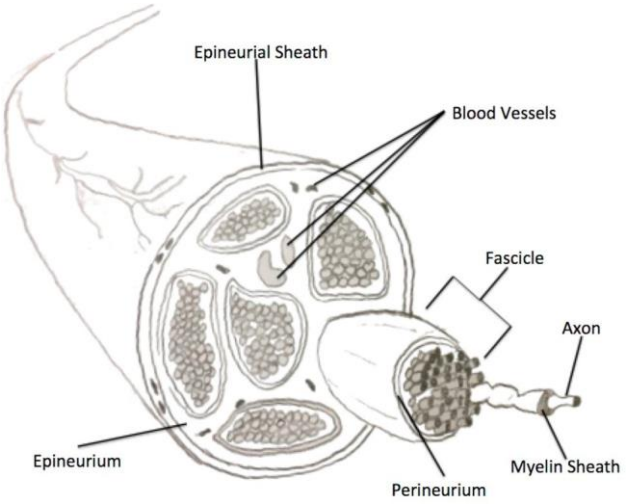

Figure 2-Structural representation of a nerve in the peripheral nervous system (5).

1.2. Nerve injury and regeneration

The complex anatomical structure of the peripheral nervous system and the mechanism of degeneration of the nerve bundles limit the strategies for repair and regeneration of the nerves, which have often failed to restore sufficient nerve function. Depending on the type of trauma, different repair strategies have been devised. When the lesion affects the peripheral nerves (PNI), cascading events occur involving the cell bodies of the spinal cord and ganglia with the aim of regenerating the damaged nerves. Nerve lesions are broken down according to severity into neurapraxia, axonotmesis and neurotmesis. Neurotraxia is the least severe lesion as it does not correspond to a long-term loss of

function. In contrast, an axonotmesis is associated with the interruption of the nervous axis and the surrounding myelin sheath. The nerve lesion that causes the most damage is neurotmesis, with complete disconnection of the nerve and therefore of nerve function (6). There is a potential risk of scar tissue formation, such as neuroma, which limits axonal regrowth. Sir Sydney Sunderland, following Seddon's scheme, creates a new PNI classification of five degrees to discriminate the extent of the damage with respect to the surrounding connective tissues. The first and second grades of the Sunderland classification are associated with neurapraxia and axonotmesis respectively. Grade III, IV, and V lesions are seen as axon damage along with the associated endoneurium, perineurium and epineurium, respectively. These types of damage cause an increase in the probability of variable recovery, incomplete at times, due to an incorrect direction of the regenerating axons. Grade IV lesions result in the generation of localized neuromas, due to internal bleeding and fibrous tissues that block the distal axonal stump. Subsequent lesions characterized by complete nervous discontinuity determine a terminal neuroma-bulb. In compression injuries, which are part of Sunderland's Grade I class, there is focal demyelination at the compression site without any damage to the surrounding axons or connective tissues. In this case there is a significant decrease in the distance between the adjacent nodes of Ranvier, known as the internodal length. Crushing injuries are caused by acute blunt force trauma, causing traumatic nerve compression. The severity of crush injuries is based on the extent of the trauma and the location of the injury. Transfection lesions, according to Sunderland's Grade V, determine a physical space between the proximal and distal ends of the nerve (7).

The current standard for neurotmesis repair is end-to-end direct suture, but this cannot be used in the case of critical size lesions, as functional failure may occur. On the other hand, there are other factors that may hinder the success of grafts for nerve regeneration, such as tissue availability or host immune response. When talking about nerve grafts, one can refer to autografts or allografts. Autografts are derived from healthy parts of the patient's body: this restricts the possibility of immunological rejection but can cause damage to the donor's tissues due to the second surgery or possible deformities in the donor's site and discrepancies between the damaged nerves and those of the donor. In the case of allografts, tissue is taken from another donor. This may result in risk of immunological rejection and functional loss in donor nerves, although it may increase availability (6).

Given the limitations of these two methods, nerve conduits made of biocompatible polymers are nowadays used, mainly for small caliber defects. As alternatives to current clinical practices, in order to guide the regeneration of peripheral nerve tissue and avoid immune rejection, inflammation and disease transmission for successful tissue regeneration, new tissue engineering techniques have been deployed, based on the fabrication of cell-holding bio-frames and capable of providing biomolecular and physical signals to cells. Among the biomaterials used, polymers have ideal properties such as high ductility and superior tensile strength, while being lightweight. For a scaffold to be successfully implanted, it must be characterised by biocompatibility, porosity, bioresorbability and mechanical strength. In this way, the biocompatible scaffold will be able to integrate the native tissue allowing its regeneration without causing a response from the immune system. The tissue integration and regeneration are particularly favoured by a scaffold with interconnected pores. At the same time, resorbability of the scaffold must be encouraged in order to prevent necrosis of the native tissue and new tissue and allow its decomposition. Finally, mechanical properties such as tensile strength are essential to ensure scaffold stability (6).

Peripheral nerve injury generally occurs by physical damage, although the most severe injury is the complete nerve transection. When a peripheral nerve is severed, Wallerian degeneration occurs at the end of the distal nerve below the point of injury. This results from protease activity and separation

from the metabolic resources of the nerve cells, causing the decomposition of the cytoskeleton and thus of the cell membrane. The proximal end of the nerve stump, on the other hand, suffering minimal damage due to retrograde degradation, is used to reform the synaptic connections with nearby tissues, allowing regeneration. The following figure represents the PNS response to an injury.

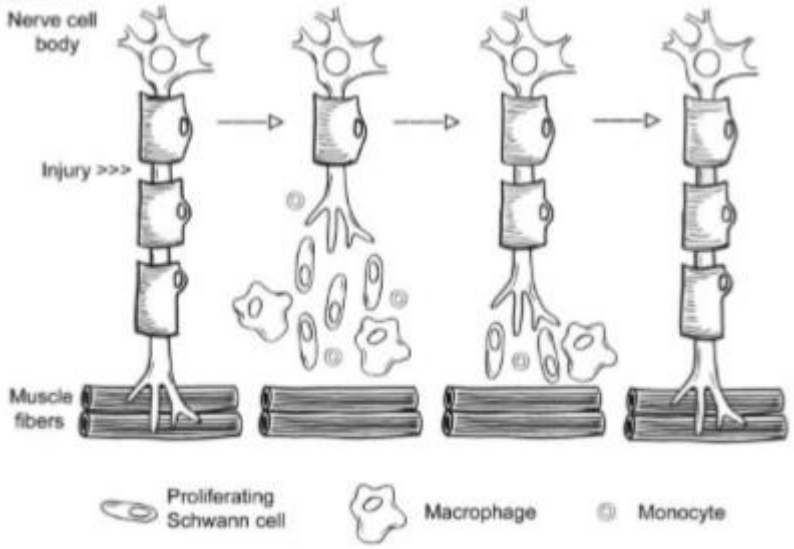

Figure 3-Schematic illustration of the response to axotomy in PNS (6).

In this axonal regeneration process, the role of Schwann cells (SC) is crucial. If the lesion affects peripheral nerves, the immune response is activated by Schwann cells and macrophages, which release myelin and axonal debris near the distal nerve stump. They contribute to the process of regeneration by secreting neurotrophic factors and cytokines, components of the extracellular matrix. The recruitment process of macrophages, neutrophils and adaptive cells (T and B cells), in addition to Schwann cells, varies from a few hours to days after the lesion with the primary aim of removing the dendrites in order to form an environment conducive to regeneration of the nerves. Despite this, the axons that have suffered the injury are intact for several days and are able to transmit action potentials when stimulated. Macrophages together with Schwann cells release extracellular matrix proteins (ECM), neurotrophins, cytokines and chemokines (8). Schwann cells grow and migrate to the damage site and guide the regenerating axon from the proximal end to the distal stump (8). Regeneration starts from axonal sprouts from Ranvier's nodes, non-myelinic axonal parts between Schwann cells. Functional reinnervation in humans has a rate of about 2-5 mm/day (9). Following an injury, if a hollow nerve conduit is used for the severed peripheral nerve, the formation of a fibrin-rich macrophage bridge through the sheath and through the defect site can be seen. As Schwann cells along with the capillaries grow, the retreat of the bridge occurs as a sign that regeneration is progressing (6).

2. Nerve conduits and electrical stimulation

2.1. Bioengineering strategies for nerve repair

In the last few years, numerous advances have been made in the field of tissue engineering and regenerative medicine in the manufacture of nerve ducts, which are used for nerve defects in place of allografts and autografts. They have taken over due to the ease of availability, reduced immune response and morbidity of the donor site. New materials are currently being tested for improved biocompatibility, biodegradation and porosity. A biodegradable implant prevents secondary surgery and decreases the invasiveness of the therapeutic approaches. Research is now focused on the combination of specific materials and biomolecules to create composite materials capable of directly activating stimulation for nerve regeneration. In Table 1, a summary of materials in use or under investigation for nerve repair applications is shown.

Table 1-Nerve grafts and nerve conduit materials (6).

Graft		**Reference**
Autologous tissue grafts		
1.	Nerve grafts (gold standard)	(10), (11)
2.	Vein grafts	(12), (13), (14)
3.	Muscle grafts	(15), (16)
4.	Epineurial sheaths	(17)
5.	Tendon grafts	(18)
Nonautologous/acellular grafts		
1.	Immunosuppression with allografts	
2.	Acellular allografts and xenografts	
	Thermal decellularization	(19), (20), (21)
	Radiation treatment	(22), (23)
	Chemical decellularization	(24), (25)
3.	Small intestinal submucosa (SIS)	(26), (27), (28)
4.	Human amnion	(29), (30), (31)
Natural-based materials		
1.	ECM protein-based materials	
	Fibronectin	(32), (33)
	Laminin	(34), (35)
	Collagen	(36), (37), (38)
2.	Hyaluronic acid-based materials	(39)
3.	Fibrin/fibrinogen	(40), (41)
4.	Other materials (alginate, agarose …)	(42), (43), (44)
Synthetic materials		
1.	Biodegradable synthetic materials	
	Poly(lactic acid) (PLA)	(45), (46)
	Poly(lactic-co-glycolic acid) PLGA	(47)
	Poly(caprolactone)	(48), (49)
	Poly(urethane)	(50)
	Poly(organo)phosphazene	(51)

	Poly(3-hydroxybutyrate)	(52)
	Poly(ethylene glycol) “glue”	(53), (54)
	Biodegradable glass	(55), (56)
2.	Electrically active materials	
	Piezoelectric	(57)
	Electrically conducting	(58)
3.	Nonbiodegradable synthetic materials	
	Silicone	(59), (60)
	Gore-Tex or ePTFE	(61), (62), (63)

Natural biopolymers possess regenerative bioactivity with good mechanical properties. High biocompatibility, biodegradability, mechanical properties and moisture absorption are only some of their properties, which allow to stimulate cell adhesion, migration, growth, proliferation and differentiation. For small defects, collagen type I is typically used, while for critical defects fibroin and silk are used as supporting materials. In order to improve the properties of the materials, as previously mentioned, in recent years attention has been paid to polymer composites, which aim to combine the advantages of natural polymers with those of synthetic materials. Synthetic materials guarantee a high degree of controllability during their manufacturing process and often better mechanical properties than natural biopolymers. Most commonly used are polylactic acid (PLA) and polylactic-glycolic acid (PLGA) (18) (64), favored for their ease of processing and for their high biocompatibility. PLGA implants are able to adhere to Schwann's cells, directing their growth. It is also possible to control the degree of degradation of PLGA by varying the ratio of its monomeric components. Rapid prototyping techniques such as 3D bio-printing are used for the production of synthetic nerve ducts. This technology allows the printing of biocompatible nerve grafts with the addition of cells and growth factors that optimize axonal regeneration. A composite nerve graft can be exemplified by a duct consisting of polycaprolactone (PCL) and collagen fibers produced by electrospinning. PCL is a synthetic polymer used in scaffolds for its excellent porosity, biocompatibility, adhesion properties and cell proliferation. On the other hand, collagen is a structural protein of the extracellular matrix. Seeding of cells on this composite shows a preferential growth and extension of the neurites (5). It is also possible to mix two synthetic polymers such as polypyrene (PPy) and poly(D, L-lactic acid) (PDLLA) (65). The first is a conductive polymer that promotes the regeneration and differentiation of new nerves. It is combined with PDLLA in order to improve the degradation rate and resistance of the composite conductive matrix. For nerve regeneration, it is also important to consider the topography of the finished scaffold and its elasticity. The latter property has a positive influence on the differentiation and growth of neuronal cells. Surface topography, similarly, can be important for greater surface proliferation and elongation of neuritis.

In recent years, nanotechnology has gradually emerged, leveraging on materials with a basic structural unit of <100 nm in at least one size (66). This has enabled new strategies to be elaborated for tissue regeneration based on the fact that nanomaterials (either in the form of nanoparticles or nanostructured scaffolds) are characterized by a high specific surface area and porosity; they can as well enable a controlled and specific release of active substances suitable for the regeneration of tissues, among which there is the peripheral nerve tissue. Nanomaterials can mimick several physico-chemical properties of the biological environment, both in structural and in functional terms. First of all, the high surface/volume ratio of nanomaterials favours cell adhesion and simplifies a possible drug loading and administration. The repair of the damage is also supported by the excellent mechanical properties and a high degree of absorption of proteins. One example is provided by nanocomposite scaffolds

based on carbon nanotubes (CNTs), which, thanks to their electrical conductivity, can promote cell adhesion and guide the growth of peripheral nerves (67).

Figure 4 shows the ideal characterics that an engineered nervous construct should have.

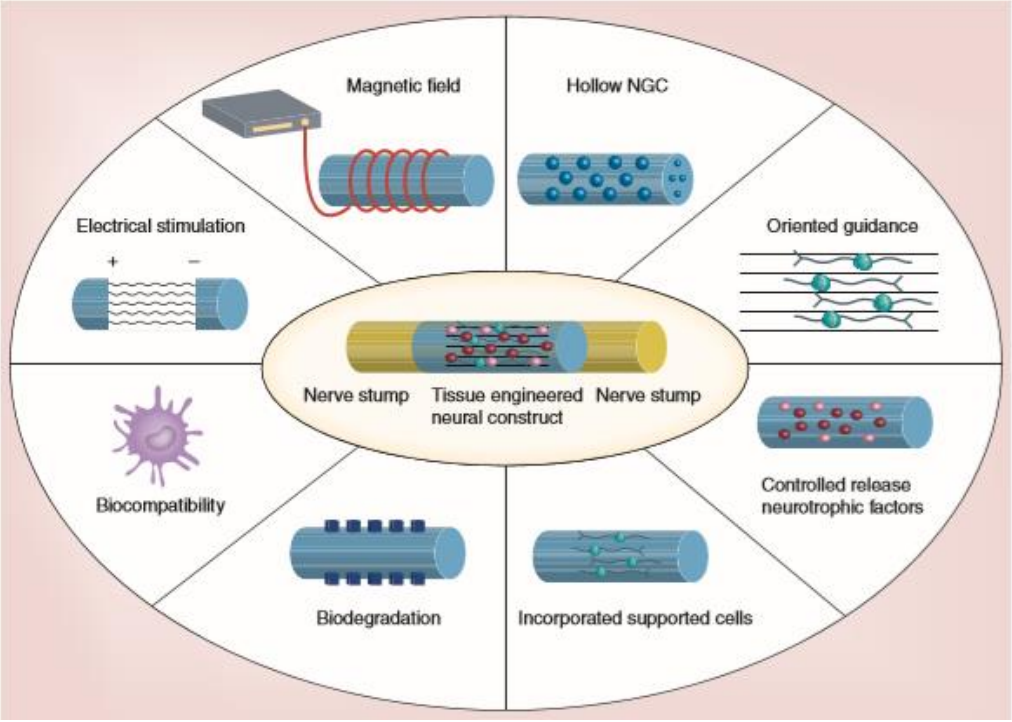

Figure 4-The key factors for an ideal nervous tissue regenerative construct (68).

2.2. Stimulation of PNS regeneration

In the regeneration of damaged tissues, the actions of cells and biomolecular signals are fundamental, although often insufficient and . In the case of nerve tissue, both chemical and electrical stimuli are capable of promoting the regeneration of axons and the differentiation of native cells. Nerve regeneration can be controlled by external physical stimuli, such as mechanical actions, electrical signals or surface topography, and by chemical stimuli, such as growth factors delivered to trigger cell signaling cascades able to promote specific functions. Similarly, electrical stimuli such as those resulting from the use of conductive polymers can initiate different cell transduction pathways, through a variation in ion influx through the cell membrane. In this section a brief description of all these parameters that stimulate the regeneration of the peripheral nervous system is provided.

2.2.1. Material properties

As previously mentioned, there are several characteristics that a nanoscaffold must have for the regeneration of peripheral nerves: it must be biocompatible, biodegradable and have mechanical intelligence. This type of structure must be easily sutrable and must continue to perform physiological functions where there is a neurological deficit. The scaffolds must also be able to promote cell migration and axonal growth of defects in order to regenerate neuronal function. In PSN lesions, Schwann cells act as support cells to stimulate myelination; they come into contact with nutritional

factors to promote axonal repair. They also play a role in reducing the degree of muscle atrophy. The adhesion and diffusion of Schwann cells are favored by the presence of nanofibers. The cells are able to synthesize and secrete many types of neurotrophins and cell adhesion molecules in order to alter the peripheral nerve microenvironment after injury and during regeneration. The biofunctionalized PHB / PHBV scaffolds are capable of increasing the metabolic activity and the proliferation of SC, much more than the unmodified scaffolds (68).

2.2.2. Surface topography

Just as the chemical characteristics of the materials used are fundamental, topography also plays a crucial role on cellular morphology and functionality. For instance, it has been observed that electrospun fibers of various types of polymers or ECM proteins favor the growth of different types of primary neurons and glial cells. A study was carried out using microchannels with grooves of different depths and widths to observe the topographical effects on neurite growth. If the channel width ranges between 20 μm and 40 μm, the neurites grow parallel to the channels, while the growth direction is perpendicular to the channels when the channel width is increased up to 60 μm. Culture of PC12 cells in microchannels was shown to have axonal growth direction and cell complexity depending on the substrate topography. If cells are grown in parallel micro-projection channels with 20-30 μm width, the complexity of the neuronal structures is decreased. At the same time, in another study, it was seen that the orientative distribution of neurites strictly depended on the orientation of poly (3-hydroxybutyrate) PHB submicrometric fibers made by electrospinning. Furthermore, graphene, through a specific surface topography, can encourage the proliferation of human neural stem cells (hNSC). Fluorinated graphene with 30 μm wide microchannels optimizes cell adhesion and proliferation of bone marrow-derived mesenchymal stem cells, exerting a neuroinductive effect (68).

The basic structure of a nerve scaffold is a single hollow nerve conduit, with a given porosity that allows to imitate the morphology of the ECM and improve the physico-chemical properties, supporting the regeneration of the nerves. In an in vivo study with Sprague-Dawley rats, the sciatic nerve was cut to implant nanofibers of silk-fiber nanofibre nanoparticles and cell-loaded gold-silk fiber nanoparticles. After 18 months from implantation, it was observed that nerve growth was completed along the interphalangeal space and neuromorphology regenerated thanks to the porosity of the duct (68).

Electrospinning is the simplest and most versatile technique for making substrates capable of providing different cells with topographical cues in vitro. Polypyrrole / poly (styrene-b-isobutylene-b-styrene) among the successfully electrospun synthetic polymers and promising results for the regeneration of the nervous system (69); poly (3-caprolactone) / gelatin (70); poly-L-lactic acid (71), (72); poly (vinylidene fluoride-trifluororoethylene) (73); and poly (acrylonitrile-co-methyl acrylate). On the contrary, among the natural polymers most used in this field there is poly (3-hydroxybutyrate) (PHB), a natural polyester easily processable and with excellent biocompatibility and biodegradability properties (74), (75). In some studies, PHB has been melt-pressed or processed by evaporation of the solvent, to produce unidirectional oriented sheets suitable for pericardial suturing (76) and peripheral nerve repair (77), (78). It has been seen that electrospun sub-micron fibers with random or parallel orientation on which neuron-like PC12 cells have been grown can act as a support for the growth of

neurites in the peripheral nervous system. In particular, it has been seen how the orientation of neurites depends on the orientation of the fibers: random or parallel.

Neurites that grow within 10 ° of the fiber axis appear to be aligned along the fiber axis (68). Thus they are able to grow on electrospun fibers aligned on micro or nanoscale. For example, in nanofibers aligned with PCL gelatin, cells grow more oriented along the direction of the nanofibers and the dendrites are connected to adjacent cells. In fact, neurons grown on aligned nanofibers show significantly longer neurites than cells grown on randomly oriented nanofibers (79).

2.2.3. Magnetic properties

Axonal growth can be stimulated by the presence of magnetic nanoparticles (MNP), which promote the regeneration of the peripheral nerve through the application of an external magnetic field.This is also able to improve the vitality of the SC, promoting its adhesion and proliferation. Research has highlighted how the application of a magnetic field can significantly increase the gene expression of neurotrophins, such as brain-derived neurotrophic factor (BDNF), glial cell line-derived growth factor (GDNF), neurotrophin-3 (NT-3) and vascular endothelial growth factor (VEGF), through a 10% magnetic scaffold. The use of MNP functionalized with nerve growth factor (NGF) and VEGF significantly increases the rate of regeneration and recovery of motor function. In other studies it has been shown how MNP nanoshuttles can stimulate the growth of adipose stem cells (ADSC) and improve the ability of ADSC to treat erectile dysfunction; in ADSC treated with MNP it is observed that the expression of smooth muscle actin α and of adhesion molecule 1 of platelet endothelial cells accelerates significantly (68). There are ongoing studies on how magnetic scaffolds can promote and improve cell proliferation.

2.2.4. Biological microenvironment

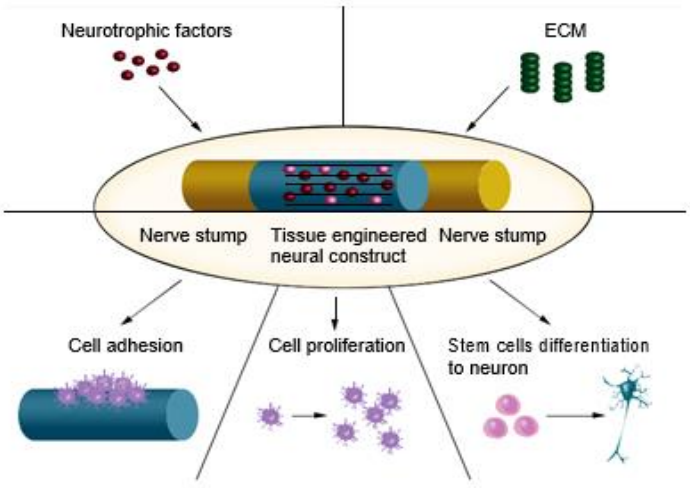

Figure 5-Schematic illustration of the biological microenvironment in the peripheral nerve regeneration [68].

Figure 5 shows the role of the biological microenvironment factors. Re-creating the biological microenvironment has proven to be fundamental for regenerating peripheral nerves. Neurotrophic factors and ECM are part of the biological microenvironment. Neurotrophic factors favor the synthesis of proteins linked to cell bodies, thus supporting the growth, development and functional integrity of neurons. ECM, through neurotrophic hormones, can indeed regulate cellular function. Recent

strategies for the biofunctionalization of nanostructured scaffolding aim to mimic the ECM properties (68).
Neurotrophins are fundamental in the survival, growth, differentiation and growth of neurites in neurons, also encouraging the regeneration of injured nerves. Several studies have seen how the combination of nanofibers, which act as a nerve conduit, and neurotrophic factors increases biocompatibility and neuronal tissue regeneration. NGF-functionalized nerve guide channels have been observed to help improve the thickness of the myelin sheath, nerve conduction velocity and even action potential of the compound muscle in a rat regenerated sciatic nerve.

BDNF is a neurotrophin which is able to promote the survival of axotomized neurons, the regeneration of wound fibers and the myelination of regenerated nerves. It has also been shown that in a model of facial nerve injury in the rat, BDNF alone or combined with CNTF (Ciliary Neurotrophic Factor) manages to direct the orderly growth of axons, optimizing regeneration and functional recovery. An in vitro study has shown how silk nanofibers loaded with BDNF and CNTF lead to significant results on the growth, alignment and migration of glial cells and PC12, increasing neurite length by up to 3 times (68).

2.2.5. Electrical stimulation

New research strategies today are aimed at restoring function after neurological damage. The fields that aspire to this ultimate goal include: enhancement of axonal regeneration with electric fields, development of hybrid neural interfaces that combine inorganic and organic elements and study of the role of modeled neuronal activity in regulating neuronal processes and neurorehabilitation. In this context, the role of external stimuli appears to be fundamental. In particular, it has been seen that by using external means such as conductive polymers it is possible to apply an electrical stimulation which affects cellular behavior (80). Electrical stimulation leads to a variation of the flow of ions through the cell membrane, triggering several intracellular transduction pathways. The cell membrane is characterized by a steady state potential, defined as resting potential, which can be altered from negative to positive when there is an electrical activity, called action potential. The action potentials ensure that the information is transported along the axons of the neurons. This generates a transport mechanism that governs growth processes through the plasma membrane. Several *in vivo* and *in vitro* studies demonstrated the effectiveness of electrical stimulation in promoting regeneration of peripheric nerves (5). In particular, electrical stimuli increase both sensory and motor nerve regeneration, reducing atrophy of the axotomized nerves, and muscle growth and remodeling following injury. Electrical stimulation, if applied within 30 days of injury, promotes the formation of myelin where the nerve is damaged, preventing apoptosis of Schwann cells. The neuronal guide must be made of electrically conductive polymers to generate an electric discharge inside the scaffold. It has also been found that the metabolic imbalance generated by electrical stimulation leads to an increase in VEGF, which favors angiogenesis, which is fundamental both for tissue regeneration and for remodeling (81). By using a minimal electrical stimulation, for instance in terms of time or voltage threshold, cell proliferation and growth can still be promoted *in vitro*. The parameters used in electrical stimulation studies typically vary in terms of voltage, frequency, stimulation time.

2.2.6. Piezoeletric effect

Recently, the field of nanotechnology has contributed to bringing numerous interesting results by creating scaffolds characterized by piezoelectric characteristics through the use of nanoparticles. Piezoelectric materials can generate electrical signals in response to applied stress and are able to

stimulate intracellular signaling pathways in order to improve tissue regeneration at the injury site. This also applies to neural tissue as electric charges play a crucial role for cellular activity. The main positive aspect of this type of material is the generation of electrical potential in a non-invasive way through the influence of mechanical forces, without the need to use invasive electrodes. Despite the difficulty in the treatment of patients suffering from lesions of the nervous system, it has been seen that the application of piezoelectric polymers as nerve guide conduits allows the direct delivery of electrical stimulation of cell growth with its electrical activity during mechanical deformation without the need for an external energy source (82). Indeed, the surface charges generated as a result of minimal mechanical deformations of the material play an important role in stimulating the proliferation or differentiation of various cell types. In this context, the use of electrically conductive polymers as interactive materials could potentially be useful in providing neuronal guidance.

Table 2 presents the main works on the application of the piezoelectric properties of different materials:

Table 2- Piezoelectric materials in nerve tissue engineering.

Material Type	Sca*ff*old Design	Cells Type Used	Ref.
	Film	Spinal cord neurons	**(83)**
	Film	Mouse neuroblastoma cells	**(84)**
	Channels	Mouse sciatic nerve model	**(85)**
	Tubes	Wıstar rats	**(86)**
Polyvinylidene Fluoride (PVDF)	Membranes	Neuronal cells	**(87)**
	Films	Stem cells	**(88)**
	Nanosheets	Rat neuronal cell line	**(89)**
	Fibers	Osteoblasts MG-63 cells	**(90)**
	Fibers	Mesenchymal stem cells	**(91)**
Poly[(vinylidene fluoride-co-trifluoroethylene] (PVDF-TrFE)	*	Poietics normal human neural progenitors	**(92)**
		Dorsal root ganglion	**(93)**
	Films	Poietics normal human neural progenitors	**(92)**
	Membranes	Osteoblasts SaOS-2 cells	**(94)**
	Tubes	In vivo implementation: rat sciatic nerves	**(95)**
	Fibers	Preosteoblasts	**(96)**
	Films	Fibroblast growth factor (bFGF)	**(97)**
Poly(3,4ethylenedioxythiophene) (PEDOT)	**Films**	-	**(98)**
Films		Neural stem cells	**(99)**
	Films	Neural stem cells	**(100)**
	Nanofibers	Brain neuroglioma cells	**(101)**
		Sprague–Dawley rats	**(102)**
Polylactic acid	Fibers	PLLA blends for vascular differentiation in vitro	**(103), (104)**
			(105)
		PLLA blends for bone formation in vitro	**(106)**
	+PANi fibers	Nerve stem cells	**(107)**
Poly(3-hydroxybutyrate-co-3-hydroxyvalerate)	**Fibers**	Human mesenchymal stem cell	**(108)**
Collagen	**Fibers**	Schwann cells	**(109)**
	3D gel matrices	Embryonic rat cerebral cortices	**(110)**
BaTiO3	**+PVDF matrix**	**Osteoblasts**	**(111)**

3. Hybrid interfaces

Interfaces between materials and biomolecules or cells reflect the cornerstone of the success of bioengineering applications, which include drug delivery systems, tissue engineering and artificial organ implants to sensor devices. In recent years, the development of smart biointerfaces has presented the possibility of imitating extracellular signals in order to trigger a series of cellular responses, thus stimulating cells and tissues. The manufacture of artificial substrates with electrical and topographical characteristics at the micro and nano scale made it possible to influence the behavior of the cells in a specific direction. As mentioned in the previous chapter, surface topography and electrical stimulation, among others, play a fundamental role in the regeneration of the peripheral nervous system. For this purpose, in this thesis work, hybrid interfaces based on poly (3,4-ethyleneoxythiophene) doped with poly (styrene sulfonate) (PEDOT: PSS) and cerium oxide nanoparticles, called nanoceria, have been developed. The aim was to combine into a single hybrid nanocomposite material electroconductivity (PEDOT:PSS matrix) and redox action/radical scavenging (nanoceria particles). In the following subsections basics about structure and properties of the aforementioned materials will be introduced, in connection with their application in biomedicine

3.1. Conducting polymers

Conjugated polymers, thanks to their mixed electrical and ionic conductivity, are thought as ideal transducers between living tissues and electronic devices, originating the conversion of electronic signals into ionic currents and vice versa. Among other applications, they have been used in electrically modulating cellular activities such as adhesion and differentiation (112). The conductivity of conducting polymers comes from conjugated double bonds along the backbone of a structure that would otherwise have been insulating. In conjugation, the bonds between the carbon atoms are alternately single and double. Each link in the polymer chain includes three localized σ bonds link which creates a strong chemical bond and each double link also contains a less localized π-bond. In the neutral state, conjugated polymers are characterized by low conductivity, showing an electronic band structure typical of semiconductors, with an energy gap between a fully filled valence band and an empty conduction band. Conduction occurs when the conjugated polymers are synthesized in an oxidized state through the oxidative chemical or electrochemical polymerization of the monomers. What happens is the removal of the π electrons with the consequent introduction of holes (polarons) in the backbone, which act as carriers of electric charge. The holes allow the charge to move along the polymer chain and between adjacent chains thanks to the delocalized π system. To neutralize the positively charged conjugated backbones, counter-ions (anions or polyanions) are introduced during the synthesis (113).

Conductive polymers are neutral systems, deriving from a close association of oxidized conjugated polymers and counter-ions (dopants). Conductive polymers can be made in different ways. A first method is chemical polymerization, such as addition reactions stimulated by radicals, cations or anions, or condensation reactions. The advantage lies in the customization of the film that is originated, although generally it requires post-manufacturing doping with low molecular weight moieties (e.g. polar solvents, polyols, among others) to increase the conductivity. Another technique used is electrodeposition, in which the sinthesys of the polymer occurs with the addition of the dopant to the electrolytic solution. In the case of oxidative polymerization, at the base of the process there is a dopant molecule with an overall anionic charge. Cationic dopants instead generate polymers through reduction reactions (113).

Recent studies have focused their attention on biological signaling factors to optimize cell-tissue interactions with polymers. The introduction of these factors can take place as ion-charged dopants or as a non-doping inclusion. An anti-doping inclusion, unlike a biological dopant, does not have a significant overall charge, therefore it does not participate in the process of balance of the charge through the backbone of the polymer. Biological dopants contain sequences of laminin peptides, hyaluronic acid or silk-like polymer with fragments of fibronectin and polysaccharides. Inclusions such as neurotrophins, non-doping peptides, whole laminin, red blood cells and human serum albumin occur by entrapment during polymerization, post-fabrication adsorption or pre-fabrication covalent attachment to the monomer (114).

3.1.1. Conductive polymers in biomedical field: PEDOT:PSS

The conductive polymers most used for biomedical applications are polypyrrole (PPy), polythiophene (PTh) and its derivatives such as poly(3,4-ethylenedioxythiophene (PEDOT). Polypyrrole (PPy) is widely studied for its stability in aqueous media and biocompatibility, its efficient and direct deposition on areas confined by electropolymerization and its conductive nature. Despite these innumerable advantages, PPY exhibits poor long-term stability due to multiple molecular defects resulting from the α - β coupling. There is a possibility that insulating and unstable interfaces may be created in a typical biomedical environment due to the high oxidation potential of PPy, which makes the polymer reducible by weak but biologically relevant reducing agents. A more stable conductive polymer, which shows a more controlled surface morphology is the poly (3,4-ethylendioxythiophene) (PEDOT), with extraordinary electrical properties (115). It is currently used in antistatic coatings for cathode ray tubes, layers for transporting holes for light emitting diodes, photovoltaic devices, organic thin film transistors and sensors. Thanks to its high degree of biocompatibility, due to the similarity of the structure with natural materials such as melanin, and thanks to the aqueous compatibility, PEDOT can be polymerized directly in living tissues.

PEDOT is characterized by stable conductivity, whose value varies according to the type of dopant and polymerization, and a high electrical conductivity (103 S cm^{-1}). (82). Some studies have been carried out to analyze the effect of the length of conjugated sequences in the polythiophene on conductivity. The results revealed that oligomers consisting of 11 thiophene units have conductivity similar to that of the higher molecular weight polythiophene. On the other hand, a shorter length of the thiophene oligomers entails polymeric properties, with conductivity and mobility of the vehicle which increase as a function of the length of the conjugation until the thiophene is examined. Transparency is one of the main characteristics based on the application in which electrical conductivity is important and can be increased with dilution. Thanks to its high electrical and ionic conductivity, PEDOT can be used to make semiconductor films through electrochemical polymerization and interfaces of biomaterial tissues. The electrical and morphological properties of PEDOT polymer film depend on the introduction of counterions. Polymerization of polythiophene does not require isolation and purification, but could cause decomposition (82).

The use of counterions such as poly (sodium 4-styrenesulfonate) polyanion, sodium chloride (NaCl), lithium perchlorate (LiClO4), (PSSNa), monobasic sodium phosphate monohydrate (NaH2PO4 · H2O) and ions in PBS (ie, KH2PO4, NaCl and Na2HPO4) has been studied. We have seen how the PSS polyanion was incorporated into the PEDOT. In some studies, Tosylate anion (TOS) or poly (styrene sulfonate) (PSS) have doped PEDOT for the manufacture of spin coating films and vapor phase polymerization. In particular, for biofunctionalization, PEDOT: TOS was used, which shows high cell adhesion, thanks to its hydrophilicity and nanotopography (82).

In particular, the polyelectrolyte complex of the conjugated polymer PEDOT and poly-styrene sulfonate (styrene sulfonate) (PSS) has become one of the cardinal conducting polymers in organic bioelectronics. In PEDOT: PSS, the holes in the oxidized PEDOT chains are counterbalanced by PSS negative sulfonic acid groups (Figure 6) (113).

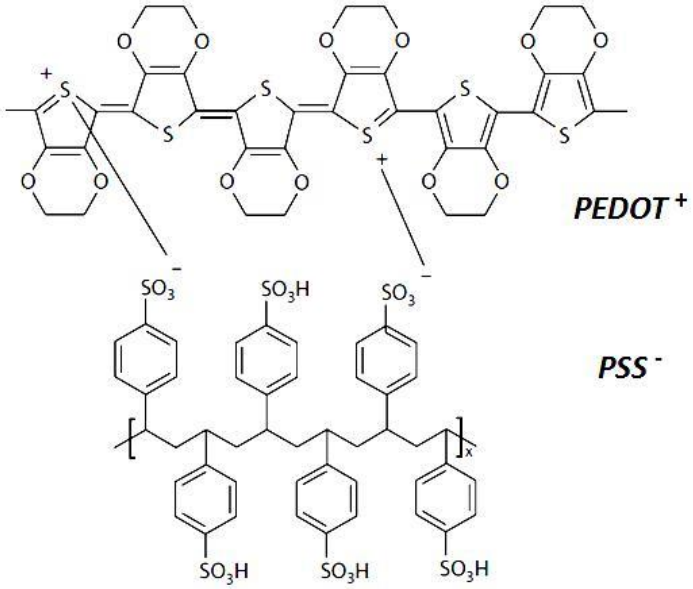

Figure 6-Chemical structure of PEDOT:PSS (113).

It is a conductive polymer with excellent properties in terms of conductivity, processability and stability. Moreover, it is characterized by good biocompatibility and transparency. The development of PEDOT formulations of the water-based PSS has found application in inkjet printing to make biomedical devices such as biosensors.

PEDOT: PSS has also proved successful thanks to its commercial availability as a polymer dispersion in aqueous solution. The particles obtained are characterized by an internal core rich in PEDOT and a hydrophilic external shell rich in PSS. PSS dispersions are commercially produced on a large scale, favoring easy processability through common techniques of deposition deposition (including screen or inkjet printing) of water based dispersions. They are suitable for production on large areas, with high efficiency, such as roll-to-roll techniques. PEDOT: PSS dispersions have the advantage of being able to be mixed directly with water-soluble additives, such as surfactants, stabilizers, crosslinkers and agents that significantly (up to around 3 orders of magnitude) increase conductivity. The conductive polymers, thanks to their soft nature, allow to interface with the biological environment thanks to the combination of electrical and mechanical properties. Furthermore, by chemically modifying these polymers, it is possible to impart specific biological functionality (116).

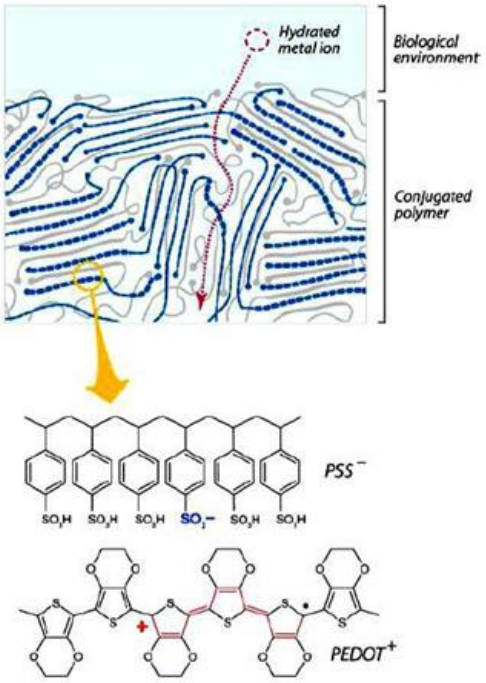

Figure 7-Structure of the conducting polymer (PEDOT:PSS) and its interface with the biological environment (116).

In figure 7, it is shown how electrical properties combine electronic conductivity with ionic mobility, thanks to the intermolecular space. In the case of PEDOT: PSS, in the event of a reduction (negative polarization) of the PEDOT chains, the electrons are injected into PEDOT, which causes a decrease in the quantity of holes (polarons), i.e. a lower conductivity. Then to balance the excess of negative charges of the PSS polyanion, small cations are brought from the electrolyte to move into the conductive polymer film or small anions are expelled. Instead in case of oxidation (positive polarization) of the PEDOT chains, the conductivity increases and to counterbalance the excess of positive charges, small anions are moved from the electrolyte to the film from the electrolyte or small cations are eliminated (82).

3.2. Nanoceria

Cerium dioxide (CeO_2) is rare earth inorganic metal oxide that is widely used for a myriad of environmental and energy-related applications, including electrochemistry, catalysis for automotive exhaust systems, chemical-mechanical planarization process, UV light shielding, adsorption and reaction of formaldehyde, oxygen storage, photovoltaics and biomedicine. It is an n-type semiconductor, with a face centered cubic arrangement (117) (118) (119). This wide variety of uses derives from the intrinsic physico-chemical properties of cerium oxide. At the nanoscale, it is also called as nanoceria, and shows an interesting redox activity thanks to the presence of crystalline defects on their surface enabling to the co-presence of both the Ce^{3+} and Ce^{4+} oxidation states. These defects are ascribable to oxygen vacancies, and mimic the activity of biological antioxidants responsible for free radical scavenging, superoxide dismutase and catalase (120).

3.2.1. Role as free radical scavengers

Free radicals are molecules with an unpaired electron in their outermost shell. ROS are produced at low levels during normal metabolism, but increase significantly during disease states, increased metabolism and cell turnover. In particular, being highly unstable and reactive, ROS can determine biomacromolecule alteration with loss of function or even acquisition of dysfunctional activity. Free radicals generated within the cell include superoxide ($O_2^{\cdot-}$), hydroxyl radical (OH •), NO, peroxynitrite (ONOO−), lipid hydroperoxides and others. Thanks to the intrinsic structure of cerium oxide nanoparticles (CeO_2 - x), numerous research studies have shown that nanoceria is able to reduce cellular structural damage by inhibiting and eliminating ROS and other inflammatory mediators in biological systems (121).

As aforementioned, cerium oxide nanoparticles mimick the biological function of superoxide dismutase. Superoxide ($O_2^{\cdot-}$), which derives from one-electron reduction of molecular oxygen (O_2), is a key species of reactive oxygen in the biological environment. Spontaneously, it decomposes into hydrogen peroxide, but it is also able to react with other radicals such as the nitric oxide radical ($^{\cdot}NO$), giving rise to other oxidants such as peroxynitrite ($ONOO^-$). When present in excess in biological environments, these species determine the so-called oxidative stress, that often leads to inflammatory cascades. For this reason, catalysts evolved with the task of minimizing the steady state concentration of superoxide in the cells, mainly superoxide dismutase and superoxide reductase. (122). In 2007, Korsvik et al. demonstrated for the first time the ability of nanoceria to mimic superoxide dismutase (SOD). Pirmohamed et al. also showed that nanoceria possesses the mimetic activity of catalase. Enzymes such as catalase, glutathione peroxidase and peroxiredoxins have the task of modulating the levels of hydrogen peroxide in mammals. Peroxides have been shown to be probably the most stable and abundant ROS in vivo, and therefore a catalyst that manages to decrease peroxide levels can be beneficial during inflammation. The catalase mimetic activity of the nanoceria is inversely related to the SOD mimetic activity in terms of the surface charge of the cerium (123). In fact, when the concentration of cerium atoms on the surface of the nanoparticle in the oxidation state +3 is more abundant, then there is a decrease in the mimetic activity of the catalase. Vicki Colvin's team has evidenced that the nanoceria deriving from a non-water based manufacturing process are good catalase-mimetics. The team also showed that oxygen vacancies play an important role in reactivity with hydrogen peroxide. When coated with oleic acid, nanoceria have high stability over a long period of time and can be used as robust catalysts for subsequent reactions. Another study has shown that nanoceria dispersed in aqueous environment has both SOD and catalase mimetic activity in vivo (124). A study highlighted nanoceria ability to protect against cellular damage caused by reactive oxygen species (ROS) and radiation. ROS influence the cytoplasmic and nuclear signal transduction pathways, and can vary the structure of DNA, as well as modulate the genes related to cell proliferation, apoptosis and differentiation processes.

Nanoceria application in biomedical research requires the elaboration of suitable synthetic protocols, and of methods for obtaining stable colloidal dispersions in water environment. The synthetic process should indeed tightly control the redox properties of nanoceria, and should ensure full removal of contaminants that may have toxic effects on the cells. Generally, nanoceria is synthesized in water medium or organic solvents, like ethylene glycol and dextran. Along with the solvent choice, that one of precursors, their concentration and the redox chemistry are fundamental during the synthetic process (125). Cerium oxide nanoparticles showed unique regenerative properties thanks to their low reduction potential and the coexistence of both Ce^{3+} / Ce^{4+} on their surfaces. Nanoceria have proven effective

against diseases associated with chronic oxidative stress and inflammation, as it will be discussed in the following paragraph.

3.2.2. Biomedical application

There are several biomedical applications of nanoceria demonstrated over the past few years, such as the inhibition of neovascular macular degeneration, protection against laser-induced eye and tissue damage due to radiation, induction of proangiogenesis and wound healing, the control of ischemic stroke, neurodegenerative diseases, anti-angiogenesis and inhibition of the interaction of the tumor stroma (125). All these studies have shown the potential of nanoceria as a therapeutic agent in diseases associated to oxidative stress.

Autoimmune diseases allow simultaneous analysis of the effects of nanoceria on inappropriately activated immune cells and ROS levels. For example, autoimmune multiple sclerosis (MS) is marked by different levels of progression as distinct immune cell populations or combinations of cell populations and their respective cell secretions are involved. It generates the loss of the myelin sheath that covers the neurons in the central nervous system, which are no longer able to efficiently transmit nerve impulses. Rodent models called experimental autoimmune encephalomyelitis (EAE) replicate the symptoms of multiple sclerosis and allow to study potential therapeutic agents. Although evidences suggest the concomitant role of nanoceria to autoimmune tissue damage, macrophage activity seems to be beneficially tuned by nanoparticles. In another study it was observed that the stabilization of sodium citrate has given rise to a sufficient quantity of nanoparticles in the brain, so as to have a therapeutic effect while maintaining intrinsic neutralization properties of ROS (123).

Nanoceria has also been shown to mitigate the noxious effect of radiotherapy on normal cells compared to cancer cells and to mediate cancer cell targeting upon suitable surface modification. Radiotherapy is indeed widely used for the treatment of cancer, but it can also damage healthy cells that are close to the irradiation site , due to the production of free radicals. Cerium oxide nanoparticles have been shown to protect normal breast cells human but not human breast cancer cells. (125). In the case of tumor tissue, the increased permeability favors the accumulation of nanometer-sized materials, thus suggesting the use of nanoparticles as a vehicle for the release of drugs. Thanks to functionalization with folic acid (FA) or methotrexate (MTX), active targeting of cancer cells can be achieved. These two molecules are recognized by the folate receptor, which is overexpressed on the surface of many cancer cells. At the same time peptides such as arginine-glycine-aspartate (RGD) can be used for targeting integrins on the tumor endothelium (125).

A NCP solution in water can lead to the healing of skin wounds, thanks to the ability of the nanoceria to improve the proliferation and migration of fibroblasts, keratinocytes and vascular endothelial cells. One study aimed to observe that oxidative stress due to increased ROS production leads to the onset and progression of cardiac dysfunction. Mice that develop myocardial inflammation until fatal ischemic cardiomyopathy have been studied. Cerium oxide nanoparticles have led to a drastic suppression of interstitial fibrosis and degeneration of cardiac myocytes in the heart of mice. Lee et al. improved nanoparticles in the protection against ischemic stroke in live animals. By injecting a selected dose of NCP intravenously, there was an important reduction in the volume of ischemic tissue, mediated by the elimination of ROS. In the field of eye diseases, NCP have been shown to have a protective effect against peroxide-induced retinal degeneration. Recently, studies have been carried out to observe the potential of cerium oxide nanoparticles in regenerative medicine in combination with stem cell therapies. NCP are able to protect the cardiac progenitor and stem cells from oxidative

stress, as well as improve the adhesion of stem cells when they were used as a bioadditive on a PLGA scaffold (124).

3.2.3. Neurological diseases

Also at the basis of neurodegenerative diseases there is the accumulation of ROS. A neuroprotective effect of NCP has been demonstrated in the prevention of lesions mediated by hydrogen peroxide to spinal cord neurons. As for the neurological field, the applications of NCP include the treatment of neurological diseases, such as Alzheimer's, Parkinson's and Gehrig (126). In the case of Alzheimer's, Cimini et al. showed an improvement in neuronal survival using nanoceria with polyethylene glycol (PEG) coating and conjugated with antibody for the selective targeting of amyloid-β 1-42 aggregates, main responsible for the disease, by modulating the brain-derived neurotrophic factor (BDNF) (127). Even when ischemia occurs, nanoceria is able to reduce reactive oxygen species and 3-nitrotyrosine levels, i.e. a modification of tyrosine residues in the proteins induced by the peroxynitrite radical. In another study, neuronal-like PC12 cells were examined, incubated with increasing concentrations of a commercial NC. There was an evident increase in differentiation by observing the length of the neurites. The antioxidant properties of the nanoparticles were confirmed by applying an oxidative insult to the cultures and by quantifying ROS species by fluorescence (128). Beneficial effects of nanoparticles have also been noted in view of Parkinson's disease treatment under proliferative conditions of the PC12 cell model (secreting dopamine, which is the neurotransmitted depleted in this morbid condition). Differentiation assessed in terms of neurite length was even promoted by nanoceria administered to the same cellular model. Far from being exhaustive, these evidences support further investigations, especially aiming at the understanding of biological phenomena and how the latter can be perturbed in order to promote tissue regeneration and maintenance.

4. Rapid Prototyping

Rapid prototyping techniques constitute a series of systems which, regardless of the constructive capacity of the object, reproduce it with additive techniques. It starts from its mathematical definition specified on three-dimensional CAD and using rapid, flexible and highly automated processes. Initially this technique was used only for commodity polymer materials, then extending it to other specialty polymer materials and then also to non-polymer materials such as metals. Prototypes and in some cases even finished products could be created (molds for small series, therefore not refined, not destined to last long and not complex). These technologies were called Rapid Tooling (RP), as the goal was to quickly produce tools for small series. With the passing of the years, the definition of Rapid Manufacturing took over by indicating technologies united by the fact that they reproduced the piece through the overlapping of successive layers of consolidated material. This type of process also goes by the name of Additive Manufacturing, as it adds material to the finished piece. In these techniques the cost of the product is independent of the geometric complexity of the piece but is only linked to the quantity of material used and the machine times. For this reason they are also called Solid-Freeform Fabrication. Since they are fully automated technologies and therefore the transition is direct from the model to the computer up to the finished product, another definition that can be used is Computer Direct Manufacturing or Computer Assisted Direct Manufacturing (129).

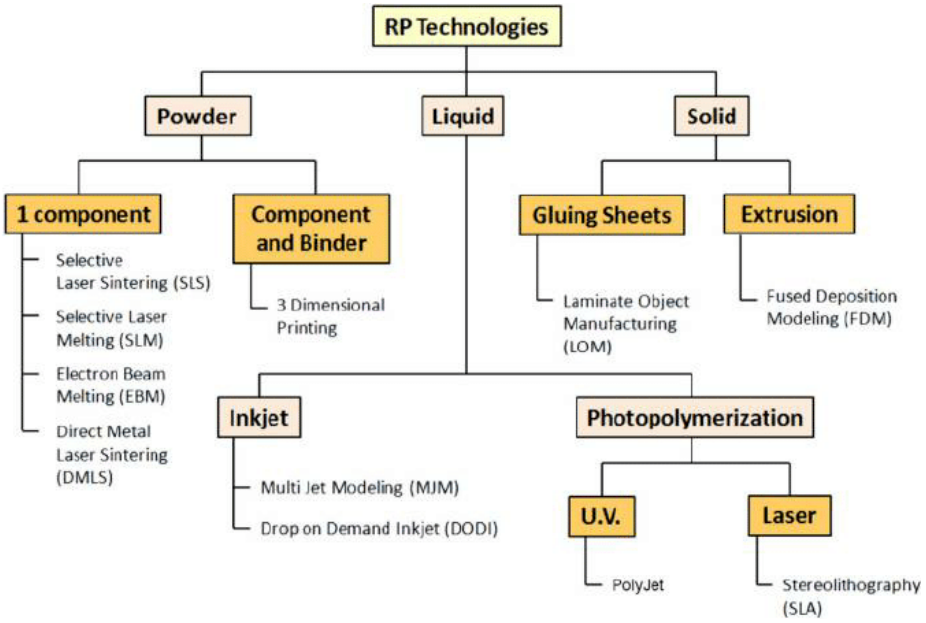

Figure 8-List of Rapid Prototyping techniques.

At the basis of RP techniques, illustrated in Figure 8, there is the material in disaggregated form, which can be of various types: granular, liquid and solid.
Among the technologies that start from the material in granular form we can distinguish:

- Selective Laser Sintering (SLS)
- Selective Laser Melting (SLM)
- Electron Bean Melting (EBM)
- 3D printing

The techniques that start from liquid material, on the other hand, consist of:

- Light-curing: Stereolithography that uses a laser to cure or the Polijet that uses UV light to cure.
- Jetting: liquid is sprayed with micropumps and then it consolidates because it is ejected at a temperature slightly higher than the melting/softening temperature. So the newly added materialsolidifies quickly as it touches the previous layer, being it at a lower temperature. Two techniques of this type are: Multi Jet Modeling and Drop on Demand.

Finally, the technologies that start in solid or filament form are Fused Deposition Modeling (FDM), where the material is extruded at a temperature close to that of melting, and the Laminated Object Manufacturing (LOM) technique.

STEREOLITHOGRAPHY

Among the characteristic elements of this technique there is a vat, which contains a photopolymer or a polymer in liquid form which polymerizes under the action of a light that belongs to a predetermined wavelength window. As shown in Figure 9, inside the vat there is a sort of lift platform that moves vertically and in the direction of the processing direction.

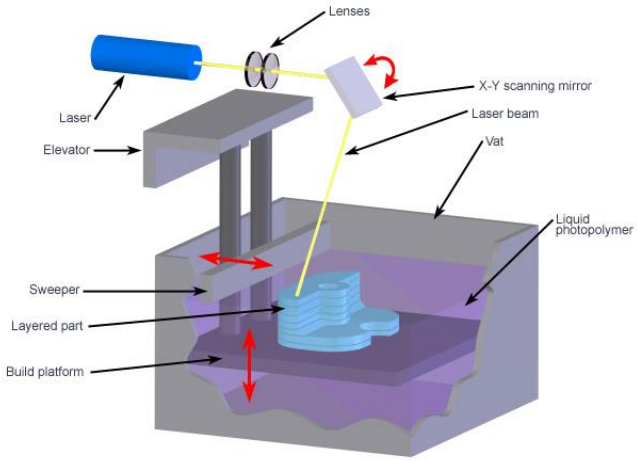

Figure 9-Schematic illustration of the stereolithography process.

In the initial phase, this platform is positioned exactly under the free surface. The tool, as in many processes, is a laser or a medium-low power monochromatic beam. It is usually a laser in the ultraviolet field because most polymers are sensitive to a wavelength window that falls back into the ultraviolet. This laser is oriented and can slide on the liquid surface thanks to a system of mirrors which are controlled by stepper motors. These motors are in turn linked to the control system, which allows you to follow the process through the use of software. The laser scratches the surface and consolidates the first layer of material. It may not be made directly on the elevator but there may be a plastic support on which the liquid resin is placed. Once the first layer has been made, the process stops and the elevator is lowered by the thickness of the next layer. Being a viscous liquid there is usually a spatula that uniforms the layer. At the end of the process, the piece emerges and must be cleaned of this resin with solvents. An additional finishing step in UV ovens may be necessary.

SOLID GROUND CURING

In this technique, the use of a mask is applied, which is prepared with a granular-shaped material and deposited on each layer, to selectively solidify. For each layer and for each geometry there is a different mask. Once the layer is consolidated, everything that is left over will be removed.

SELECTIVE LASER SINTERING

It is a process that uses a material in the form of powder, placed in a tank with an elevator that can move along z. The laser consolidates the material by partially melting the material particles, which bind together. After this consolidation, the elevator is lowered by the thickness necessary for the next layer. The newly fabricated layer is again powder coated and the process is repeated. The powder layer must be spread and flattened on the surface through a roller in order to make the thickness preset and uniform. Finally, the elevator rises and brings the finished piece out of the dust. The success of this technology is due to its simplicity combined with its great versatility in terms of materials that can be used, unlike the stereolithography in which light-curing resins are used that degrade easily and toxic. It can be applied to both plastic and metal materials but the same system is not used because with metals I work at much higher temperatures.

FUSED DEPOSITION MODELING

It is used for the creation of conceptual models. The material, contained in a reel, is introduced into a heated head which brings the material to the plasticization temperature. The head has a vertical development, therefore it can move on the xy plane; extrudes the filament and deposits it creating paths. The work plane, on the other hand, lowers along the z plane.

LAMINATE OBJECT MANUFACTURING

The most common process is that which uses paper rolled in a roller, which is stretched and spread on a work surface and then rolled up in another roller. The tool used is a laser that has the role of cutting the contours of the piece geometry. All the rest of the material is cut into chess so as to be eliminated at the end of the manufacture. Consolidation is done by passing a heated roller over the deposited layer before cutting with the laser. The temperature is such as to melt the plastic layer, which adheres to the previous layer. Once the adhesion phase has taken place, cutting can be carried out. The finished element can be coated with a water-repellent material. The mechanical resistance of the product obtained is high and could be used to create sheet metal molds.

Modern studies are oriented towards new manufacturing techniques for the creation of suitable scaffolds capable of combining multiple stimuli in a single therapy for the regeneration of the peripheral nervous system. The structures created must faithfully and functionally imitate the architecture of the nerve. The production of these constructs can take place through various methods, such as injection molding, the manufacture of free form solids and the printing of inkjet polymers.

INJECTION MOULDING

Through immersion molding technique, it was thought to create guide channels containing smaller chambers, or subluminates, in order to imitate the natural fascicular organization of the nerve. Poly (lactic acid) and poly (lactic-co-glycolic acid) tubes showed regeneration capacity. Using this type of approach, specific neurotrophic factors can be integrated into sublamines with the aim, for example, of guiding the elongation of certain types of nerve fibers.

Various experimental tests have been conducted to study the use of extruded or collagen spun fibers or other biodegradable materials that are placed in the lumen of the ducts. Tong et al.showed good regeneration by exploiting collagen tubes filled with bundles of collagen fibers with double coating in laminin and fibronectin. Matsumoto et al. have shown that the poly (glycolic acid) -collagen ducts filled with collagen fibers allow the regeneration of defect lengths greater than 80 mm in dogs. The internal collagen fibers optimize axonal elongation. A subsequent research study has shown that an internal collagen sponge is a preferred substrate over fibers due to its ease of preparation.

FREEFORM SOLID MANUFACTURE AND PRINTING OF INK-JET LIQUID POLYMERS

In recent years, there has been the opportunity to design more complex and functional structures for peripheral nerve repair thanks to the advancement of new advanced processing techniques, such as free-form solid fabrication (SFF) and jet printing ink for liquid polymeric solutions. Three-dimensional printing (3DP) is a process that starts from powders for the layered construction of devices. 3DP, like other SFF methods, realizes a structure starting from a computer model. A thin layer of polymer powder is initially deposited on a plate. A solution of liquid binder that acts as an adhesive is selectively passed through a print head on the powder bed in order to consolidate only the desired parts. The elevator is then lowered, another thin layer of dust is placed and the process is repeated. By using SFF you have more control over the type of material the structure is made of. On the other hand, the inkjet printing technique provides for a high manufacturing speed, low material consumption and suitability for mass production. But despite the many advantages of this printing technique, some points for trying to print good quality films still remain unresolved.

Among these challenges appears the formulation of appropriate inks to be able to generate spherical drops (Figure 10) and show a stable jet. The use of halogenated solvents for the ink formulation is not allowed for industrial applications, as they can cause serious health and environmental risks. After inkjet printing on a substrate, problems such as "the effect of the coffee ring" can occur, which can lead to the formation of uneven films. For this purpose, to prevent these side effects, it is essential to optimize the ink and the printing parameters. Therefore, for each layer of the device, it is necessary to refine the ink with regard to the formulation, the film formation capacity and the performance in the device (130). Subsequently, a section (see 6.1.3.) will be dedicated to the printing method used in this thesis project.

Part II
Methods and materials

5. Materials

Table 3 lists the materials used in this thesis work.

Table 3-List of used materiasl and tools for samples' fabrication.

Abbreviation	Company	Product name	Description
PET-ITO	Aldrich 639303-1EA	Polyethylene terephthalate film, ITO coated	Control substrate
PJet 700	Heraues	Clevious™ PJet 700	PEDOT:PSS ink, water based; high conductivity, ink-jet printable formulation
NC	Aldrich 643009-100ML	Cerium oxide nanoparticles	242 mg/ml, dispersion nanoparticles, size < 25 nm, 10 % wt in water
Glycerol	Aldrich	G5516-1L	≥99%, ink additive

Table 4 presents necessary materials for biological characterisation.

Table 4-List of used materials and tools for biological characterisation.

Abbreviation	Company	Product name	Description
PDMS	Dow Corning®	Polydimethylsiloxane, DOWSIL 184 Silicone elastomer KIT	Silicone elastomer
SH-S5Y5	ATCC®	CRL-2266™	Cells
DMEM/F12	Aldrich	Dulbecco's Modified Eagle's Medium D6421	Medium
FBS	Gibco	Fetal Bovine Serum	Cell culture
L-Glutamine	Gibco	25030081	Cell culture
P/S	Gibco	Penicillin/Streptomycin	Cell culture
DPBS 1X	Gibco	Dulbecco's phosphate-buffered saline	Balanced salt solution
Hoechst 33342	Invitrogen	V23201	Blue fluorescent nucleic acid stain
TRITC	Aldrich	Phalloidin–Tetramethylrhodamine B isothiocyanate	Immunofluorescent stain
TRITON	Aldrich	Triton™ X-100	Non-ionic surfactant and emulsifier

DIMEM	Aldrich	Dulbecco's Modified Eagle's Medium	Medium with high glucose
RA	Aldrich	All-trans-retinoic-acid	≥98%
TERT	Aldrich	Luperox® TBH70X	Tert-butyl-hydroperoxide solution

Table 5, instead, shows the different tools used during this thesis project.

Table 5-List of tools used in this project.

Abbreviation	**Company**	**Product name**	**Description**
Filter CA	DIA-Nielsen GmbH & Co. KG	FCA300020	0.20 µm syringe filter Cellulose Acetate
Filter PTFE	DIA-Nielsen GmbH & Co. KG	FPT150020	0.20 µm syringe filter Polytetrafluoroethylene
Syringe	Aldrich Z118400-30EA	NORM-JECT® syringe	Sterile, eccentric, luer slip ip syringe without needle
Needle	Aldrich HSWNH201-100EA	FINE-JECT® needles	Gauge 20, hypodermic, disposable, sterile needles
Micropipette	Aldrich Z646563-1EA	BRAND® Transferpette® S pipette	Volume 500-5000 µL, D-5000, adjustable single channel
Petry	Aldrich	CLS430599-60EA	Culture cell dish
24-multiwell plates	Corning®	3337	1.9cm² growth area per well
Tube	Corning® Centristar	430790	15 L capacity

5.1. Substrate

A transparent polyethyleneterephtalate (PET) film coated with a thin, transparent, conductive indium tin oxide (ITO; In_2O_3 / SnO_2) layer was used as a substrate. ITO/PET films had the following properties: surface resistivity = 60 Ω/sq, thickness = 130 µm, thickness of ITO coating = 130 nm, transmittance @ 550 nm > 78%) (131). The indium tin oxide coated polyethylene terephthalate (PET) film is optically transparent. The whole is covered by a thin, removable transparent film, which acts as protection.

Figure 10-PET-ITO sheets.

To check which side is conductively coated with ITO, a multimeter can be used. PET/ITO sheets have great flexibility and temperature resistance up to 120 °C. Due to their high optical transmission and conductivity, these films can be applied in various fields. PET/ITO sheets can be laser cut easily in customized shapes, allowing a high versatility and ease of processing.

5.2. Ink preparation

This section presents the preparation and processing of the inks. Table 3 shows the distributors of the materials used in printing. In particular, PEDOT:PSS ink is commercially available, while nanoceria ink has been modified and optimized before reaching the final composition useful for printing.

PJet 700 (PEDOT:PSS)

PJet 700 is an aqueous PEDOT:PSS dispersion with a solid content of 0.6-1.2%, blue color, mainly used as ink in printing. Before use PJet 700 was first placed in a syringe and filtered with a 0.20 µm CA filter to remove any aggregate or residual mechanical impurities. It was then mixed with 10% wt glycerol (used here as both a conductivity enhancer dopant and an humectant, for improving the quality of printing) and stirred overnight to reduce the formation of air bubbles. It has a minimum specific conductivity of 650 S/cm (132).

NC ink

The commercially available nanoparticles dispersion, with a concentration of 10 wt. % in H_2O, has been 1:5 diluted in distilled water. Then glycerol was added in 1:1 volume ratio and stirred.. In the first experimental tests used to resolve the best concentration of nanoparticle-based ink, a small amount of surfactant (0.5 µL/mL of BYKJET 9171) was added to the solution. The ink thus formed had a very low viscosity and problems were encountered during printing. This is the reason why the surfactant has been removed.

6. Deposition and characterisation methods

This chapter describes in detail the methods used for the fabrication of composite substrates based on PEDOT:PSS and nanoceria. A brief background on the various methods is given, with the aim of providing an understanding of their basic principles.

6.1. Deposition and fabrication methods

This section provides an introduction to the methods used for cutting base substrates, activating their surface by plasma treatment and printing composite films on them. Inkjet printing was chosen as a deposition method since it is one of the most promising in terms of resolution, film thickness, homogeneity; it also enables low cost and upscalable manufacturing. PET-ITO sheets were chosen as convenient substrates since they were combining good mechanical and electrical properties while being fully transparent in the whole visible range. Moreover, PEDOT:PSS is known to create smooth, stable and perfectly matched films and interfaces with ITO, as used e.g. in organic photovoltaics (133). A plasma activation treatment was necessary in order to increase the wettability of the surface by the inks, with the final aim to improve printing quality and film homogeinity.

6.1.1. Pre-deposition treatment: laser cutting

Prior to printing, the PET-ITO sheets were laser cut into 2.8 x 8 cm^2 rectangles. The cutter used was a Universal Laser Systems VLS 2.30. The system was equipped with a CO_2 laser source (emission wavelength 10.6 µm) with a power of 30 Watt. Laser cutting parameters (P: power, S: speed; PPI: resolution; Z: focal distance) were set at: P= 27%, S=24%, PPI= 500, Z= 0 mm.

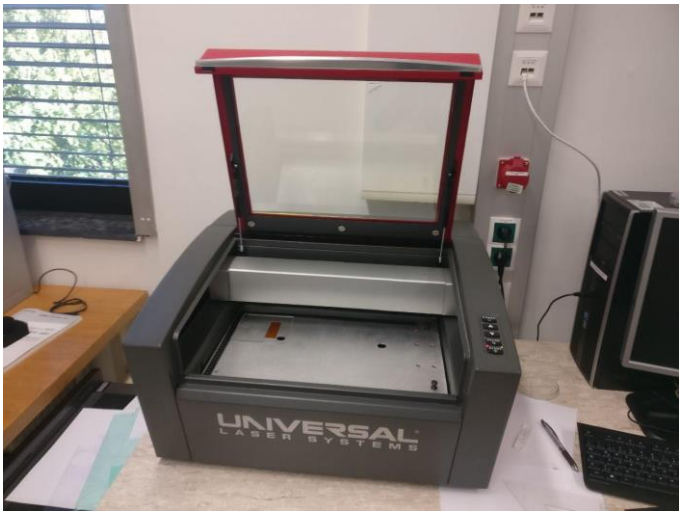

Figure 11-Laser system used during the project.

6.1.2. Pre-deposition treatment: plasma activation

A prerequisite for printing is good surface wettability. This is often associated with the surface energy of the substrate. It is very difficult to deposit a coating from a waterborne solution/dispersion onto a non polar surface. The surface energy of the liquid that is made to adhere to the substrate must be lower than that of the substrate. This derives from the study of the wettability of a surface. Assuming that a drop of water is deposited on an ideal surface (smooth and chemically homogeneous), along the entire contact line (place of the points of coexistence of the liquid, solid and gaseous phases) a contact angle is defined as the internal angle between the surface and the plane tangent to the contact point. By projecting the different surface tensions acting on the plane, since the drop is in equilibrium, the Young-Dupré law can be written:

Equation 1

$$\gamma_{SG} = \gamma_{SL} + \gamma_{LG}\, cos\theta_c$$

γ_{SG} = the solid-gas interfacial tension

γ_{SL} = the solid-liquid interfacial tension

γ_{LG} = the liquid-vapor interface tension

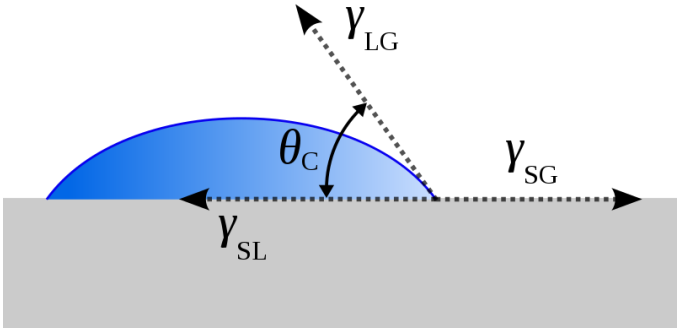

Figure 12- The contact angle of a liquid on a surface (134).

Under these hypotheses, the contact angle is associated with minimization of the surface free energy of the system for thermodynamical reasons. At room temperature for water it is possible to observe the condition of total wettability ($\theta = 0$) in spite of that of completely dry surface ($\theta = 180^{\circ}$). An air or oxygen plasma treatment is usually required to partially degrade and activate the polymer surface, whose functional groups are then partially replaced with different polar moieties to increase the surface energy.

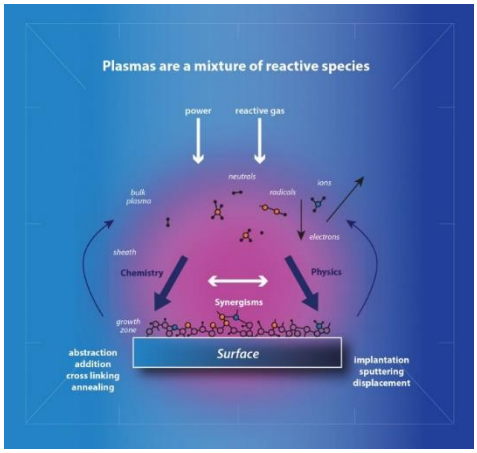

Figure 13- Simple design of a plasma treatment (135).

As shown in Figure 14, plasma is an ionized gas with neutral electrical charge and consists of electrons, ions, radicals and photons. It can be defined by the gas used, the pressure and the plasma mode. It is essential to know which gas to choose for the desired application as completely different effects may occur. For example, oxygen-plasma increases while flourine-plasma decreases surface tension.

Atmospheric air plasma is sometimes used in manufacturing, which does not need vacuum and shows fast processing. The plasma technique using air or oxygen plasma causes the non-polar hydrogen bonds of polymers to be replaced by oxygen bonds (136).

Figure 14-Femto Plasma chamber used in this project.

6.1.3. Inkjet printing

The use of inkjet printing was considered fundamental for this thesis work. The operating principle at the base of an inkjet printer is the ejection through a nozzle of fixed quantities of ink (drops), present in a reservoir chamber. There are two different types of printers for droplet generation, known as continuous inkjet printing (CIJ) and drop-on-demand (DOD) inkjet printing (137). DOD inkjet printing has been used in this project, which allows droplet generation only when an activation pulse is

provided. This technique can be thermal or piezoelectric. The FUJIFILM - Dimatix DMP2800 printer is in the second category.

a) 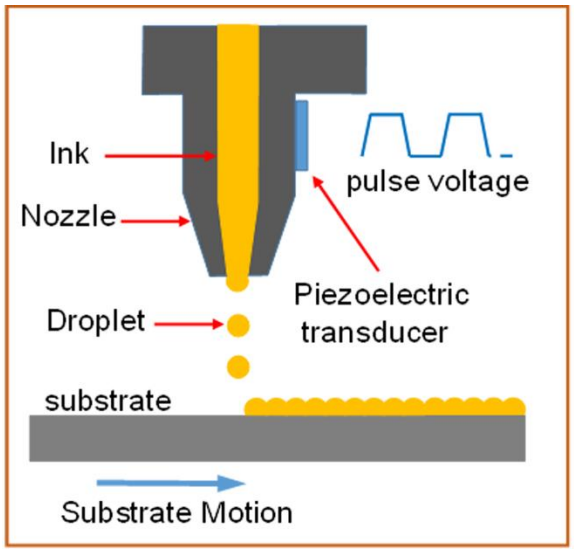

b) 

Figure 15-a)DoD inkjet printing system.b) Fujifilm Dimatix DMP2800.

As displayed in Figure 16, the figure representing the operating principle of a DoD-inkjet piezo printer, there is a piezoelectric actuator whose functioning can be adjusted through a software user interface. The piezoelectric membrane deforms when external voltage is applied, producing ink compression down to the nozzle. The surface tension, viscosity and inertia are essential for the creation of droplets. The operating system includes a waveform editor which can alter the electronic pulses to be supplied to the piezoelectric inkjet device and a drop control camera system to watch the droplets ejected from each nozzle. This aims to improve the characteristics of jetting from the nozzle.

The schematization process to generate ink droplets on the desired substrate can be described in five steps: drop ejection, flight, drop impact, drop diffusion and drop solidification (138).

- Drop ejection and flight - An electrical signal is sent to the piezoelectric actuator to decrease the volume of the chamber where the ink is located. This generates an increase in pressure and kinetic energy, which leads to a drop ejection if the surface tension is exceeded. The shape of the drop, which may vary during flight, may depend on several factors such as the properties of the fluid, the nozzle geometry and the signal applied to the piezoelectric actuator.
- Drop impact and diffusion - The parameters that determine the drop behavior at this stage are: drop impact velocity, its diameter and surface tension, as well as substrate hydrophobicity/hydrophilicity, its surface energy and roughness. Other parameters such as the volume and speed of a droplet depend on the amplitude of the piezoelectric drive voltage, frequency and pulse width. Different measurements such as Reynolds, Weber and Ohnesorge numbers allow to determine which of the two phenomena, impact and diffusion, is predominant. The contact line expands radially, with viscous forces and surface tension dampening diffusion. The kinetic energy associated with the drop is dissipated by the impact and transformed into surface energy in the form of diffusion.

- Drop solidification: The last step involves evaporation of the solvent lying on the substrate. The evaporation produces a high volume variation that will be relevant for the final characterization of the printed layer. In this phase the hydrophobic/hydrophilic character of the surface is of considerable importance. If the surface is hydrophobic, a line of contact that moves away or even rebounds is highlighted. If the surface is hydrophobic the drop continues to spread until it reaches a state of final equilibrium. A drying phenomenon, known as the coffee ring effect, is also detected, which determines the final resolution and quality of the printing path. The evaporation rate of the solvent increases towards the edge, where there is the interface with a dry substrate. This increase causes the fluid to move towards the edge to balance the evaporated solvent.

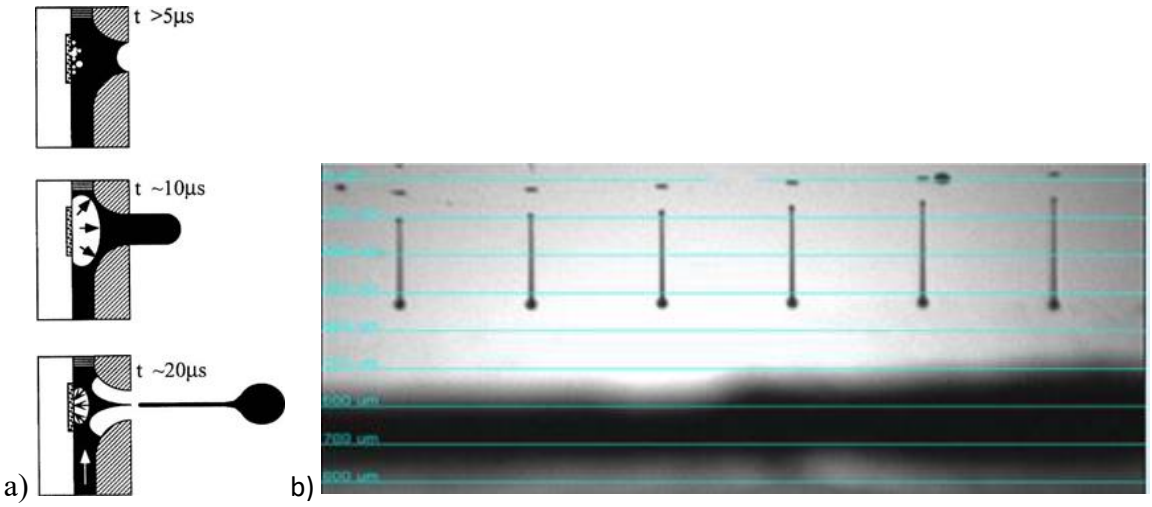

Figure 16-a) Mechanism of droplet formation in a piezo-driven DoD inkjet printing. b) Camera view of ink drops jetting from a printhead.

An important print parameter that will also affect the results of the various tests carried out is the spacing between the drops, from which the resolution and density of the print is determined (Figure 18) (139). This is done by adjusting the printhead angle. The 16 tunable and piezo-actuated nozzles of the printhead are arranged along a row. The printhead can be adjusted to different angles for tuning the actual dot spacing. When the cartridge is placed perpendicular to the printing direction, there is a maximum spacing in the y-axis of 254 µm between individual jetted droplets. If the cartridge is set at an angle of less than 90°, the spacing is reduced, allowing for high-resolution printing.

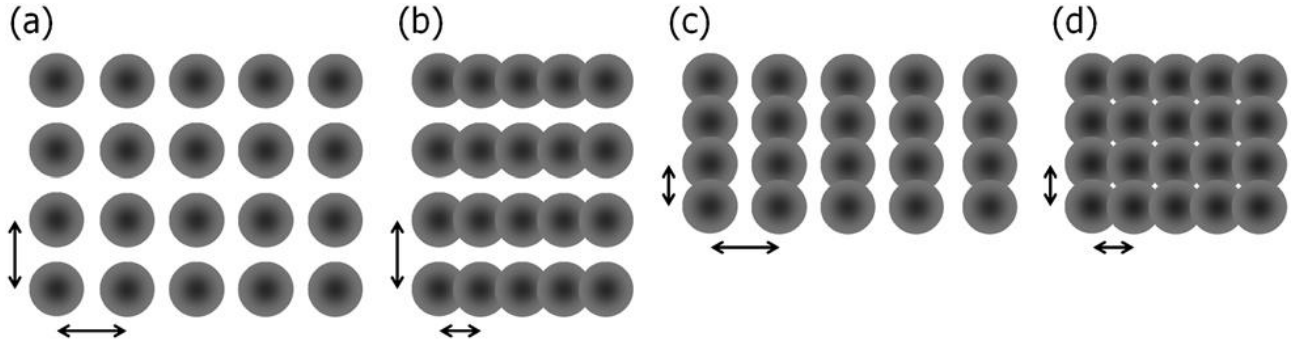

Figure 17-Schematic representation of the variations in point spacing, indicated by the arrow: (a) single drop condition, obtained when the dot spacing in the x and y direction is greater than the diameter of the drops on the substrate, (b) horizontal line condition if the dot spacing in the x direction is reduced, (c) vertical line condition if the dot spacing in the y direction is reduced, (d) continuous film condition if the dot spacing in the x and y direction is smaller than the diameter of the drops on the substrate.

6.2. Characterisation methods

The characterization of the materials investigated in this project involved the evaluation of properties such as thickness, film homogeneity, conductivity and redox/electrochemical behaviour. In this section the basics of several characterization techniques are provided, together with those used for the biological part.

6.2.1. Profilometry: thickness

The stylus profilometer is mainly used for step height assessment in thin films research and technology (e.g. semiconductors, optics, etc.). The profilometer is equipped with a stylus tip which is gently placed on the surface of the sample to be examined and pressed against it by a controlled force. The tip is scanned along a user-defined length line and the measurement of the height variation can be made through a linear variable transducer differential, an optical lever or a linear variable capacitor differential. Stylus size has the advantage of being direct and independent of material properties (140).

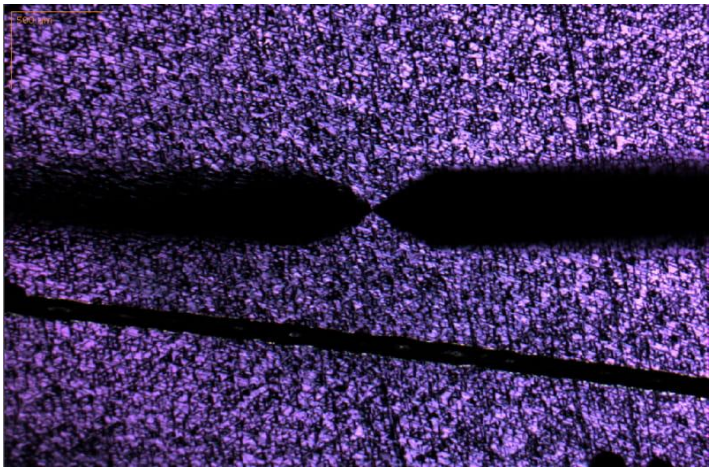

Figure 18-Stylus tip on a surface (140).

The measurement is easier if there is a sharp edge on a smooth surface below, because it ensures that small heights can be detected and are not disturbed by roughness. The instrument sensitivity can be optimized by reducing external vibrations from the environment (air fluxes, building and instrument vibrations). This can be achieved by placing the measuring system on an optical table or on an active vibration damping device. The device also has a cover or enclosure to minimize air fluxes within the measuring area.

6.2.2. Optical microscopy: film homogeneity

The thesis project uses an optical microscope to evaluate the uniformity of the printed film. The main basic functions are:

1. Magnification of an image of a sample
2. Illumination of a sample

The optical observation system allows the implementation of the first function, which includes obtaining a clear and sharp image, changing an enlargement and focusing the image. This part of the device projects the sample and the projection is collected by the eyes or by a sampling device such as

the charge coupled device (CCD). The optical lighting system, on the other hand, provides light, collects it and changes its intensity. It focuses the light generated by a light source to illuminate the desired sample (141).

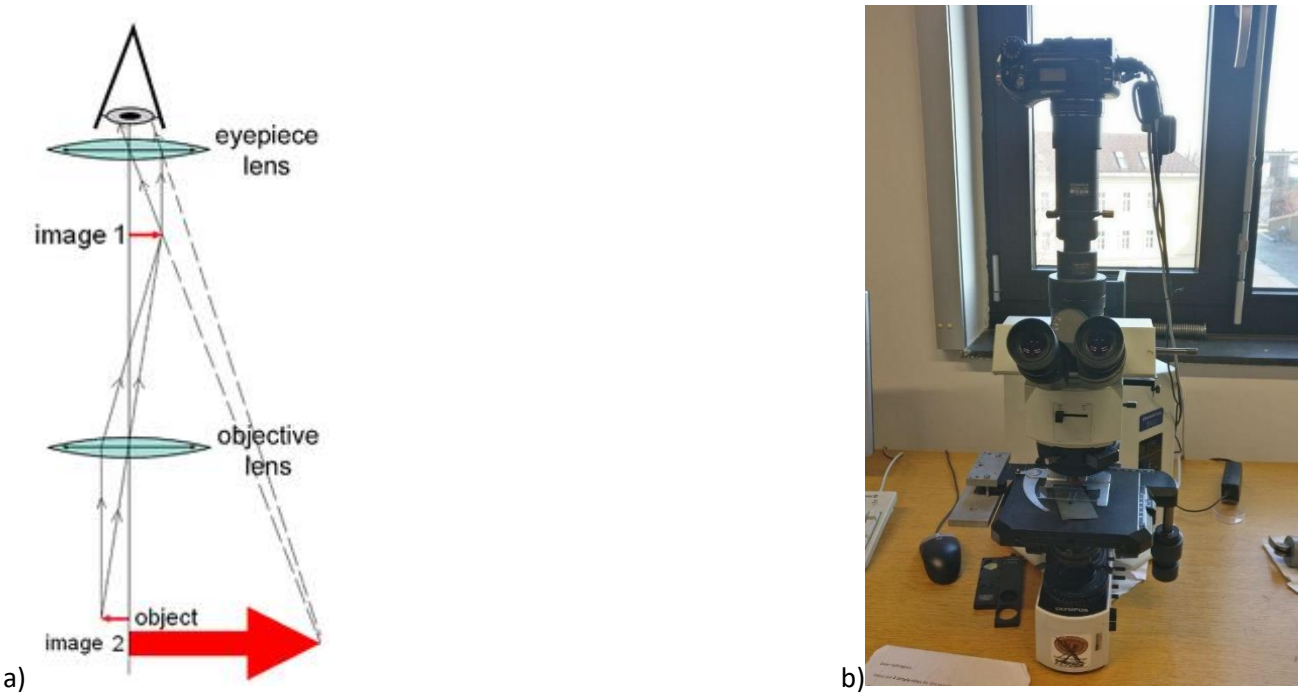

Figure 19-a)Schematization of the operation of an Optical Microscope (141). b)Optical Microscope used in this thesis.

The creation of a magnified image of a sample is done through an objective lens. The microscope further magnifies the image with an eyepiece so that it is visible to the user even with the naked eye. The instrument sets the objective lens close to the sample to focus the image of the object. Through an eyepiece the acquired image is magnified, being closer to the eyepiece than the front focal point, so that a virtual magnified image of the sample to be examined is presented to the user.

6.2.3. Four-point-probe method: conductivity

The purpose of the 4-point probe is to determine the sheet resistance of a material from which its specific conductivity can be derived, if the thickness of the thin film is known. The four equidistant tungsten metal tips with finished radius are in linear arrangement and come into contact with the surface. The current I passes through the external electrodes, while the potential V is measured across the internal electrodes 1,2 in Figure 21 (142).

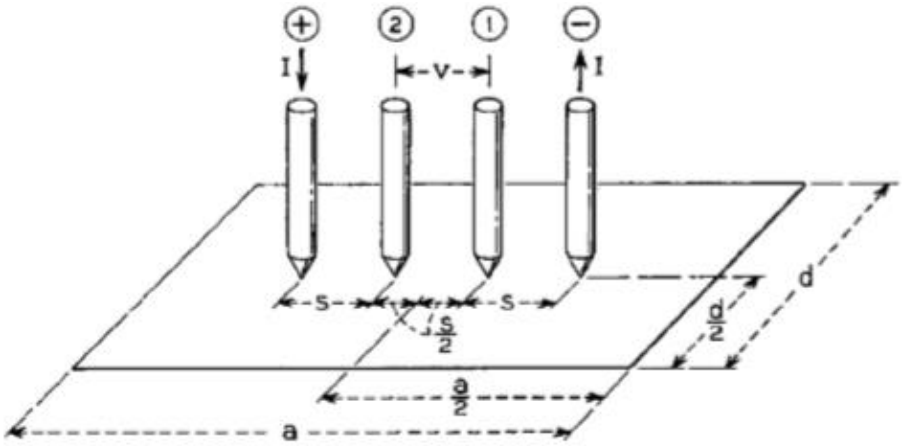

Figure 20-Schematic illustration of a four-point-probe on a 2D rectangular sample. I (current), V (voltage), s (distance between probes), a (lenght of sample area), d (width of sample area).

The sheet resistance can be calculated through the Equation 1:

Equation 2

$$\rho_s = \frac{V}{I}\frac{\pi}{\ln 2}\,C(a,s,d)$$

ρ_s = sheet resistance

V = voltage

I = current

a = lenght of sample area

d = width of sample area

s = spacing of probes

C(a,s,d) = correction factor depending on a, s and d

The correction factor is 1 if the sample area is large and may depend on the film thickness in other cases. In literature it is also possible to find the term constant in the correction factor. If the condition occurs where the thickness is less than half of the probe spacing, then the following equation that relates the measured sheet resistivity to the mass resistivity (143), applies:

Equation 3

$$\rho = \rho_s\, t$$

ρ = bulk resistivity

t = thickness

The Equation 2 was used to calculate the conductivity of all the samples made. The conductivity can be quickly obtained from the Equation 3:

Equation 4

$$\sigma = \rho^{-1}$$

6.2.4. Cyclic voltammetry: electrochemistry

Cyclic voltammetry is a type of potentiodynamic electrochemical measurement used to study the reduction and oxidation processes of molecular species. If an electrode is considered, the oxidation or reduction that occurs on its surface is related to the potential of the electrode. Therefore it is possible to control the redox reaction that takes place on the electrode through the electrode potential of an electrochemical cell. This makes it possible to analyse the electrochemical behaviour of a system by studying the current-voltage measurements of a given electrochemical cell.

The cyclic voltammetry considers the configuration of the three electrodes: a reference electrode, a working electrode and a counter electrode (144). As can be seen from Figure 22, the potential is applied between the working electrode and the reference electrode and the current is measured between the working electrode and the counter electrode.

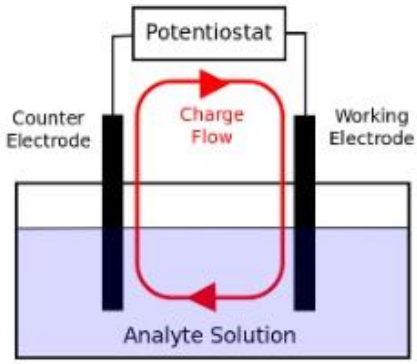

Figure 21-Schematic illustration of basic operation (144).

In the experiment, there is a linear and cyclic variation with respect to time, of the working electrode potential for a given scanning speed. When this reaches the set threshold, the trend of the current, traced with respect to the applied voltage, is reversed in order to return to its initial potential. This can also occur several times within a single experiment. Typically a triangular waveform is used and the cyclic voltammeter provides the graph of the current to the working electrode with respect to the applied potential. The peaks for oxidation and reduction are similar if the reaction is more reversible.

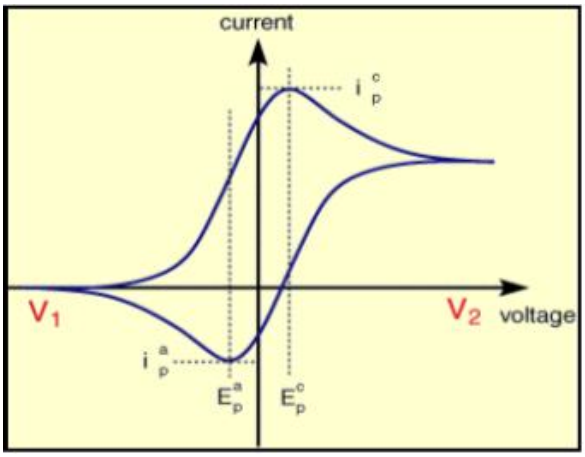

Figure 22-An example of cyclic voltammogram.

The figure 23 presents a graph of a typical cyclic voltammetry. As shown, the potential is first increased. Because of the analytic species, the cathodic current also increases and there is therefore a reduction. Once the threshold potential is reached, the current decreases as the concentration of the analyte decreases. From this moment the reduced analyte begins to reoxide, generating an anodic current of reverse polarity to before (145).

The scanning speed of the experiment is important, because the scanning speed of the applied potential depends on it. A high scanning speed leads to a decrease in the size of the diffusion layer, therefore higher currents. In the case of the transfer of electrochemically reversible electrons freely involving diffusing redox species, Randles-Sevcik equation shows how the peak current ip (A) increases linearly with the square root of the scan rate υ (V s^{-1}), where n is the number of electrons transferred in the redox event, A (cm^2) is the surface of the electrode, D_o (cm^2 s^{-1}) is the diffusion coefficient of the oxidized analyte, and C^0 (mol cm^{-3}) is the mass concentration of the analyte.

Equation 5

$$i_p = 0.446nFAC^0\left(\frac{nF\upsilon D_o}{RT}\right)^{\frac{1}{2}}$$

Through this equation it is possible to calculate diffusion coefficients. Analytes can adsorb to the electrode surface, so it is essential to see the homogeneity of the analyte in solution before evaluating its reactivity (144).

6.2.5. Immunocytochemistry and fluorescence microscopy

Immunocytochemistry (ICC) is a technique used for the indirect visualization of proteins and peptides present in cells. This technique uses biomolecules, generally antibodies bound to fluorophores or enzymes, which are capable of binding to a protein of interest, also termed antigen. The signal consisting in fluorescence or a color resulting from an enzymatic reaction is then detected under an optical microscope.

In the case of antibodies coupled to enzymes, the latter, after the addition of a substrate, catalyze a reaction which gives place to a colored product visible at the site of interaction between the antibody

coupled to the enzyme and the sample. Fluorophore molecules conjugated to antibodies are instead brought to a higher energy state by interaction with light of specific wavelength. Subsequently, by returning to their original energetic state, they emit light of a longer wavelength. The fluorescence microscope is able to excite fluorophores and simultaneously acquire their emission. It is also possible to observe multicolor images in which each color describes a specific antigenic target. In this case, care must be taken to ensure that there is no spectral overlap of the excitation and emission profiles of the fluorophores (146).

The detection method for immunostaining used for the thesis is indirect. A primary antibody targets a specific protein in a cell and several secondary antibodies conjugated to a fluorophore bind to the primary antibody. In this way the signal to be detected by the microscope is amplified.

In the thesis work, a Nikon Eclipse Ti fluorescence inverted microscope was used with the NIS elements software for image acquisition after immunocytochemistry.

Figure 23-The inverted fluorescence microscope used in this thesis work.

Fluorescence microscopy makes it possible to determine the distribution of a single species of molecule, its quantity and its location within a cell, by exploiting the emission of light from the fluorophores after being excited with light of a certain wavelength.

The typical components of a fluorescence microscope are presented in Figure 25:

- a light source (xenon arc lamp for bright field or phase contrast imaging, and a mercury vapour lamp for fluorescence imaging);

- the optical excitation filter;
- the dichroic mirror (or dichroic splitter), which reflects the excitation light to the sample and transmits only the emitted light from the sample to the detector (a CCD camera) and to binoculars;
- the emission filter, through which the light emitted by the sample passes before it reaches the detector;
- a CCD camera that detects the light from the sample and is connected to a computer.

Light of a specific wavelength impacts on the sample through an excitation filter and the fluorophores emit light at longer wavelengths after absorption. The microscope uses a spectral emission filter that is transparent only towards the light emitted by the sample, separating it from the unwanted background light. The spectral excitation and emission characteristics of the fluorophore used to mark the sample are fundamental parameters in the choice of filters and dichroic splitter (147), (148).

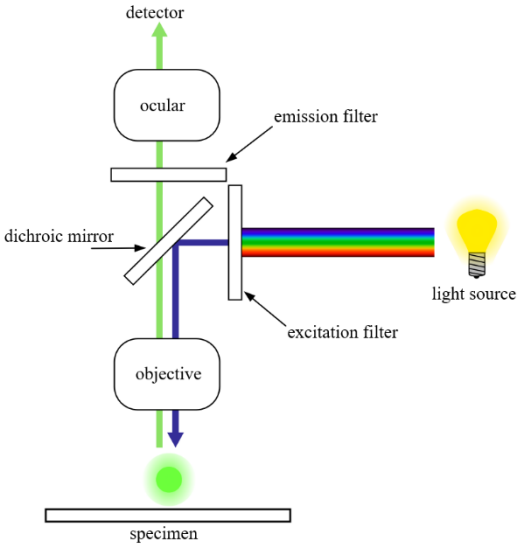

Figure 24-Schematic diagram of the ptical path of a Fluorescence Inverted Microscope (147).

6.2.6. Fluorimetry

Fluorimetry is an important analytical method characterized by a high degree of sensitivity and selectivity for many compounds. It consists in the measurement of emitted fluorescence light. In this fluorescence technique, the sample is exposed to radiation of a specific wavelength, interacts with it and emitts a radiation of equal or greater wavelength. The intensity of the emitted radiation is directly proportional to the concentration of the fluorescent species. Fluorescence begins immediately after light irradiation and stops as soon as the incident light is interrupted (149).

Figure 25-The microplate reader used for Pico Green® Assay.

In this thesis work, the fluorescence was measured through the Perkin Elmer Victor X3 microplate reader suitable to excitation of a fluorophore at 485 nm, and to detection of the emitted light at 535 nm. The fluorescence measurement time was kept constant for all samples in order to minimize photobleanching effects.

Victor X3 is a multilabel and multitasking plate reader, equipped with:

- interchangeable high quality filters;
- a heated plate holder that can be adjusted to the appropriate temperature:
- a built-in shaker;
- bells and whistles provided for high-end plate readers.

A dispenser module can also be added for plate stackers in high productivity applications. It is reliable in reading, with minimal well-to-well variability. The instrument uses a continuous light source for fluorimetric and photometric measurements (150).

6.2.7. Flow cytometry

Flow cytometry is a technique used to detect and evaluate the physico-chemical characteristics of a population of cells or particles. It allows simultaneous multiparametric analysis of single cells. A sample consisting of fluid within which cells or particles are suspended is injected into the instrument. Through a laser beam, the sample is focused in such a way that it ideally flows one cell at a time. The light emitted in a wavelength band is characteristic of the cells, marked with a fluorophore, and their components (151).

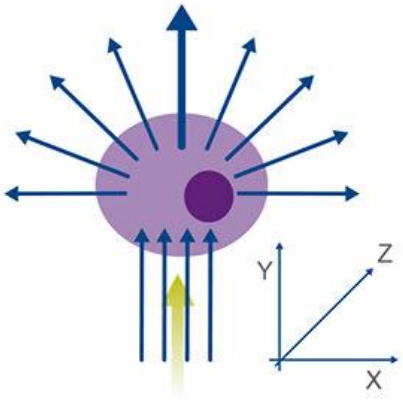

Figure 26-Light scatter as the laser interrogates the cell (151).

Placed in front of the light beam, a detector measures forward scattering (FS) and lateral scattering (SS). FS is an indicator of cell size and SS is related to cell granularity. For this reason, different cell populations can be classified according to differences in their size and granularity. Cells can also be distinguished by the expression of a particular protein.

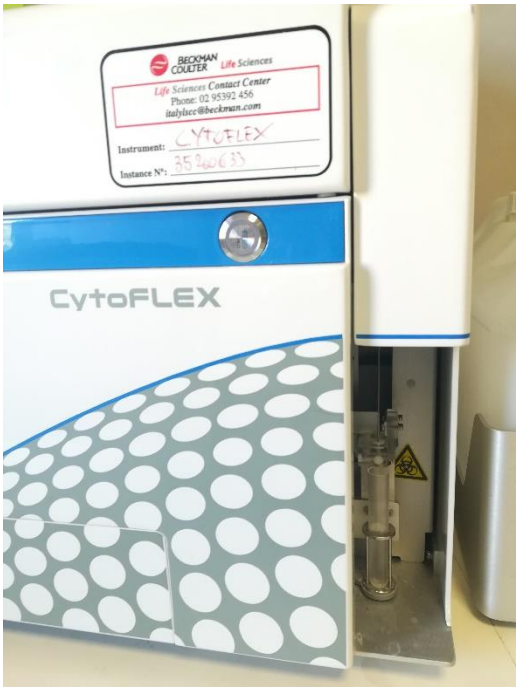

Figure 27-Flow cytometer used in this work.

In this thesis work, the CytoFLEX flow cytometer was used, characterized by high sensitivity and resolution. The operating principle is based on the row arrangement of the individual cells inside a flow chamber, which reflect the light of a laser beam and emit fluorescence once hit by the light. The signals generated are converted into digital signals and sent to a computer (152). The instrument is equipped with:

- a fluidic system that allows the passage of the suspended cells in the analysis cell. By exerting pressure, the sample is pushed into the flow chamber, where the individual cells align in a single row;

- an excitation system consisting of one or more light sources. Monochromatic and unidirectional signals are generated which intercept the cells in the test cell;
- an electronic optical system that processes the collected signals. It consists of lenses, mirrors and standard and non-standard optical pass band filters that transmit the signals to the photomultipliers. They amplify the filtered light signal, allowing it to be acquired in the form of digital data. There are no multiple dichroic filters to direct the light path, thus increasing the luminous efficiency as the loss of light due to refraction is minimized;
- an optional plate loader module for high productivity applications to allow rapid processing of multiple samples;
- a computer which enables the analysis and processing of the data by means of specific programmes of graphic representation. An offline analysis software with accessory tools is present to improve the data acquisition workflow.

7. Experimental setups and methods

7.1. Methodology

A detailed overview of the manufacturing and characterization of the composite biointerfaces created is given in this section. Hybrid substrates have been studied in terms of thickness (profilometry), film homogeneity (optical microscopy), electroconductivity (four-point probe measurements) and electrochemistry (cyclic voltammetry). In the second instance the samples created were also characterized at biological level, performing proliferation and differentiation tests by immunocytochemistry, fluorometry and flow cytometry tests.

After determining the most suitable substrate, PET-ITO, chosen mainly because of its high conductivity, the study investigated how to print onto it a film of PEDOT:PSS, cerium oxide NP and their composites. In addition, it was also essential to determine how many layers could be deposited on the control substrate to achieve the goal.

At first, PET-ITO substrates were preliminarily cut with the laser into 2.8 x 8 cm^2 pieces. Preliminary tests were carried out without plasma activation: it was noticed by eye that the deposited film was not uniform. For this reason, all subsequent tests were carried out with a plasma activation (see section 6.1.2. for description). As described in section 5.2., several preliminary printing tests were performed for the NC ink in order to identify the best composition. The use of the surfactant has led to problems of low viscosity with consequent difficulty of exit from the head of the printer. This was the reason why it was decided to eliminate the additive. Therefore a printing process was found that proved useful for this new nanoparticle-based ink without the use of surfactant and the printing parameters were determined for a commercial PEDOT: PSS ink and NC ink. NC and PEDOT:PSS ink was deposited on the top of the PET-ITO substrates with the Fujifilm Dimatix printer. The following samples were examined:

1. (P), PET-ITO as reference;
2. (P-PP1), PEDOT:PSS (1 layer) on PET-ITO;
3. (P-PP2), PEDOT:PSS (2 layers) on PET-ITO;
4. (P-NC1), NANOCERIA (1 layer) on PET-ITO;
5. (P-NC2), NANOCERIA (2 layers) on PET-ITO;
6. (P-NC3), NANOCERIA (3 layers) on PET-ITO;
7. (P-PP-NC), PEDOT:PSS + NANOCERIA on PET-ITO;
8. (P-NC-PP), NANOCERIA + PEDOT:PSS on PET-ITO.

Through the surface and electrochemical analysis of the different types of samples mentioned above, the P-NC-PP sample was discarded due to the impossibility of measuring the thickness using the profilometer. The instrument provided very different measurements even on a small scale. This was an indication of an uneven film. Based on preliminary results obtained from the different materials characterization tests, it was decided to include only 6 types of samples in further cell culture studies:

1. (P), PET-ITO;

2. (P-PP), PEDOT:PSS on PET-ITO;
3. (P-NC30), NANOCERIA on PET-ITO (nominal drop spacing 30 µm);
4. (P-NC200), NANOCERIA on PET-ITO (nominal drop spacing 200 µm);
5. (P-PP-NC30), PEDOT:PSS + NANOCERIA (nominal drop spacing 30 µm) on PET-ITO;
6. (P-PP-NC200), PEDOT:PSS + NANOCERIA (nominal drop spacing 200 µm) on PET-ITO.

The drop spacing to investigate how different distances between the individual ink droplets (and the resulting morphology and composition of the film) can influence the cellular response. Four type of cell test were carried out, with cells of neuronal origin. They were carried out twice in order to have comparable results. The section 10 will be dedicated to cell culture studies.

7.2. Devices and setups

The table below shows the different devices. The next subsections show the self-made setup for CV.

Table 6-Device list.

Device / setup	**Company**	**Model**
Laser cutter/engraver	Universal Laser Systems	VLS 2.30
Plasma chamber	Diener electronic	Femto
Inkjet printer	Fujifilm	DMP2850
Profilometer	KLA-Tencor	D-500
Optical microscope	Olympus	DP SOFT
Four-point-measurement	Vötsch	VT4002
Centrifuge	Hettich Zentrifugen	Universal 320R
Incubator	Thermo Scientific	BB-15
Fridge	Joint Lab	
Sonicator	Sonopuls-Bandelin	Mini20
Flow cytometry	Beckman Coulter	Cytoflex
Inverted fluorescence microscope	NIKON	ECLIPSE Ti
Shake	Heidolph	Rotamax 120

Microplate reader	PerkinElmer	Victor3
Potentiostat	Gamry Instruments	G 600/ZRA

7.3. Experimental methods

This part of the chapter presents all the experimental procedures carried out during the surface and electrical characterisations of the samples. A brief description of inkjet printing is also provided.

Laser cutting

The laser cutter/engraver used for cutting the PET-ITO substrates (See Section 5.1), was a ULS 2.30 by Universal Laser Systems. After removing the blue protective film, the PET-ITO film has been placed on the laser cutter working table. Through the user interface, the appropriate laser cutting parameters were used, as summarized in the following Table 7:

Table 7-Laser cutting parameters.

Parameters	Values
Mode	Vector
Power	27%
Speed	24
PPI	500
Offset	0 mm (focused state)

Plasma activation

The plasma activation was carried out using the "Femto" plasma system from Diener electronics. In order to ensure good wettability of the inks used and thus to achieve a uniform printed layer, it is necessary to modify the surface energy of the PET-ITO control substrate. For this purpose a weak air plasma (4W) and a short duration (90s) at a pressure of 0.4 mbar were applied.

Inkjet printing

Inkjet printing of PJet700 and NC ink was made with a Dimatix Materials Printer DMP2850 from Fujifilm operating with inks filled in 10pl cartridges. This section provides the printing parameters of the inks. The most important parameters to be examined are the wave function of the jet, the frequency of the tickle, the suction of the meniscus and the cleaning cycle. The setting of the jet voltage can be done for each individual nozzle, since the drop velocity depends on it. Piezoelectric actuators send as a signal the jetting wave function, which is primarily responsible for the shape of the droplets. It is

possible that the desired droplets will not form due to incorrect setting of the wave function, which would cause no ejection or spraying.

Thanks to the tickle frequency, the ink can be kept in constant movement, thus avoiding the drying of the ink at the air/nozzle interface (and related clogging of the nozzle). Cleaning cycles (also during the printing process) are carried out to prevent clogging and are also used when dirt has accumulated around the nozzle or ink drops have formed. However, this could lead to high ink consumption. For this reason, in the thesis work, cleaning cycles were carried out before printing and, in the case of composite substrates, also in the change of the different ink. First of all, the parameters influencing the shape of the drop, the size and the speed were set, which remained sent while the jetting voltages were changed. Other parameters can be varied, such as drop spacing, plate temperature and amount of printed layers. The drop spacing, measured in dots-per-inch dpi, is responsible for the spreading of the droplet and therefore the resolution of the printed pattern. It can be controlled by manually setting the angle of the printhead. A printed pattern through the native pattern editor or by importing a bitmap, ensuring that the dpi set coincides with the drop spacing. The surface properties of the substrate on which the print is made are fundamental since the drop spacing is influenced by the overlapping of individual printed droplets, which is in turn affected by wettability. For this reason, a pre-deposition treatment such as plasma activation may be required.

Table 8-Print parameters indication for used inks: JV (Jetting voltage), Tf (Tickle frequency), MV (Meniscus vacuum), Tp (Temperature of print plate), Ds (Drop spacing).

Ink	JV	Tf	MV	Tp	Ds
PJet 700 (PEDOT:PSS)	30-35 V	5 kHz	5 inches H_2O	Ambient temperature	200 µm
NC ink	30-35 V	5 kHz	5 inches H_2O	Ambient temperature	40-200 µm

Another important parameter concerns cleaning cycle. Cleaning is important to ensure stable jetting from nozzles during the whole duration of printing of a specific pattern. The parameters of cleaning cycles, that have been performed for both inks, are listed below:

Table 9-Cleaning Cycle Editor.

Action	Time	Frequency	Post Delay
Split	500 ms	1.5 kHz	2 s
Purge	0.2 s		2 s
Split	500 ms	1.5 kHz	2 s
Blot	0.3 s		

Profilometry: thickness

Thickness was measured with a stylus profilometer AlphaStep D-500 from KLA Tencor. The profilometer was installed on top of an optical table and an anti-vibration plate from Halcyonics (Micro 40). For characterisation of the hybrid substrates, measurements were performed in three different points for each type of sample. This operation was preceded by scratching with tweezers on thin deposited films in the middle and just in two edges, aimed at assessing the coating thickness. The parameters for the different measurements have been set using the AlphaStep Development Series

software. The scanned profile length depends on the spacing of scratches, so it was varied in the range of (0.5-2) mm. The scan speed was maintened constant for all materials at 0.10 mm/s. After several tests on different substrate materials, the highest range of the instrument was kept at the value of 10 μm. A stylus force of 10 mg was applied to each investigated samples.

Optical microscopy: film homogeneity

In order to observe the uniformity of the layer deposition by means of inkjet, it was necessary to use an optical microscope. The homogeneity of the films was measured using the Olympus Dp Soft optical microscope. At least three measurements per sample were made.

Four-point-method: sheet resistance and conductivity

To the aim of measuring the sheet resistance of thin film specimen, and consequently its specific conductivity from the known thickness, a 4-point probe technique. The experimental setup consisted of four metal tips, linearly spaced of 1.5 mm. The custom four-point probe setup was connected to a Keithley 2602B multifunction sourcemeter. An auto-mechanical phase that moves up and down during measurements also includes the four metal tips. The 8×8 mm sample sheet resistance was evaluated with a current of few mA, which varied slightly depending on the sample. The current is supplied through the outer two probes. The voltage was measured across the inner two probes in oder to determinate the sample sheet resistance and thus its resistivisty. The conductivity was calculated from the measured thickness and sheet resistance values, through the Equation 3.

Cyclic voltammetry: electrochemistry

In order to evaluate the current/voltage (I/V) characteristic curve resulting from cyclic voltammetry, a three-electrode setup was employes, with gold electrodes as counter electrode and working electrode and SCE (saturated calomel electrode) as reference electrode.

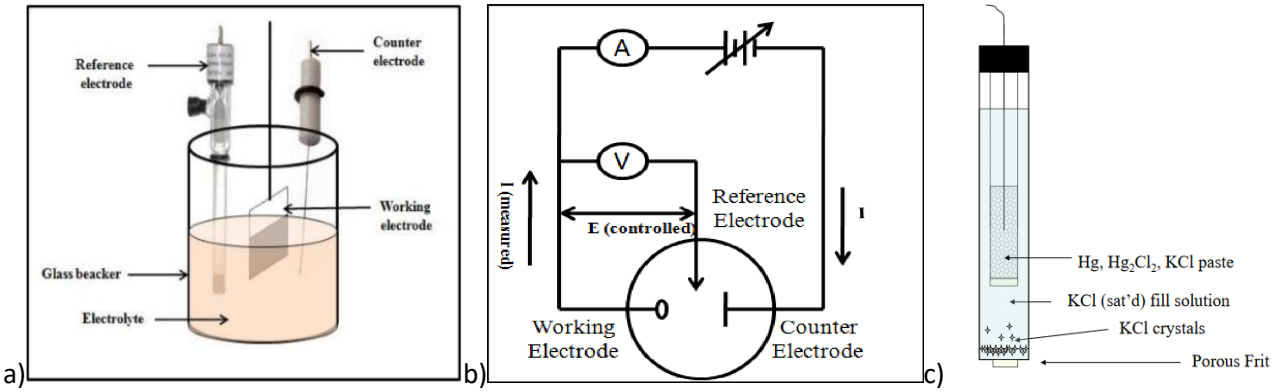

Figure 28-a) Schematic illustration of electrochemical cell (145); b) Simplified circuit for cyclic voltammetry Setup; c) Design of Saturated Calomel Electrode (SCE) (153).

Cyclic voltammetry was performed with a G 600 Potentiostat/ZRA (Gamry Instruments). All electrochemical experiments took place at room temperature. The potential is applied between the reference electrode and the working electrode and the current is measured between the working electrode and the counter electrode. Phosphate buffered saline solution (PBS), dissolved in 200 mL H_2O at pH = 6.9, was used as an electrolyte during electrochemical experiments. Cyclic voltammetry (CV) was performed at 25 mV s-1 and in the range from (-0.3) to (0.7) V,. This range was chosen

specifically to prevent hydrolysis signals (oxidation at ~-0.32 V and reduction at ~0.8 V). Other parameters used during CV measurements are shown in the table below:

Table 10-Parameters for CVs.

Parameters	**Values**
Total time	30 s
Step	0.5 s
Scan rate	25 mV/s
Step size	2 mV
Cycles	5
Initial delay	30 s
Equivalent time	10 s
Zeta potential	0

Part III
Characterisation and results

8. Printing and surface characterisation

This chapter presents the samples obtained by printing and their results in terms of surface characterization, concerning the thickness and homogeneity of the films deposited on the chosen control substrate.

8.1. Fabrication of the samples

The realization of the samples starts from the laser cutting of the film of the selected substrate and the plasma activation of the various pieces obtained. One of the parameters which have been investigated was the number of printed composite layers above the PET-ITO substrate. As seen previously, the samples manufactured for the purpose of characterization are listed below:

1. (P), PET-ITO;
2. (P-PP1), PEDOT:PSS (1 layer) on PET-ITO;
3. (P-PP2), PEDOT:PSS (2 layers) on PET-ITO;
4. (P-NC1), NANOCERIA (1 layer) on PET-ITO;
5. (P-NC2), NANOCERIA (2 layers) on PET-ITO;
6. (P-NC3), NANOCERIA (3 layers) on PET-ITO;
7. (P-PP-NC), PEDOT:PSS + NANOCERIA on PET-ITO;
8. (P-NC-PP), NANOCERIA + PEDOT:PSS on PET-ITO.

After printing, the obtained samples underwent a thermal treatment in oven at 110°C for 1h. Aim of this thermal treatment is to stabilize the PEDOT:PSS film by making it not dissolvable in water (as requested for further processing and in the final application, i.e. cell culture studies). The hybrid samples (NC+PEDOT:PSS) have only one layer of PEDOT:PSS and only one layer of NC ink. The strategy to prepare hybrid materials by subsequent printing of the two different materials was chosen after some failed attempts to obtain a composite film by direct printing of a mixture NC+PEDOT:PSS. Indeed the addition of NC dispersions (in various composition range) to the pristine PEDOT:PSS ink caused irreversible precipitation of a solid. Also in the case of hybrid films, after the deposition of the conductive polymer, heat treatment 110°C for 1h was carried out.

The samples P, P-PP1 and P-NC1 are taken as control samples for subsequent characterizations.

8.2. Profilometer measurements

For thickness measurements with the profilometer, the samples were examined as described in section 7.3. Scratches were made on each sample by means of a needle in three different positions, close to the centre. Three thickness values per sample were obtained and then averaged. The results are presented in the following graph:

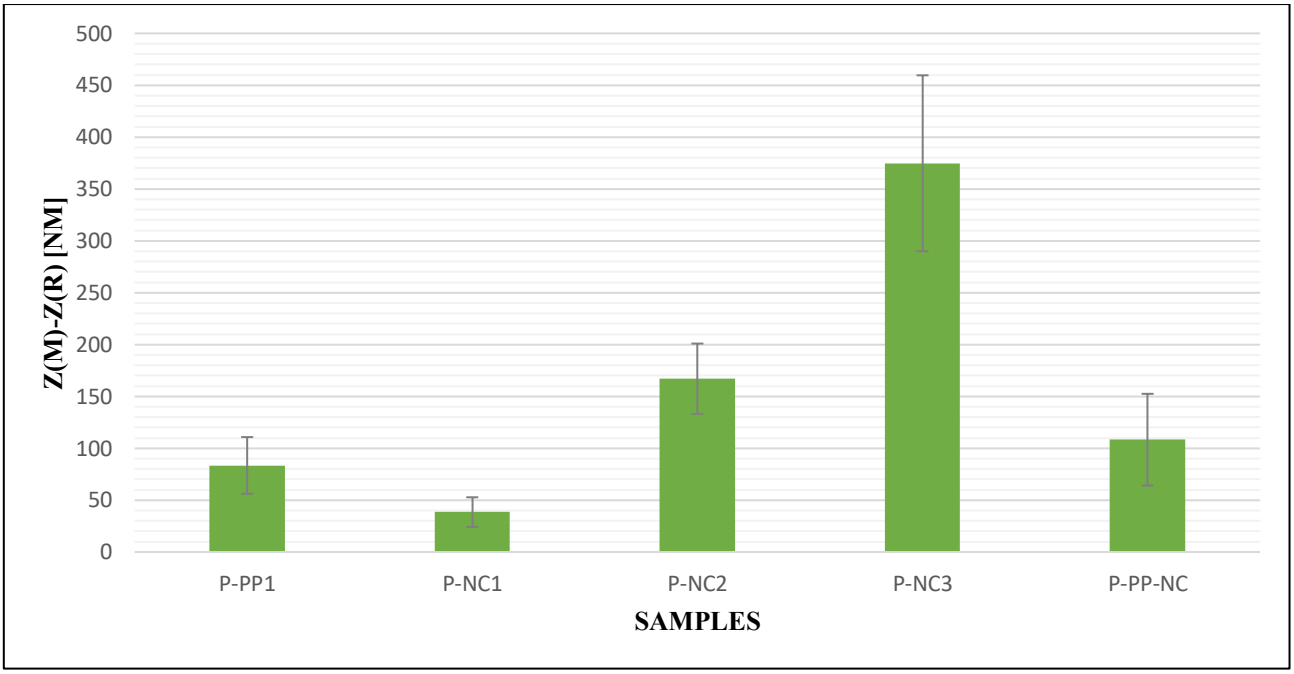

Figure 29- Thickness of ink-jet printed materials: results of profilometry analysis.

For P-NC-PP the graph was omitted because of the large thickness dishomogeinity caused by poor printing quality. As a result of this, it was decided to discard this sample.

There are enough significant observable differences. As expected, all the films prepared by ink-jet printing had a thickness in the tens-hundreds nanometer range, even if several layers were deposited. In the latter case, each layer was heat treated before the next layer was laid down. P-NC1 is thinner than the P-PP sample. Interesting is the fact that the hybrid P-PP-NC sample has a thickness that is almost the sum of the two individual thicknesses of the P-PP and P-NC1 samples, as it could be expected in this additive process, although the deviation is quite high.

Contrary to what was imagined, the histogram shows that the P-NC2 and P-NC3 samples, made up of two layers and three layers of NC ink respectively, show a high thickness, more than double the thickness of the sample consisting of a single layer of nanoceria. The cause of this effect has not been identified yet and will be the object of further investigation in future. Nevertheless, since the films obtained had a thickness in the suitable range, they were included in the study .

8.3. Optical microscope measurements

The surface characterization included the evaluation of the homogeneity of the films deposited on the P substrate. In Figure 31 the images of the various samples under the optical microscope are displayed. The samples are the same as those of the profilometry, also adding the P-NC-PP sample.

Blurring in some images is caused by shallow depth of focus at higher magnification.

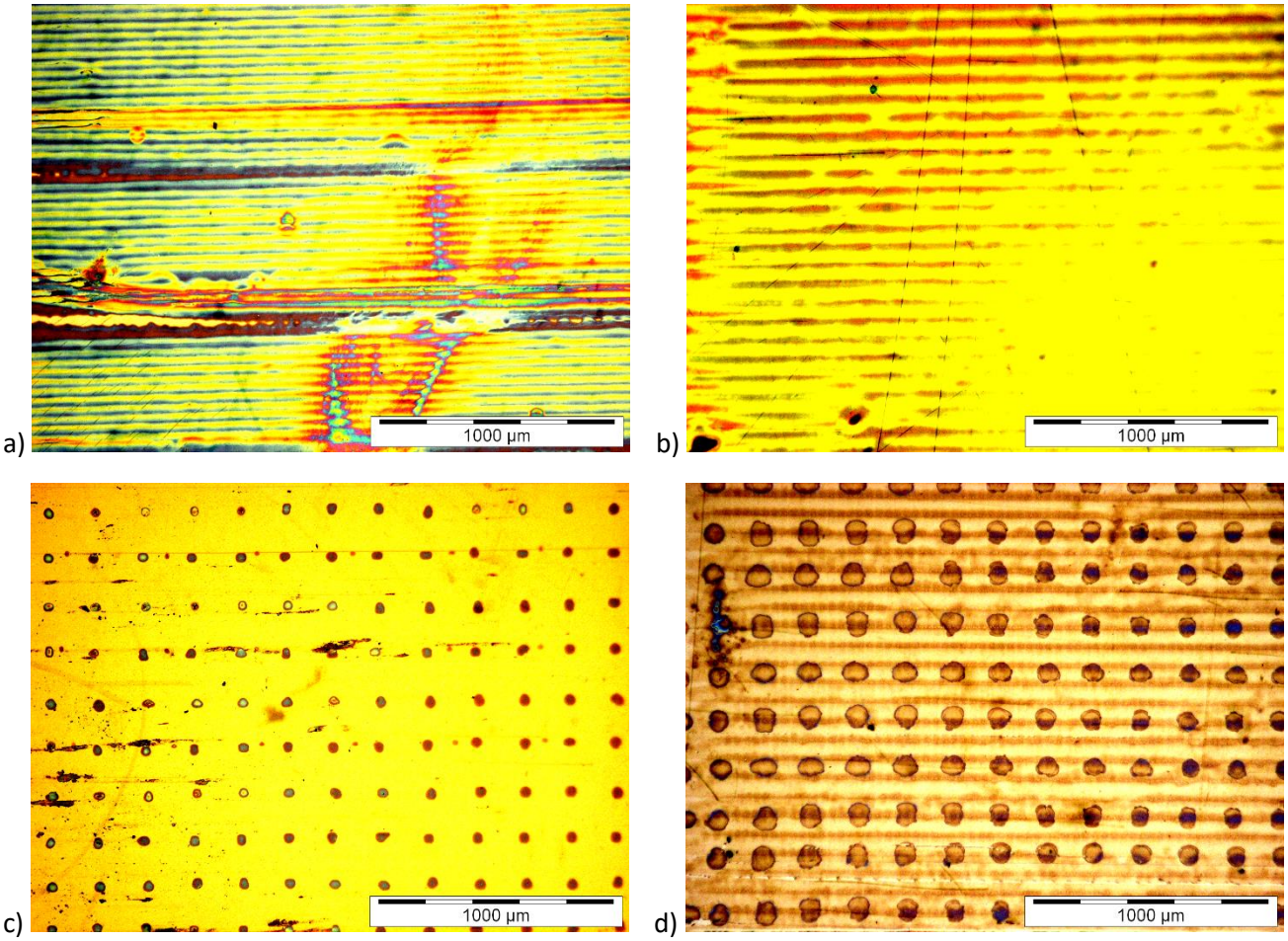

Figure 30-Optical microscope pictures of a) and b) P-NC1, c) P-NC200, d) P-PP-NC200.

Figure 31 a) is a representative image of the P-NC1 sample and is quite colorful, which is due to the interference and any scratches already present on the control substrate or deriving from the process conditions. For the rest, no obvious features are visible, except for some scratches due to the profilometric measurements. Image b) refers to sample P-NC1 and considers another region of the surface. In both a) and b) it is possible to observe lines, corresponding to the continuous printing of the ink based on nanoparticles. The images c,d) resulting from the analysis of the samples P-NC200 and P-PP-NC200, respectively (prepared with a a dot spacing of 200 µm, see Table 8) are quite interesting. In both it is possible to clearly identify individual dots (differently from continuos line, as in Figure 31 a,b), due to the jet of each single nozzle As far as sample d) is concerned, there appear to be two different morphologies: a filiform and a drop-like one. This is due to the fact that both inks (NC and PEDOT:PSS) are present together, printed with two different dpi settings. However in figure d) the NC droplets have a larger diameter with respect to c). Such broadening can be ascribed to difference in wettability and interaction of the NC ink with the PEDOT:PSS printed film.

9. Electrical characterisation

In this section the results of the electrical characterization are reported. First of all the sheet resistance of the samples has been evaluated, with the aim of comparing the conductivity of the substrate PET-ITO, PEDOT:PSS and the various materials under investigation. Then an electrochemical characterization was carried out by means of cyclic voltammetry (CV). Aim of the latter was to analyze the redox behaviour of the samples, in particular how the presence of cerium oxide nanoparticles affected the usual CV curves of PEDOT:PSS.

9.1. 4PM measurements

Depending on the obtained thickness, the resistivity (and thus its conductivity) of the various samples was calculated from the measured sheet resistance by using Equations 2 and 3. As mentioned before, the P-NC-PP samples were not included in this characterization (and no longer considered in the study) because of unsatisfactory quality of printed films (i.e. dishomogeneity, partial coating).

The following graph shows the conductivity of the samples:

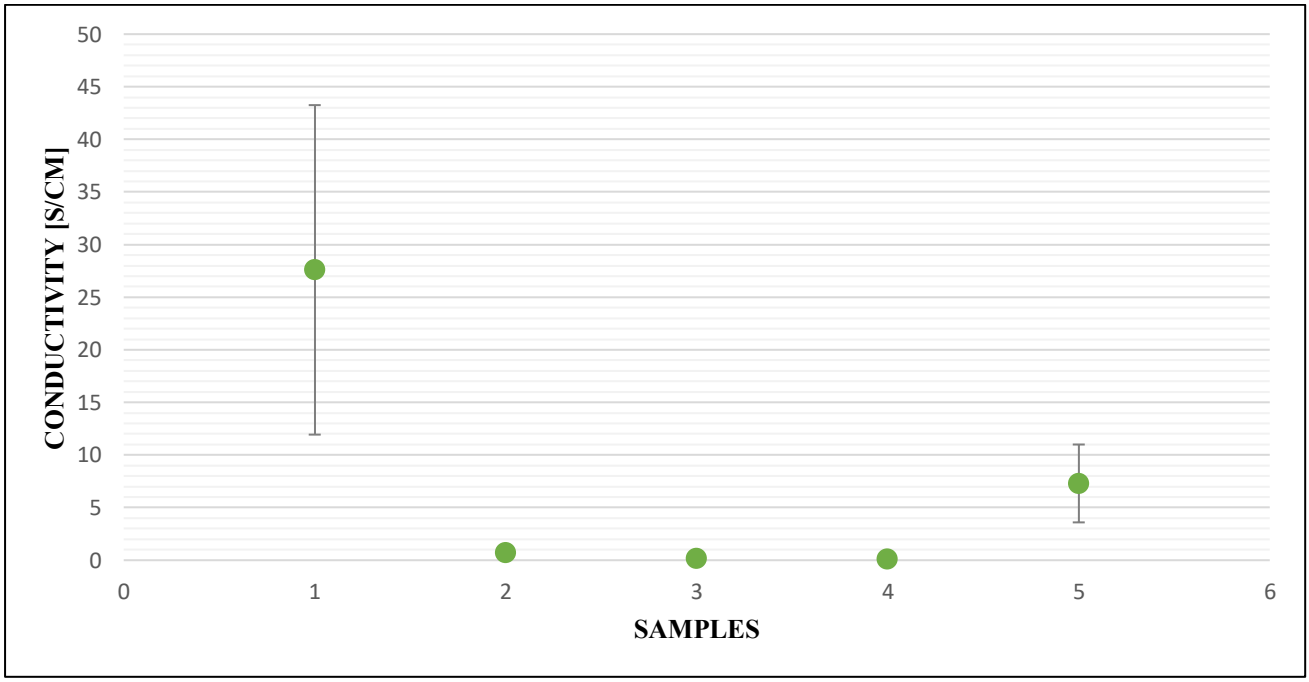

Figure 31-Results of four-probe-method measurements.

The results obtained are in line with what is expected. The P-PP1 sample shows a conductivity value similar to that found in the literature (132), with a thickness of around one hundred nanometres. Nevertheless, the uncertainty of the conductivity measurement is high. This may be due to both the ink composition and the processing conditions of the sample. The prototypes on which the NC ink is deposited have a conductivity value more than one order of magnitude lower than the P-PP1 sample. It is also noted that conductivity becomes lower and lower as the number of nanoceria layers increases, underlining an inverse proportionality between conductivity and thickness. More interesting is the

value derived from the hybrid sample. It is clear that the nanoceria dampens the high conductivity value characterizing the PEDOT:PSS without reducing it much. Observing also the thickness that has been calculated previously, it is found to be a satisfactory result.

9.2. CV measurements

The results from the cyclic voltammetry experiments are shown in Figures 33-37. The axes are not set equally for all the graphs, but they have been set in such a way as to have a better visualization. In the analysis of the sample treated only with the nanoceria, a comparison has been made with what is already present in literature in order to have a meaningful reference (154).

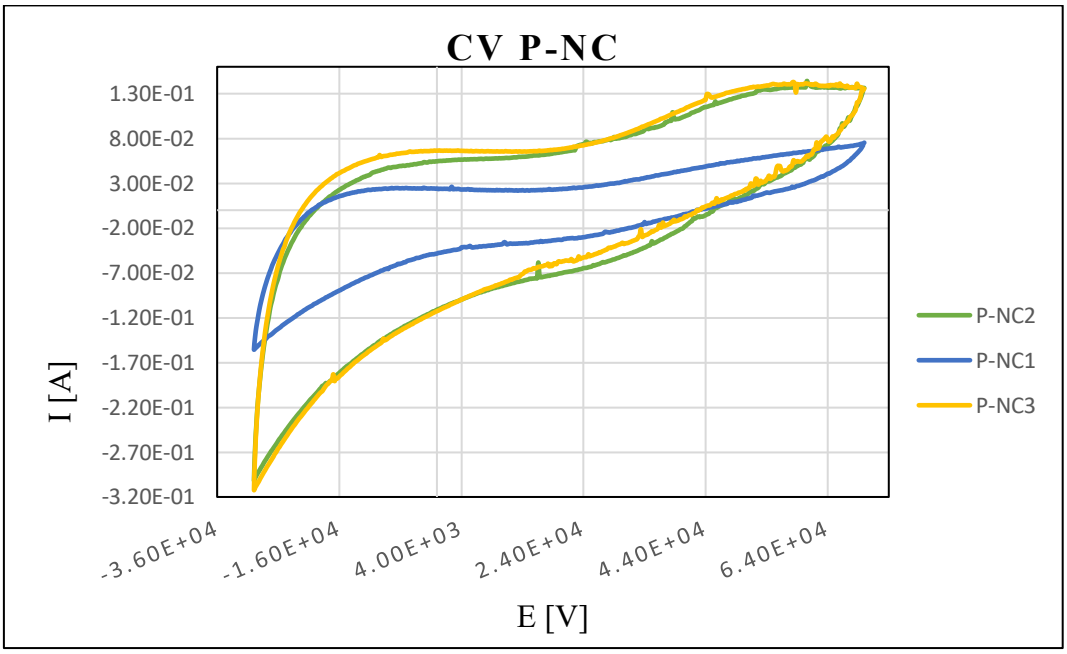

Figure 32- CV curves of P-NC sample: three consecutive scans (1-3).

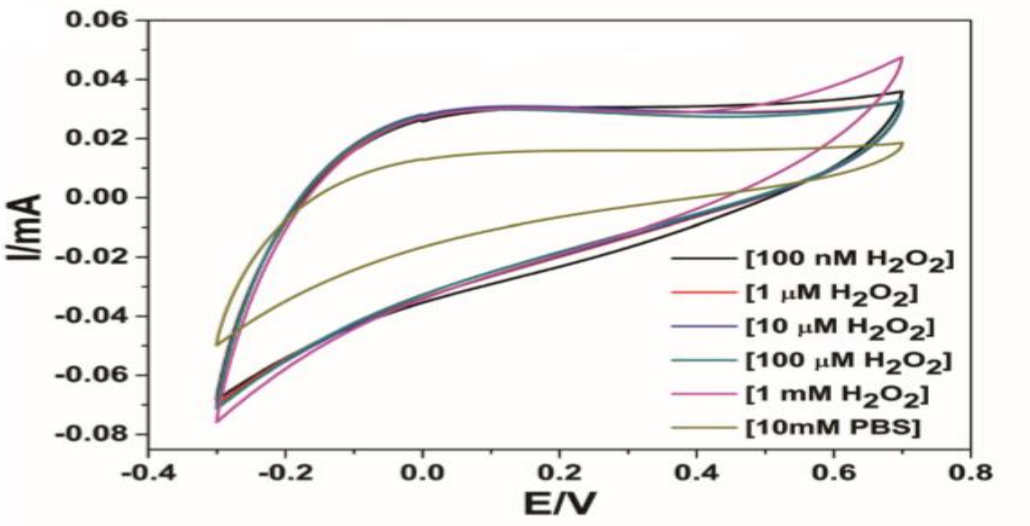

Figure 33-Cyclic voltammograms response of 200 cycles in 10 mM PBS electrolyte at 50 mV s^{-1} scan rate with varying [H_2O_2] (154).

The case presented in the literature sees the execution of cyclic voltammetry in the presence of H_2O_2, mimicking the effect of oxidating species in the biological case. Voltammetry was performed in the range of (−0.3) to (0.7) V at 50 mV s^{-1}. This interval is the same as the one chosen in the experiment done (see section 7.3). The measurements show an increase in the reduction current to −0.3 V in the presence of H_2O_2 and a positive correlation between concentration and current at this potential. This observation is supported by other results in related works and represents the reduction of peroxide groups at the CeOx surface. A similar trend is observed in the case with PBS, which is the same as that treated during the thesis project. The absence of an obvious corresponding oxidation peak suggests that this reaction is irreversible.

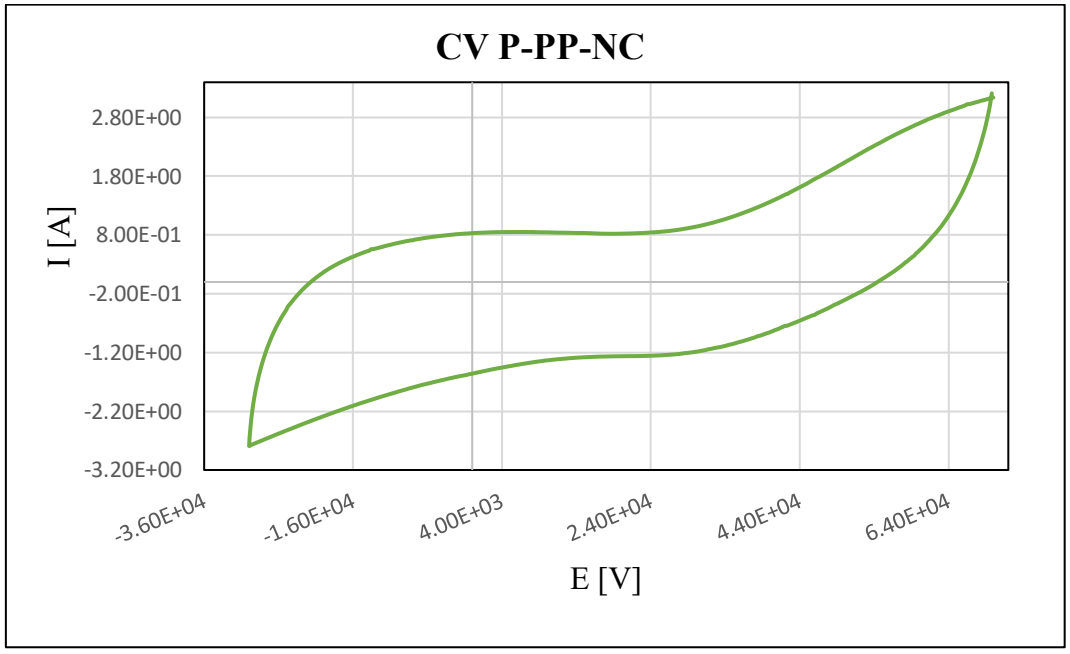

Figure 34- Cyclic voltammetry of the hybrid sample P-PP-NC (nanoceria topmost layer).

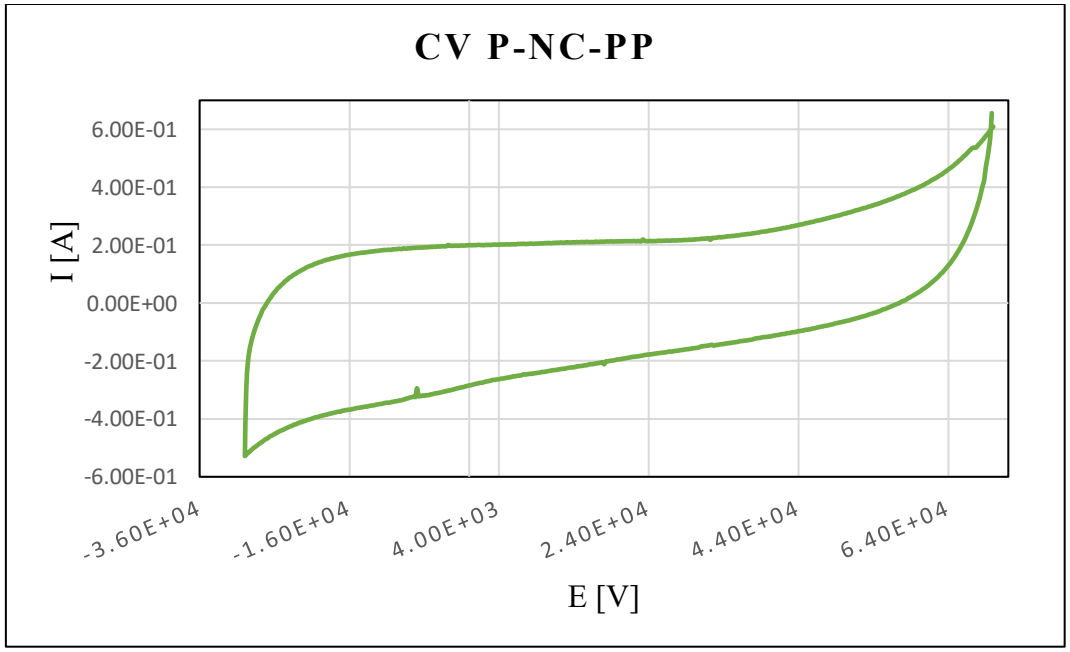

Figure 35- Cyclic voltammetry of the hybrid sample P-NC-PP (PEDOT:PSS topmost layer).

During the voltage scan, there is an exchange of electrons with the working electrode, which in turn causes a variation of the measured current which produces a peak in the voltammogram. What can be observed from Figures 35 and 36 is that the peak produced by the current occurs at the same voltage value (0.7 V) for both samples, as described in section 7.3. The peak reaches a higher value for the P-PP-NC sample. The process is reversible, given that when the voltage inversion occurs, it will reach the value that will re-oxidize (or reduce) the product formed in the first part of the scan, producing a current of opposite polarity. As desirable, the new reverse polarity peak reaches a lower value for the P-NC-PP sample. The cyclic voltammogram relating to the P-NC-PP sample is more wide-ranging and less symmetrical than that of the P-PP-NC sample.

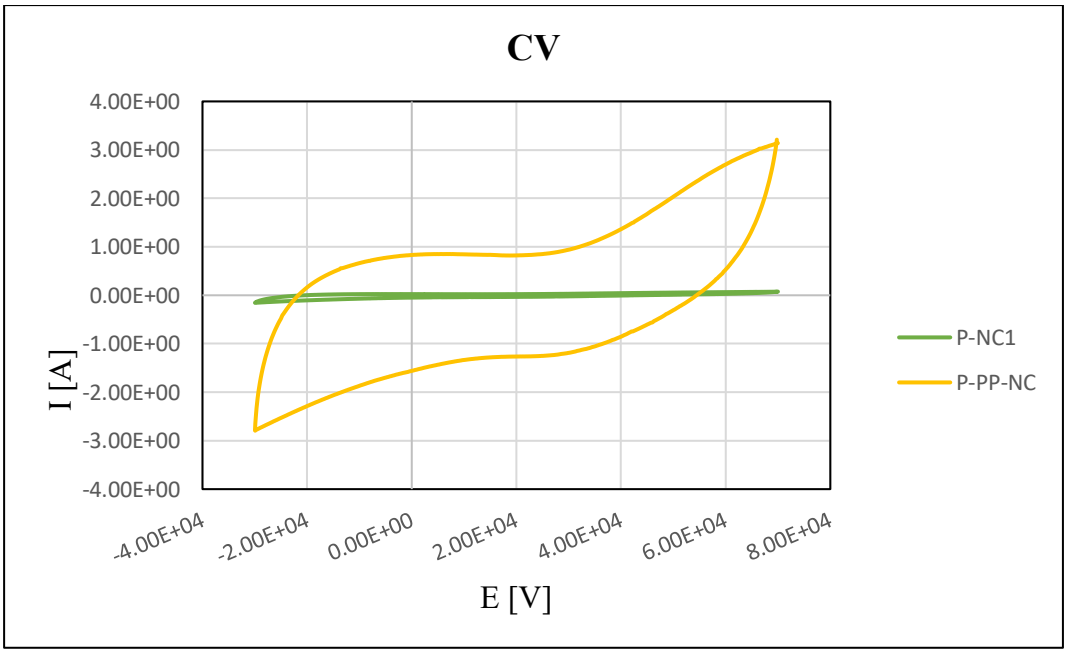

Figure 36- Comparison of CVs of the composite sample P-PP-NC and the sample with only nanoceria, P-NC1.

As can be clearly seen from Figure 37, it has been chosen to show the superposition of the two cyclic voltammograms of the samples P-NC1 and P-PP-NC. The shape of the cyclic voltammogram of the P-PP-NC sample is almost the same as that taken by the P-NC1 sample only. They differ only in the fact that the hybrid sample shows a higher peak value of the current than the other sample analyzed. This is certainly due to the interposition of the layer formed by the PEDOT: PSS.

10. Biological characterisation

The fabricated substrates were used for cell culture studies under both proliferation and differentiation. Particular attention was dedicated to the evaluation of cell response on the substrates following pro-oxidative insult. Proliferating cultures underwent analyses performed by optical microscopy (due to sample transparency) and fluorimetry techniques. Differentiating cultures instead underwent analyses performed by immunocytochemistry/optical microscopy and flow cytometry techniques. SH-SY5Y neuroblastoma cells were chosen as a neuronal model for cell culture. They are widely used in neurological experiments, including analysis of neuronal differentiation, metabolism and function related to neurodegenerative processes, neurotoxicity and neuroprotection. In this thesis, their behavior was evaluated on the following substrates:

1. PET-ITO
2. PEDOT:PSS on PET-ITO
3. NANOCERIA on PET-ITO (nominal drop spacing 30 μm)
4. NANOCERIA on PET-ITO (nominal drop spacing 200 μm)
5. PEDOT:PSS + NANOCERIA (nominal drop spacing 30 μm) on PET-ITO
6. PEDOT:PSS + NANOCERIA (nominal drop spacing 200 μm) on PET-ITO

Of the abovementioned substrates, the first four were considered as controls. For proliferating cultures, immunocytochemistry followed by optical microscopy was aimed at the evaluation of the cytoskeletal actin filaments and of cell focal adhesions. Fluorimetry analysis was conducted by using PicoGreen assay, which enabled quantification of double-stranded DNA in solution, and therefore directly correlated with cell number and proliferative capability. For differentiating cultures, immunocytochemistry followed by optical microscopy aimed at the staining of cytoskeletal beta-tubulin and to the qualitative assessment of neurite length. Flow cytometry was performed to quantify the number of cells positive to a staining specific for intracellular reactive oxygen species.

10.1. Substrate preparation for cell cultures

In order to perform biological experiments, all samples were visually inspected for defect evaluation at the optical microscope. Then, they were cut with a scalpel into 0.8 x 0.8 cm^2 pieces and the latter were anchored to the bottom of the wells of 24-well multiwell plates through pieces of an adhesive polydimethylsiloxane (PDMS) layer. This silicone layer was prepared by mixing polymer base and crosslinking agent with 20:1 ratio (w/w), by casting 10 gr of the obtained mixture on a 15 cm-diameter Petri dish, and by accelerating cross-linking through thermal treatment at 60°C for 2 h. Substrate positioning in multiwell plates was performed under biological hood, and sample sterilization was then performed by exposure to UV lamp for 20 min.

10.2. Cell culture

Once isolated from their natural tissues, cells must be maintained in physiological conditions in order to live. Cell culture is a process that allows cells to be kept alive and grown in an artificial environment (typically: Petri dishes and multiwell plates fabricated in polystyrene made hydrophilic by plasma treatment) under a culture medium, and under appropriate conditions of temperature, pH, humidity and nutrition. This technique allows the physiology and biochemistry of a given cell line to be

evaluated. Cell culture medium provides fundamental energy resources and includes compounds that regulate the life cycle of the cell.

In this thesis work, SH-SY5Y cell proliferation was obtained with culture under Dulbecco's Modified Eagle Medium: Nutrient Mixture F-12 medium (DMEM/F-12) supplemented with:

- 10% fetal bovine serum (FBS);
- 2 mM L-glutamine;
- 100 IU/ml penicillin;
- 100 µg/ml streptomycin.

DMEM/F-12 is commonly used as a basal medium, which contains glucose as the main source of energy for cellular metabolism. DMEM/F-12 uses sodium bicarbonate buffer system (3.7 g/L) and requires a 5-10% CO_2 environment to maintain the neutral pH during culture. It also contains a pH indicator, phenol red, which enables visual monitoring of cultures by color shifts: based on the metabolic activity of the cells, it can exhibit either a yellow color corresponding to acidic pH, or a violet color corresponding to alkaline pH. FBS is the most used animal serum, containing hormones, vitamins, embryonic growth factors, and inorganic minerals. L-glutamine is an amino acid involved in protein synthesis and is an energy source through the Krebs cycle along with glucose and pyruvate. It is necessary for cell growth, but not stable. Penicillin and streptomycin are antibiotics used to prevent bacterial contaminations.

SH-SY5Y cells were routinely cultured as follows. First of all, cell suspensions (containing less than 1 million cells) stored in liquid nitrogen were thawed at room temperature, transferred from 2 ml cryovials to 15 ml centrifugation tubes where they were added with 6 ml of complete proliferation medium, and then centrifuged at 700 g for 5 min. The supernatant was discarded, and then the cell pellet was resuspended in 1 ml of cell culture medium. Cells were seeded in a 10 cm-diameter Petri dish pre-filled with 10 ml of medium. At 48 h from thawing, SH-SY5Y cells were ready for subculture on the experimental substrates.

Before starting any manipulation of the cells, both native and coated substrates were pre-conditioned with cell culture medium in order to favor cell adhesion: the samples were indeed incubated with 500 µl of cell culture medium at 37°C for 1 h in a 5% CO_2, saturated-humidity atmosphere. Thereafter, cell culture medium was refreshed and cell subculture started with the procedures described in the following.

First of all, cell culture medium was removed and transferred to an empty 15 ml tube. Cell were thus rinsed with Dulbecco's phosphate-buffered saline (DPBS) to remove any traces of serum, and then their delamination from Petri dishes was induced by incubation with a 0.05% trypsin-EDTA solution at 37°C for 2 min. Trypsinization was stopped by addition of exhausted cell culture medium. Cells were then centrifuged at 700 g for 5 min and cell pellet was resuspended in 1 ml of cell culture medium.

The cells were then observed and counted under the inverted fluorescence microscope with the help of a Bürker chamber. To this purpose, 10 µl of cell suspension were positioned by precision micropipette inside the chamber covered with cover glass, and the cells were counted in a square grid comprising 16 smaller squares engraved on the bottom of the chamber. This number was then multiplied by the fixed dilution factor of 10,000, and a volume adequate to a seeding with cell density of 4,500 cells/cm^2 was withdrawn from the suspension. This volume was adjusted by dilution with cell culture medium in order to dispense 200 µl of cell suspension in each well of the multiwell plate. After seeding, the cultures were again positioned in the incubator set at 37°C and with 5% CO_2 atmosphere.

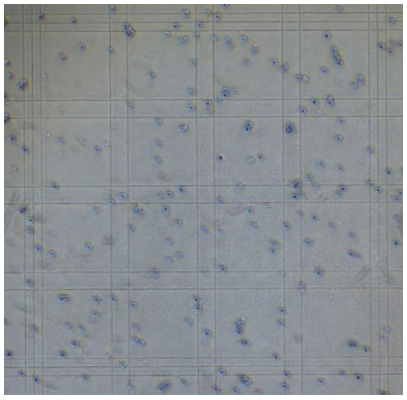

Figure 37-Cell count on the Bürker chamber.

At day 3 from seeding, cell differentiation was induced by administration of a cell culture medium composed by DMEM supplemented with

- 1% FBS;
- 2 mM L-glutamine;
- 100 IU/ml penicillin;
- 100 µg/ml streptomycin;
- 10 µM all-trans-retinoic acid.

Cell differentiation was allowed for 3 dd before performing oxidative stress tests 1) in a pilot experiment with increasing concentrations of a pro-oxidant reagent administered to cells adherent to traditional cell culture plastic and 2) in an experiment with three selected concentrations of the same reagent administered to cultures adherent to the PET-ITO based substrates.

10.3. Cell proliferation analysis: PicoGreen assay

To evaluate any possible toxic effects of the substrates on the cell cultures during proliferation, Quant-iT™ PicoGreen® dsDNA assay was performed. This assay is used in many biological applications for detecting and quantitating double-stranded DNA (dsDNA) in solution. Quant-iT™ PicoGreen® dsDNA reagent is an ultra sensitive fluorescent nucleic acid stain. It is a tertiary amine, a member of quinolines, a member of benzothiazoles and a cyanine dye (155).

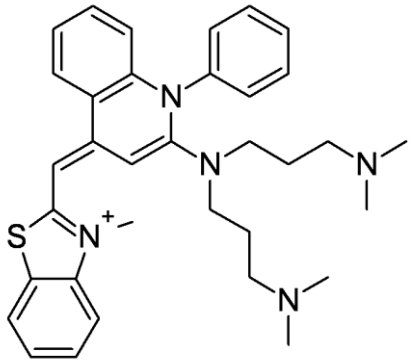

Figure 38-PicoGreen dye structure.

The assay was carried out on samples obtained by two independent experimental runs by taking into consideration two time points: 3 and 6 dd from seeding and maintenance under proliferation cell culture medium.

First of all, the cell culture medium was removed and discarded. 500 µl of DPBS w/o calcium and magnesium was thus placed in each well for washing: two rinses were performed to remove any residues (such as bovine serum) that are known to interfere with the assay. Samples were transferred to low-absorption microcentrifuge tubes (Eppendorf LoBind, 0.5 ml), previously filled with 500 µl of ultrapure sterile water for cell lysis by osmotic rupture. The tubes were then stored at -20°C until time of analysis.
To ensure full disruption of cell and nuclear membranes, samples underwent three freeze-thaw cycles followed by ultrasonication for 10 min. Cell lysates and reagents from the assay kit were then mixed in wells of a black 96-well plate by following the protocol detailed below.

- A 1X TE working solution was prepared by performing a 1:20 v/v dilution of the concentrated buffer in water to a final volume of 200 µl. 100 µl were manually dispensed (for each sample in duplicate) in the 96-well multiwell plate.
- 50 µl of cell lysate were then manually dispensed in each well of the black multiwell plate;
- An 1X working solution of the Quant-iT™ PicoGreen® reagent was prepared in a tray by performing a 1:200 v/v dilution of the concentrated DMSO solution in 1X TE to a final volume of 300 µl. 100 µl of PicoGreen solution were then added with the aid of a multichannel precision pipette.
- The 96-well black plate, coated with aluminum foil to protect the solution from light (the PicoGreen reagent is sensitive to photodegradation), was kept on an orbital shaker for 10 min.
- Fluorescence was detected with Victor X3 plate reader: excitation wavelength was 480 mn, and emission wavelength was 520 nm.

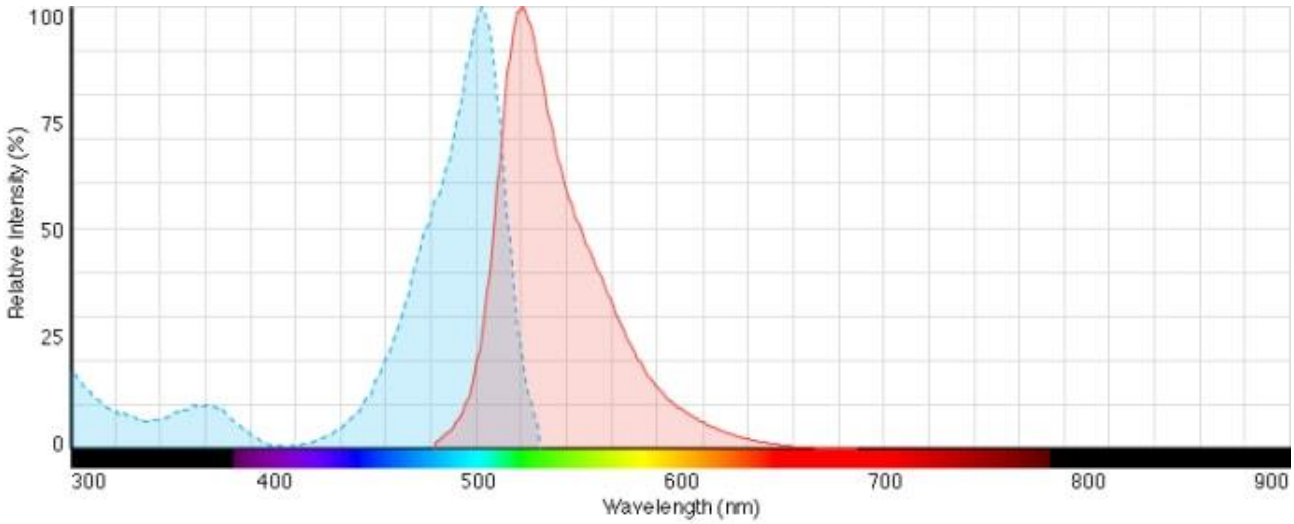

Figure 39-Excitation (blue) and emission (red) spectra of PicoGreen Reagent (155).

10.4. Cell differentiation analysis: immunostaining of β3-tubulin

Cell morphology was analyzed after 3 and 6 dd from differentiation induction by immunocytochemistry, followed by fluorescence microscopy. To this purpose, the cell culture medium was removed, and the cells were rinsed with DPBS and fixed with a 4% formaldehyde solution in DPBS for 20 min at 4°C. Fixative solution was then removed and permeabilization of the cell membrane was performed with a 0.1% Triton X100 solution in DPBS for 15 min. Incubation with a 10% goat serum solution in DPBS was then performed for 1 h at 37°C in order to saturate aspecific binding sites for antibodies. Samples were then incubated with a β3-tubulin rabbit IgG antibody solution (1:75 diluted in 10% goat serum) for 1 h at 37°C, and then rinsed with DPBS four times for removal of unbound primary antibodies. Tubulin is a constituent of cytoskeletal microtubules, and undergoes high expression in mature neurons. Samples were incubated with a solution containing Alexa Fluor 488-IgG anti-rabbit secondary antibody (1:200 diluted in 10% goat serum) and 2 µg/ml Hoechst 33342 dye for nuclei staining for 45 min at room temperature. Alexa Fluor 488 dye is a bright, green-fluorescent dye that has an excitation peak at 488 nm and a maximum emission at 525 nm.

Finally, two DPBS washes were performed, then the samples were observed and imaged through a Nikon TiE Inverted Microscope.

10.5. Flow cytometry

Flow cytometry was performed to verify if the different substrates could exert a protective role on cell cultures against an oxidative stress applied by administration of a pro-oxidant agent. Oxidative stress typically results from an imbalance between the production of ROS and the ability of cells to scavenge them. In this thesis work, oxidative stress was obtained through tert-butyl hydroperoxide (tBH), that causes an increment of reactive oxygen species, resulting in subsequent alteration of membrane lipids, proteins, and nucleic acids. Tert-butyl hydroperoxide (tBH) is an alkyl hydroperoxide in which the

alkyl group is tert-butyl. It is a watery odorless colorless liquid, used in many oxidation processes as an antibacterial agent and an oxidising agent (156).

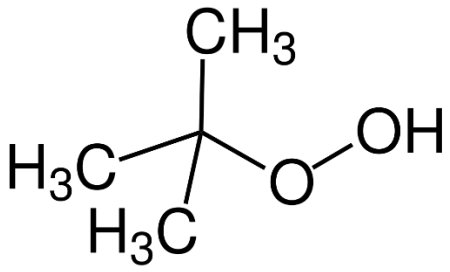

Figure 40-Chemical structure of tBH.

First, a pilot experiment was conducted with a large range of concentrations of pro-oxidant agent administered to cultures adherent to the different experimental substrates. This was done to identify sublethal concentrations of tBH for simulating both short-term and long-term oxidative stress conditions. After oxidative stress induction, cell were stained with CellROX Green reagent. It belongs to a class of fluorogenic probes used for measuring reactive oxygen species (ROS) in live cells. The cell-permeable reagents are very weakly fluorescent in a reduced state and exhibit bright green photostable fluorescence upon oxidation by ROS, subsequently binding DNA in the nucleus and mitochondria. The fluorescent cells stained with CellROX Green can be quantified by using flow cytometry.

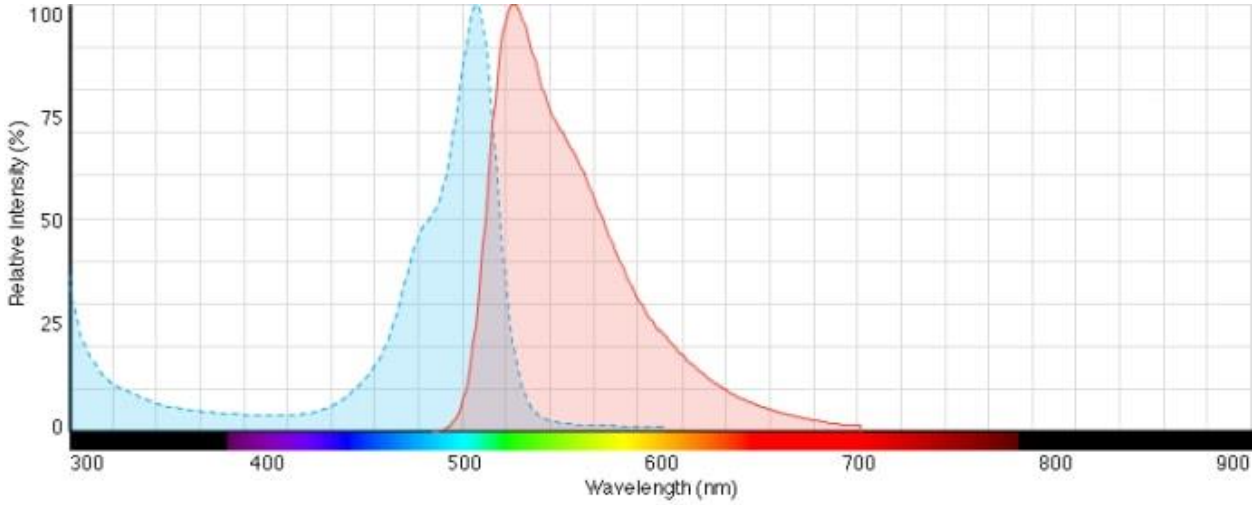

Figure 41-Fluorescence excitation and emission spectra of oxidized CellROX® Green Reagent.

For this experiment, SH-SY5Y were seeded at a density of 10,000 cells/cm^2 in 24-well multiwell plates. At 72 h from seeding, cell differentiation was induced by administration of 700 µl of differentiating medium in each well. The cultures were then incubated at 37°C and 5% CO_2 for three days. Oxidative stress conditions were applied by removing the cell culture medium and by supplying the cultures with 500 µl of fresh solutions with increasing concentrations of tBH. Cell culture medium composition is detailed in Table 11.

Table 11-volumes of reagents used to prepare cell culture media added with increasing concentrations of tert-butylhydroperoxide-tBH. P/S stands for "penicillin-streptomycin" solution.

[tBH]	L-Glutamine	P/S	FBS	tBH	DMEM
0 µM	70 µl	70 µl	70 µl	-	6790 µl
20 µM	70 µl	70 µl	70 µl	280 µl (Sol. B)	6510 µl
50 µM	70 µl	70 µl	70 µl	700 µl (Sol. B)	6090 µl
100 µM	70 µl	70 µl	70 µl	1.4 ml (Sol. B)	5390 µl
500 µM	70 µl	70 µl	70 µl	3.5 µl (Sol. A)	6786.5 µl
1000 µM	70 µl	70 µl	70 µl	7 µl (Sol. A)	6783 µl

Solution A was obtained by mixing 10 µl of tBH with 67 µl of high glucose DMEM to have 1M, as tBH has an initial concentration of 7.7 M (1:7.7 dilution). Solution B was obtained by mixing 1.5 µl of tBH with 2998.5 µl of high glucose DMEM to have a final concentration of 500 µM (1:2000 diluition).

Each experimental condition was evaluated by pooling the content of four wells of a 24-well multiwell plate. After 1, 4 and 8 h of incubation with pro-oxidant, the cultures were stained with CellROX Green dye as described in the following. First, the supernatant was collected in 15 ml tubes. Cell were rinsed with 500 µl of PBS without calcium and magnesium for each well and PBS was collected in the tubes to ensure maximum cell recovery. Each well was administered with 200 µl of trypsin solution and the 24-wells plates were incubated for 2 min. Trypsin was aspirated and transferred to the tubes, then the wells were rinsed with 500 µl of PBS, which was also recovered. 1 ml of proliferation medium was added in the tubes to stop the action of trypsin. The cells were then centrifuged at 1,000 g for 7 min at 4°C and resuspended in 300 µl of PBS with calcium and magnesium. A small volume of cell suspension (100 µl) was used to read "blank" at the flow cytometer. During flow cytometry, the tubes containing cell suspensions were sitting on ice. 160 µl of cell suspension were incubated for 15 min at room temperature in the dark with 40 µl of CellROX Green prediluted a hundred times in PBS with calcium and magnesium, in order to reach a final dye concentration of 5 µM. Again, cells were sitting on ice during flow cytometry runs. At each step, pipetting was carefully counted and repeated for each experimental class. The tubes were vortexed for a few seconds before being placed in the flow cytometer. After each counting, a washing cycle was carried out using a tube containing only water.

Based on the results achieved with the pilot experiment, cell cultures were repeated on the different experimental substrates by administering cell culture media with three selected concentrations of tBH (0, 100 and 1000 µM) and by performing flow cytometry at 6 h from oxidative stress induction.

11. Biological responses

This chapter provides and discusses the results achieved upon culture of a selected neuronal model on the substrates fabricated for this experimental thesis work. Biological responses were assessed during both proliferation and differentiation. The ultimate goal is to verify possible protective effects exerted by the substrates on cells from oxidizing insults.

All tests were performed with the experimental configuration reported in Figure 43, that shows 24-well multiwell plates containing transparent substrates anchored to the well bottom through a thin PDMS layer, and covered by cell culture medium characterized by pinkish color due to phenol red.

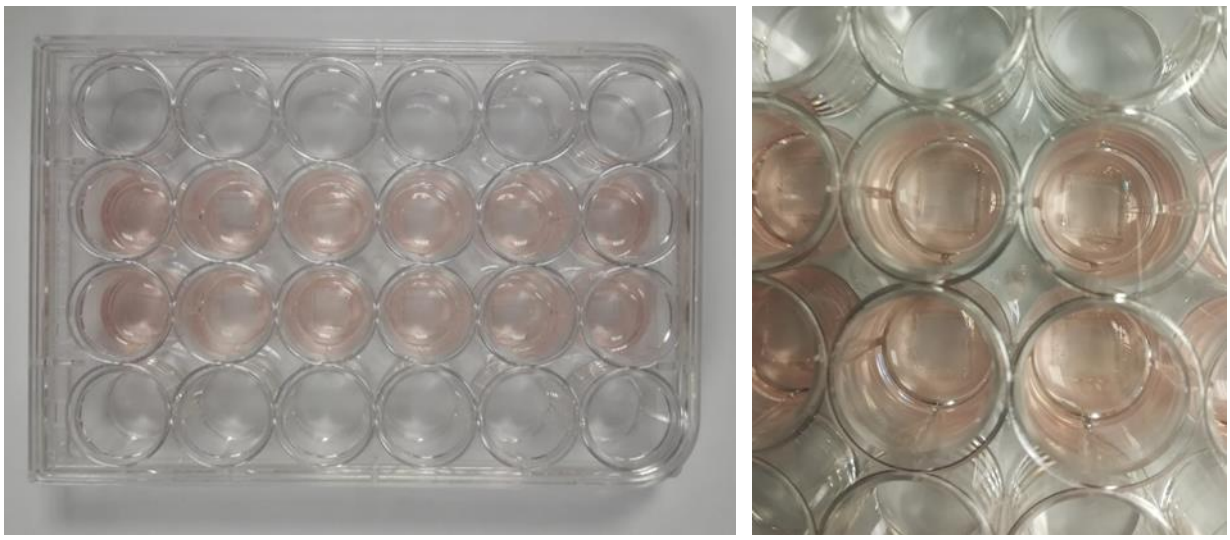

Figure 42-24-well multiwell plates containing the tested samples anchored through PDMS layer.

11.1. Cell proliferation results: PicoGreen assay

The results of the PicoGreen assay are reported as histograms in Figure 44, enabling comparisons of the cellular responses to five substrate typologies at two different time points (3 days and 6 days). In the following, samples will be identified shortly as:

- (P), PET-ITO used as control;
- (P-PP), PEDOT:PSS on PET-ITO;
- (P-NC30), NC30 on PET-ITO;
- (P-PP-NC30), PEDOT:PSS + NC30 on PET-ITO;
- (P-PP-NC200), PEDOT:PSS + NC200 on PET-ITO.

The experiment was repeated under the same conditions twice, by considering two different cell densities. The statistical analysis was carried out on several samples of the same day. The histogram on top of Figure 24 shows the results obtained from the first test, which was performed by seeding 4,500 cells/cm^2. The histogram below shows the results of the second experiment, in which cells were seeded on the different substrates at a density of 10,000 cells/cm^2. The absorbance values shown on

the y-axis were derived from the measurement of light with a wavelength of 485 nm that was absorbed by each sample.

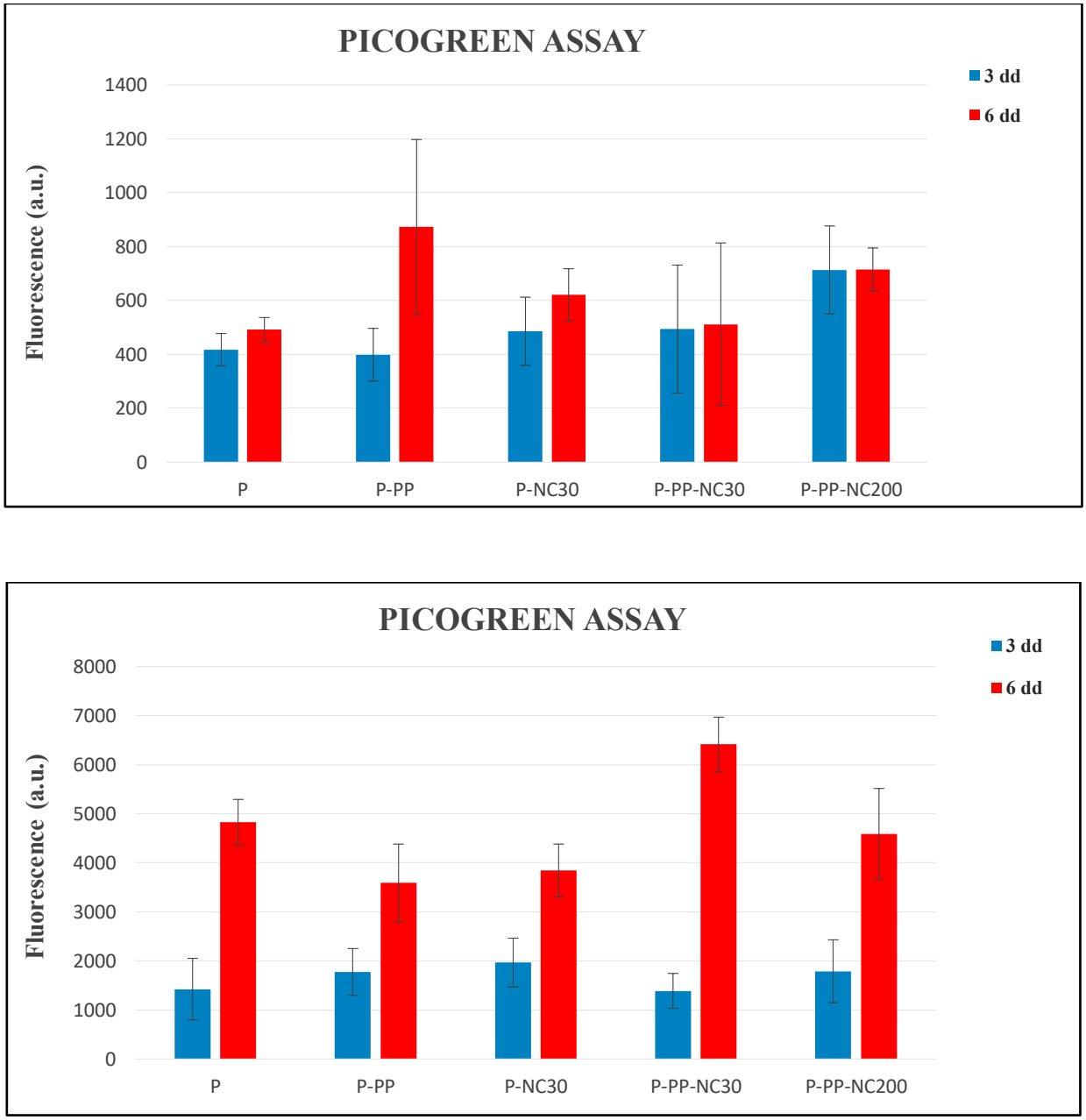

Figure 43-Results of Pico Green Assay, considering 4,500 cells/cm2 (top histogram) and 10,000 cells/cm2 (bottom histogram).

At low cell density (4,500 cells/cm^2), the fluorescence values were comparable on all substrates after 3 days of culture. The fluorescence values remained nearly constant and comparable among substrates after 6 days of culture, denoting limited SH-SY5Y cell proliferation capability. At higher cell density (10,000 cells/cm^2), the fluorescence values were again comparable on all substrates after 3 days of culture, whereas they increased after 6 days of culture, suggesting cell number doubling. In the case of cultures on P-PP-NC30 substrates, the fluorescence value seems to be even higher than that one obtained on the control substrate for reasons yet to be ascertained. In consideration of the results

achieved at the end of the second experiments, the comparable results achieved at the end of the first experiment on all substrates at both time points can therefore exclusively be ascribed to the low cell density.

11.2. Cell differentiation results: immunostaining of β-3 tubulin

Representative images of SH-SY5Y cell cultures on the different substrates at different time points from differentiation induction (3 and 6 days) are reported in Figure 45. These images were obtained by using a fluorescence microscope and were made comparable in terms of intensity and contrast with the aid of ImageJ software. All images show high cell adhesion to the substrates, and regular emission of neurites which are markers of cell differentiation. Some images demonstrate the presence of diffuse, aspecific fluorescence associated to the staining with Hoechst dye, which may be partially ascribed to an undesired contamination of the staining solution but also to partial sample degradation upon detachment from the PDMS adhesive layer for inversion during imaging procedures. Further investigations in this concern are therefore under way, as well as the elaboration of strategies for optimizing film deposition and interlayer adhesion.

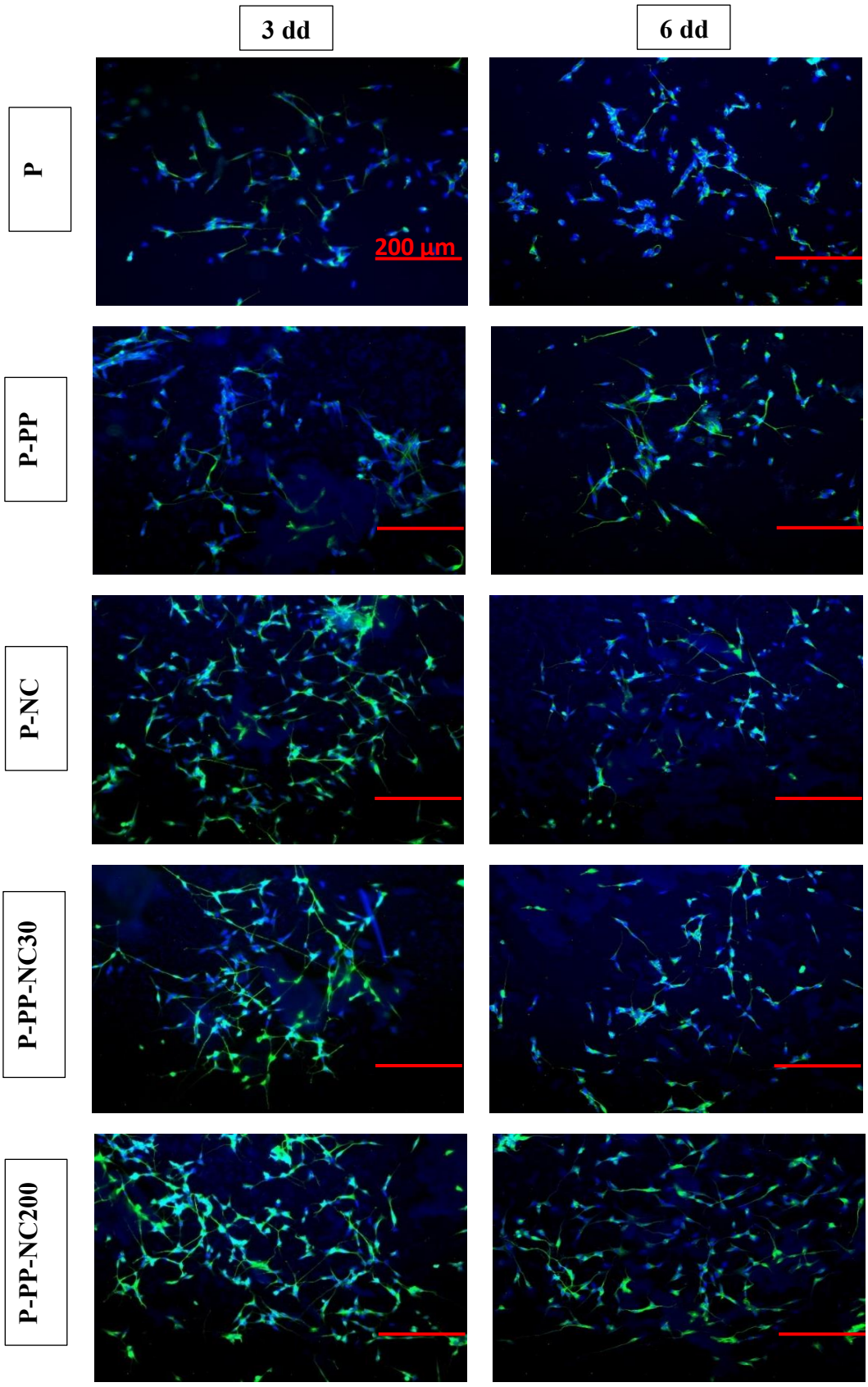

Figure 44-Representative images of fluorescence microscopy performed on fixed cultures at different time points from differentiation induction (3 dd on the left and at 6 dd on the right): β-3 tubulin is visible in green and nuclei in blue.

11.3. Flow cytometry results

As described in section 10.4, a pilot experiment was carried out with different concentrations of a pro-oxidant agent supplied to SH-SY5Y cells cultured on the different experimental substrates in order to test their protective antioxidant effect. Figure 26 reports the plots obtained for each sample after 1, 4 and 8 h from pro-oxidant reagent administration to the cultures pre-differentiated for 3 days.

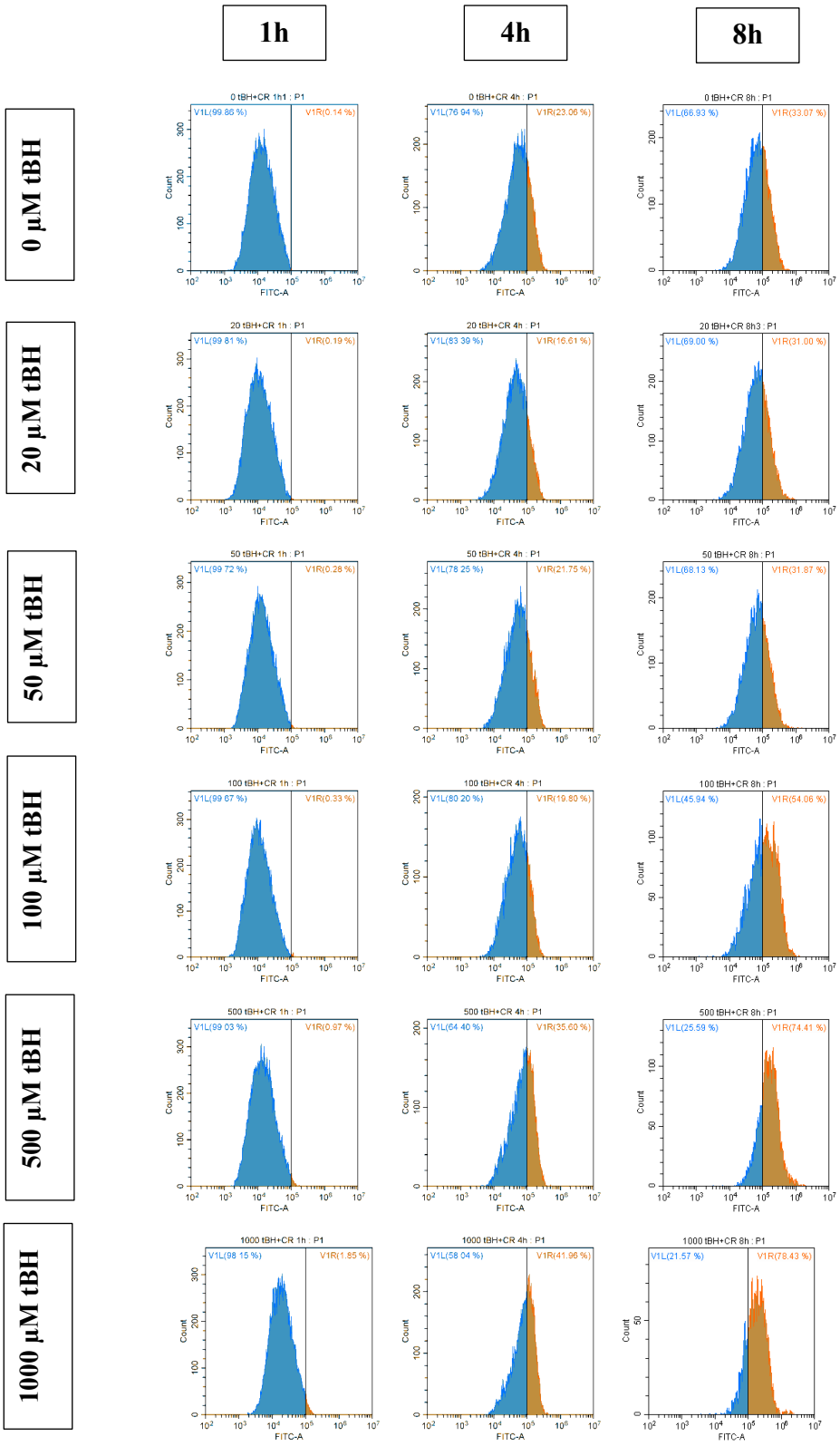

Figure 45- Curves obtained by flow cytometry at different time intervals, that is 1h (first column), 4h (second column) and 8h (third column) since administration of different tBH concentrations (0 µM, 20 µM, 50 µM, 100 µM, 500 µM, 1000 µM) to 3 dd-differentiated cell cultures.

Table 12-V1R: percentages of ROS relating to the curves obtained by flow cytometry.

	1 h	4 h	8 h
0 µM	0.14	23.06	33.07
20 µM	0.19	16.61	31.00
50 µM	0.28	21.75	31.87
100 µM	0.33	19.80	54.06
500 µM	0.97	35.60	74.41
1000 µM	1.85	41.96	78.43

In each diagram, a threshold line was manually set to 10^5 based on the results achieved for cultures on the control substrates untreated with tBH, upon staining with CellROX dye. On the left of this threshold line, there are cells considered to be negative for CellROX dye staining, whereas on the right there are those considered to be positive. As clearly reported in Table 12, the percentage of CellROX dye-positive cells increased with incubation times. The percentage of CellROX dye-positive cells instead clearly increased only when tBH concentrations exceeded 100 µM, reaching >40% after 4 h of incubation and ~80% after 8 h of incubation with the highest tBH concentration tested. Unexpectedly, increasing values of CellROX dye-positive cells were found at 0 µM tBH over time, suggesting a significant increase in the basal ROS levels of SH-SY5Y cells: this may be explained by taking into consideration that the differentiation medium was deprived of retinoic acid for the oxidative insult experiment. Up to 50 µM tBH, it therefore seems that retinoic acid deprivation may have played a more significant role in the culture oxidative stress conditions than tBH addition.

Based on these results, another experiment was conducted with the same cell model on the substrates fabricated during this thesis work. For the sake of simplicity, only one time point was considered after tBH administration, that is 6 h. The pro-oxidant reagent concentrations were 0 µM and 100 µM. The experiment was performed on 6 substrate typologies, by taking into consideration also an additional substrate for the sake of completeness: NC200 on PET-ITO (P-NC200). Figure 47 reports the curves obtained for both unstained and CellROX dye-stained cultures whereas Table 13 reports the percentages of cells either negative or positive to staining.

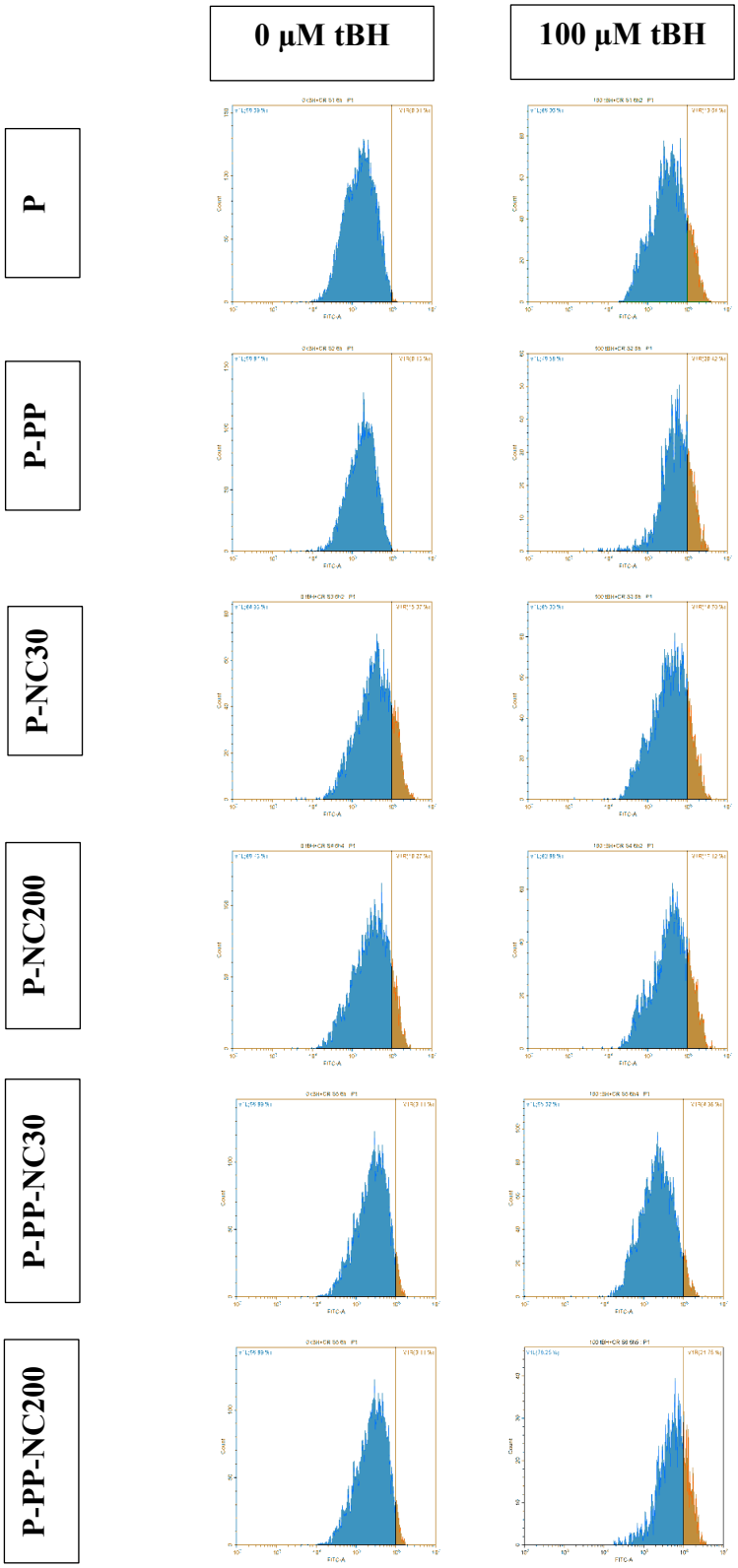

Figure 46-Curves obtained by flow cytometry at 6 h from administration of 100 µM tBH to 3 dd-differentiated cell cultures on different experimental samples.

Table 13-V1R: percentages of ROS relating to the curves obtained by flow cytometry at 6h.

	P	P-PP	P-NC30	P-NC200	P-PP-NC30	P-PP-NC200
0 µM	0.31	0.13	15.07	10.27	3.11	2.27
100 µM	13.64	20.42	14.70	17.12	4.38	21.75

In this experiment, the threshold line was manually set at 10^6. Negligible percentages of CellROX dye-positive cells were found for the cell cultured on the control substrates represented by plain PET-ITO and PET-ITO + PEDOT:PSS in the absence of a pro-oxidant insult. Slightly higher percentages were found for the cells cultured on multilayered substrates, whereas the highest concentrations were found on substrates with nanoceria ink-jet printed on plain PET-ITO. This seems to suggest mild oxidative stress induced by the latter substrates, and complex effects of multilayered substrates. When tBH was administered, the multilayered substrate with minimal nanoceria spacing instead seemed to protect cells from oxidative stress, unlike the one with maximal nanoceria spacing, that demonstrated a percentage of CellROX dye-positive cells comparable to all of the other substrates. This seems to suggest that density of antioxidant nanoparticles on the surface of the substrates may play an important role in scavenging of reactive oxygen species, and how this parameter should be carefully tuned to ensure maximal cell protection against mild oxidative stress. The results achieved on plain PET-ITO substrate at the end of this experimental run seem to be in disagreement with the ones obtained on regular PS substrates at the end of the previous experimental run, in particular as far as percentages of CellROX dye-positive cells: for this reason, both experiments will be repeated in the future.

Part IV
Summary, conclusion and outlook

12. Summary

The ultimate aim of this thesis was to create composite multifunctional printed interfaces based on conductive polymer and cerium oxide nanoparticles for the regeneration of peripheral nervous tissue. Therefore, different materials and printing strategies were considered. Surface and electrical characterization permitted to identify and select materials to be tested in susbsequent cell culture studies with neuronal cell models. Biological responses were assessed during both proliferation and differentiation. The ultimate goal of the cell culture studies was to verify possible protective effects exerted by the substrates on cells from oxidizing insults. in both proliferative and differentiating conditions.

First of all, the two inks based on PEDOT:PSS and nanoceria were created for inkjet printing for subsequent deposition on the PET-ITO substrate. Composite hybrid films (PEDOT:PSS+Nanoceria) were fabricated by sequential deposition of the two different inks in various combinations: variation in number of printed layers, printing resolution/spacing of printed droplets (and related composition), nature of topmost layer.

Thickness and homogeneity of the printed materials were then assessed by means of stylus profilometry and optical microscopy, while the electrical properties (namely, conductivity). were analysed by means of a 4 point probe technique. . The redox properties of the created systems were also studied through Cyclic Voltammetry, comparing the results of the two composite samples with the individual PEDOT:PSS and nanoceria curves.

The biological characterization of the substrates included a proliferative analysis at two different cell densities and an immunostaining analysis under differentiation conditions. A preliminary flow cytometry experiment was also conducted to observe the ability of the substrates to exercise a protective role against oxidative stress, administered to cell cultures by means of a prooxidant agent.

13. Conclusion and outlook

In order to provide topographical and electrical stimuli for the regeneration of the peripheral nervous system, hybrid biointerfaces have been developed using the inkjet printing technique. The aim was to create these innovative multifunctional biointerfaces capable of stimulating neuroregeneration by exploiting topographic and antioxidant signals, the latter obtained by doping the structures with cerium oxide nanoparticles. The topographical, antioxidant and pro-regenerative effects of scaffolding have been studied on neuron-like SH-SY5Y cell cultures.

The surface and electrochemical characterizations have brought to light fairly satisfactory results. By analysing several types and combinations of samples, the results of profilometric analysis showed that the printed layers on the control substrate had nanometric thickness, The uniformity of the films was validated by optical microscopy, highlighting how the ink was deposited on the starting substrate. The electroconductivity of the samples was then tested. As expected, nanoceria lowers the intrinsic electroconductivity of the PEDOT:PSS but not to such an extent to prevent charge injection and redox behaviour typical of PEDOT:PSS conjugated polymer. Cyclic voltammetry (CV) in PBS permitted to appreciate a CV shape similar to that found in the literature for nanoceria and a combined effect of the two constituent materials.

In the subsequent cell culture studies, interfaces have been effective in inducing axonal driving effects in SH-SY5Y neural cells, driving neurite growth. It has also been seen by the flow cytometric experiment that the density of antioxidant nanoparticles on the surface of substrates plays a crucial role in scavenging reactive oxygen species upon exposure to a oxidative insult. In future experiments, this parameter will be optimized in order to have maximum cellular protection even in case of minimum oxidative stress.

With the aim of repeating the experiments in the future to optimize different parameters, collectively, these results underline that the work done can be considered encouraging for a potential application in peripheral nerve regeneration.

Bibliography

1. **Giuseppe Anastasi, Silvano Capitani, Maria L. Carnazza, Saverio Cinti, Raffaele De Caro, Rosario F. Donato, Virgilio F. Ferrario, Luciano Fonzi, Adriano Tito Franzi et all,.** *Trattato di Anatomia Umana.* s.l. : Edi Ermes, 2010.

2. **OpenStax.** Wikimedia Commons. [Online] 18 May 2016. https://commons.wikimedia.org/wiki/File:1201_Overview_of_Nervous_System.jpg.

3. **Attilio Marino, Chiara Tonda-Turo, Daniele De Pasquale, Francesca Ruini, Giada Genchi, Simone Nitti, Valnetina Cappello, Mauro Gemmi, Virgilio Mattioli, Gianluca Ciardelli, Gianni Ciofani.** Gelatin/nanoceria nanocomposite fibers as antioxidant scaffolds for neuronal regeneration. *Biochimica et Biophysica Acta, Elsevier.* November 2016.

4. **C. Wang, H. Koh, S. Ramakrishna, S. Liao.** Nerve Tissue Regeneration. *Biomaterials.* 2011, p. 168-201.

5. *Review: Bioengineering approach for the repair and regeneration of peripheral nerve .* **Joshua Moskow, Bryan Ferrigno, Nikhil Mistry, Devina Jaiswal, Ketan Bulsara, Swetha Rudraiah, Sangamesh G. Kumbara.** 4, 2019, Bioactive Materials, p. 107-113.

6. *NEURAL TISSUE ENGINEERING: Strategies for Repair and Regeneration.* **Leach, Christine E. Schmidt and Jennie Baier.** 5, 2003, Annual Review of Biomedical Engineering, p. 293-347.

7. **Antonio J. Flores, Carlos J. Lavernia, Patrick W. Owens.** Anatomy and Physiology of Peripheral Nerve Injury and Repair. *The American Journal of Orthopedics.* p. 167-173.

8. *Functional polymeric nerve guidance conduits and drug delivery strategies for peripheral nerve repair and regeneration.* **Ohan S. Manoukian, Jiana T. Baker, Swetha Rudraiah, Michael R. Arul, Anthony T. Vella, Abraham J. Domb, Sangamesh G. Kumbar.** 2020, Journal of Controlled Release, Vol. 137, p. 78-95.

9. *An electro-physiological study of the early stages of peripheral nerve regeneration.* **S. Jacobsen, L. Guth.** 1964, Exp. Neurol., Vol. 11, p. 48-60.

10. **G., Lundborg.** *Nerve Injury and Repair.* New York : Longman Group UK, 1988.

11. **Mackinnon SE, Dellon AL.** *Surgery of Peripheral Nerve.* New York : Thieme Med. Publ., 1988.

12. **DT, Chiu.** Special srticle; the development of autogenous venous nerve conduit as a clinical entity. *P&S Medical Review.* New York : Columbia-Presbyterian Med. Cent., 1995.

13. *Autogenous vein graft as a conduit for nerve regeneration.* **Chiu DT, Janecka I, Krizek TJ, Wolff M, Lovelace RE.** 1982, Surgery, Vol. 91, p. 226-233.

14. *Clinical results and thoughts on sensory nerve repair by autologous vein graft in emergency hand reconstruction.* **G. Risitano, G. Cavallaro, T. Merrino, S. Coppolino, F. Ruggeri.** 2002, Chir. Main. , Vol. 21, p. 194-197.

15. *Nerve repair by means of vein filled with muscle grafts I. Clinical results.* **B. Battiston, P. Tos, TR Cushway, S. Geuna.** 2000, Microsurgery, Vol. 20, p. 32-36.

16. *Muscle grafts and alternatives for nerve reapir.* **MF Meck, AS Varejo, S. Geuna.** 2002, J. Oral Maxillofac. Surg., Vol. 60, p. 1095-1096.

17. *Nerve regeneration through an epineurial shealth: its functional aspetc compared with nerve and vein grafts.* **E Karacaoglu, F Yuksel, F Peker, MM Guler.** 2001, Microsurgery, Vol. 21, p. 196-201.

18. *Autologous tendons used as grafts for bridging peripheral nerve defects.* **J Brandt, LB Dahlin, G Lundborg.** 1999, J. Hand Surg., Vol. 24, p. 284-290.

19. *Long acellular nerve transplants for allergic grafting and the effects of basic fibroblast growth factor on the growth of regenerating axons in dogs: preliminary report.* **C Ide, K Tohyama, K Tajima, K Endoh, K Sano, et al.** 1998, Exp. Neurol., Vol. 154, p. 99-112.

20. *Reconstruction of peripheral nerves using acellular nerve graft with implanted cultured Schwann cells.* **O. Frerichs, H. Fansa, C. Schicht, G. Wolf, W. Schneider, et al.** 2002, Microsurgery, Vol. 22, p. 311-315.

21. *Immunogenicity and regenerative potential of acellular nerve allograft to repair peripheral nerve in rats and rabbits.* **AK Gulati, GP Cole.** 1994, Acta Neurochir. (Wien), Vol. 126, p. 158-164.

22. *Freeze dried irradiated nerve homograft: a preliminary report.* **Hiles, RW.** 1972, Hand, Vol. 4, p. 79-84.

23. *The repair of peripheral nerves by irradiated homografts.* **L., Marmor.** 1964, Clin. Orthop., Vol. 34, p. 161-169.

24. *Regeneration of the rat sciatic nerve into allografts made acellular through chemical extraction. .* **Sondell M, Lundborg G, Kanje M.** 1998, Brain Res., Vol. 795, p. 44-54.

25. *Vascular endothelial growth factor stimulates Schwann cell invasion and neovascularization of acellular nerve grafts.* **Sondell M, Lundborg G, Kanje M.** 1999, Brain Res., Vol. 846, p. 219-228.

26. *Identification of extractable growth factors from small intestinal submucosa.* **Voytik-Harbin SL, Brightman AO, Kraine MR, Waisner B, Badylak SF.** 1997, J. Cell Biochem., Vol. 67, p. 478-491.

27. *Small intestinal submucosa: a substrate for in vitro cell growth.* **Badylak SF, Record R, Lindberg K, Hodde J, Park K.** 1998, J. Biomater. Sci. Polym. Ed, Vol. 9, p. 863–78 .

28. *A new artificial nerve graft containing rolled Schwann cell monolayers. .* **Hadlock TA, Sundback CA, Hunter DA, Vacanti JP, Cheney ML.** 2001, Microsurgery., Vol. 21, p. 96-101.

29. *Human amnion membrane serves as a substratum for growing axons in vitro and in vivo.* **Davis GE, Blaker SN, Engvall E, Varon S, Manthorpe M, et al.** 1987, Science, Vol. 236, p. 1106-1109.

30. *Amnion tube for nerve regeneration. .* **Meek MF, Coert JH, Nicolai JP.** 2001, Plast. Reconstr. Surg., Vol. 107, p. 622-623.

31. *Extracellular matrix of human amnion manufactured into tubes as conduits for peripheral nerve regeneration. .* **Mligiliche N, Endo K, Okamoto K, Fujimoto E, Ide C.** 2002, J. Biomed. Mater. Res. , Vol. 63, p. 593-601.

32. *Orientated mats of fibronectin as a conduit material for use in peripheral nerve repair. .* **Whitworth IH, Brown RA, Dore C, Green CJ, Terenghi G.** 1995, J. Hand Surg. (Br.), Vol. 20, p. 429-436.

33. *Adhesion, alignment, and migration of cultured Schwann cells on ultrathin fibronectin fibres. .* **Ahmed Z, Brown RA.** 1999, Cell Motil. Cytoskelet., Vol. 42, p. 331-343.

34. *A laminin graft replaces neurorrhaphy in the restorative surgery of the rat sciatic nerve. .* **Kauppila T, Jyvasjarvi E, Huopaniemi T, Hujanen E, Liesi P.** 1993, Exp. Neurol., Vol. 123, p. 181-191.

35. *Evaluation of peripheral nerve regeneration across an 80-mm gap using a polyglycolic acid (PGA)–collagen nerve conduit filled with laminin-soaked collagen sponge in dogs. .* **Toba T, Nakamura T, Lynn AK, Matsumoto K, Fukuda S, et al.** 2002, Int. J. Artif. Organs, Vol. 25, p. 230-237.

36. *30 mm regeneration of rat sciatic nerve along collagen filaments. .* **Yoshii S, Oka M, Shima M, Taniguchi A, Akagi M.** 2002, Brain Res., Vol. 949, p. 202-208.

37. *Magnetically aligned collagen gel filling a collagen nerve guide improves peripheral nerve regeneration. .* **Ceballos D, Navarro X, Dubey N, Wendelschafer-Crabb G, Kennedy WR, et al.** 1999, Exp. Neurol., Vol. 158, p. 290-300.

38. *Guided neurite elongation and Schwann cell invasion into magnetically aligned collagen in simulated peripheral nerve regeneration.* **Dubey N, Letourneau PC, Tranquillo RT.** 1999, Exp. Neurol. , Vol. 158, p. 338-350.

39. *Hyaluronic acid through a new injectable nerve guide delivery system enhances peripheral nerve regeneration in the rat.* **Seckel BR, Jones D, Hekimian KJ, Wang KK, Chakalis DP, et al.** 1995, J. Neurosci. Res., Vol. 40, p. 318-324.

40. *Low concentrations of fibrinogen increase cell migration speed on fibronectin/fibrinogen composite cables.* **Ahmed Z, Underwood S, Brown RA.** 2000, Cell Motil. Cytoskelet. , Vol. 46, p. 6-16.

41. *Effects of fibrin micromorphology on neurite growth from dorsal root ganglia cultured in three-dimensional fibrin gels. .* **Herbert CB, Nagaswami C, Bittner GD, Hubbell JA, Weisel JW.** 1998, J. Biomed. Mater. Res., Vol. 40, p. 551-559.

42. *Peripheral nerve regeneration through alginate gel: analysis of early outgrowth and late increase in diameter of regenerating axons. .* **Hashimoto T, Suzuki Y, Kitada M, Kataoka K, Wu S, et al.** 2002, Exp. Brain Res., Vol. 146, p. 356-368.

43. *Agarose gel stiffness determines rate of DRG neurite extension in 3D cultures.* **Balgude AP, Yu X, Szymanski A, Bellamkonda RV.** 2001, Biomaterials, Vol. 22, p. 1077-1084.

44. *Studies on nerve cell affinity of chitosan-derived materials. .* **Haipeng G, Yinghui Z, Jianchun L, Yandao G, Nanming Z, et al.** 2000, J. Biomed. Mater. Res. , Vol. 52, p. 285-295.

45. *Clinical long-term in vivo evaluation of poly(Llactic acid) porous conduits for peripheral nerve regeneration. .* **Evans GR, Brandt K, Niederbichler AD, Chauvin P, Herrman S, et al.** 2000, J. Biomater. Sci. Polym. Ed. , Vol. 11, p. 869-878.

46. *.Bioactivepoly(L-lactic acid) conduits seeded with Schwann cells for peripheral nerve regeneration. .* **Evans GR, Brandt K, Katz S, Chauvin P, OttoL, et al.** 2002, Biomaterials, Vol. 23, p. 841-848.

47. *Regeneration of peripheral nerve through a polyglactin tube. .* **Molander H, Olsson Y, Engkvist O, Bowald S, Eriksson I.** 1982, Muscle Nerve , Vol. 5, p. 54-57.

48. *In vivo and in vitro degradation of poly[(50)/(50) ((85)/(15)(L)/(D))LA/ epsilon-CL], and the implications for the use in nerve reconstruction. .* **den Dunnen WF, Meek MF, Grijpma DW, Robinson PH, Schakenraad JM.** 2000, J. Biomed. Mater. Res, Vol. 51, p. 575-585.

49. *Superior muscle reinnervation after autologous nerve graft or poly-Llactide-epsilon-caprolactone (PLC) tube implantation in comparison to silicone tube repair. .* **Valero-Cabre A, Tsironis K, Skouras E, Perego G, Navarro X, et al.** 2001, J. Neurosci. Res., Vol. 63, p. 214-223.

50. *Manufacturing and microscopicalcharacterisation of polyurethane nerve guidance channel featuring a highly smooth internal surface.* **Soldani G, Varelli G, Minnocci A, Dario P.** 1998, Biomaterials, Vol. 19, p. 1919-1924.

51. *Guided regeneration with resorbable conduits in experimental peripheral nerve injuries. .* **Nicoli Aldini N, Fini M, Rocca M, Giavaresi G, Giardino R.** 2000, Int. Orthop. , Vol. 24, p. 121-125.

52. *Poly-3-hydroxybutyrate (PHB): a resorbable conduit for long-gap repair in peripheral nerves.* **Young RC, Wiberg M, Terenghi G.** 2002, Br. J. Plast. Surg., Vol. 55, p. 235-240.

53. *Rapid induction of functional and morphological continuity between severed ends of mammalian or earthworm myelinated axons.* **Lore AB, Hubbell JA, Bobb DS Jr, Ballinger ML, Loftin KL, et al.** 1999, J. Neuroscie., Vol. 19, p. 2442-2454.

54. *Behavioral recovery from spinal cord injury following delayed application of polyethylene glycol. .* **Borgens RB, Shi R, Bohnert D.** 2002, J. Exp. Biol. , Vol. 205, p. 1-12.

55. *In vitro nerve repair—in vivo. The reconstruction of peripheral nerves by entubulation with biodegradeable glass tubes: a preliminary report.* **Gilchrist T, Glasby MA, Healy DM, Kelly G, Lenihan DV, et al.** 1998, Br. J. Plast. Surg., Vol. 51, p. 231-237.

56. *Biodegradable controlled release glass in the repair of peripheral nerve injuries.* **Lenihan DV, Carter AJ, Gilchrist T, Healy DM, MillerI A, et al.** 1998, J. Hand Surg. [Br.] , Vol. 23, p. 588-593.

57. *Patterned neuronal attachment and outgrowth on surface modified, electrically charged fluoropolymer substrates.* **Valentini RF, Vargo TG, Gardella JA Jr, Aebischer P.** 1993, J. Biomater. Sci. Polym. Ed., Vol. 5, p. 13-36.

58. *Stimulation of neurite outgrowth using an electrically conducting polymer.* **Schmidt CE, Shastri VR, Vacanti JP, Langer R.** 1997, Proc. Natl. Acad. Sci. USA, Vol. 94, p. 8948-8953.

59. *The use of silicone tubing in the late repair of the median and ulnar nerves in the forearm. .* **Dahlin L, Lundborg G.** 2001, J. Hand Surg. [Br.] , Vol. 26, p. 393-396.

60. *Silicone rubber sheathing as an adjunct to neural anastomosis.* **Midgley RD, Woolhouse FM.** 1968, Surg. Clin. N. Am., Vol. 48, p. 1149-1154.

61. *Facial nerve repair with expanded polytetrafluoroethylene and collagen conduits: an experimental study in the rabbit.* **Vasconcelos BC, Gay-Escoda C.** 2000, J.Oral Maxillofac. Surg. , Vol. 58, p. 1257-1262.

62. *Use of Gore-Tex tubing as a conduit for inferior alveolar and lingual nerve repair: experience with 6 cases. .* **Pitta MC, Wolford LM, Mehra P, Hopkin J.** 2001, J. Oral Maxillofac. Surg. , Vol. 59, p. 493-496.

63. *Low-level laser effect on neural regeneration in Gore-Tex tubes. .* **Miloro M, Halkias LE, Mallery S, Travers S, Rashid RG.** 2002, Oral Surg. Oral Med. Oral Pathol. Oral Radiol. Endod. , Vol. 93, p. 27-34.

64. *Regeneration of peripheral nerve through a polyglactin tube. .* **Molander H, Olsson Y, Engkvist O, Bowald S, Eriksson I.** 1982, Muscle Nerve, Vol. 5, p. 54-57.

65. *Conductive PPY/PDLLA conduit for peripheral nerve regeneration.* **H. Xu, J. M. Holzwarth, Y. Yan, P. Xu, H. Zheng, Y. Yin, S. Li, P. X. Ma.** 2014, Biomaterials, Vol. 35, p. 225-235.

66. **Zhang L., Webster J. T.** Introduction: Nanotechnology and Nanomaterials-Biomimetic Tools for Implants. *Handbook of Nanophysics: Nanomedicine and Nanorobotics.* 2010.

67. *Nanofiber containing carbon nanotubes enhanced PC12 cell proliferation and neuritogenesis by electrical stimulation.* **Su, Wen-Ta, Shih, Yi-An.** Shanghai, China : s.n., 2015. Frontiers in Biomedical Engineering and Biotechnology – Proceedings of the 4th International Conference on Biomedical Engineering and Biotechnology, .

68. *Nanoscaffolds in promoting regeneration of the peripheral nervous system.* **Chen Aijie, Lai Xuan, Liang Huimin, Zhang Yanli, Kang Yiyuan, Lin Yuqing & Shao Longquan.** 2018, Nanomedicine.

69. **Liu X, Chen J, Gilmore KJ, Higgins MJ, Liu Y, Wallace GG.** Guidance of neurite outgrowth on aligned electrospun polypyrrole/poly(styrene-beta-isobutylene-beta-styrene) fiber platforms. *Wiley Periodicals.* 2010.

70. *Influence of Gelatin Cues in PCL Electrospun Membranes on Nerve Outgrowth.* **Marco Antonio Alvarez-Perez, Vincenzo Guarino, Valentina Cirillo, Luigi Ambrosio.** 2010, Biomacromolecules , p. 2238-2246.

71. *Enhancement of neurite outgrowth using nano-structured scaffolds coupled with laminin.* **H. S. Koh, Thomas Yong, C. K. Chan, S. Ramakrishna.** 2008, Biomaterials, Vol. 29, p. 3574-3582.

72. *The odontogenic differentiation of human dental pulp stem cells on nanofibrous poly(l-lactic acid) scaffolds in vitro and in vivo.* **Jing Wang, Xiaohua Liu, Xiaobing Jin, Haiyun Ma, Jiang Hu, Longxing Ni, Peter X. Ma.** 2010, Acta Biomaterialia, Vol. 6, p. 3856-3863.

73. **Gwang-Geun Lee, Eisuke Tokumitsu, Sung-Min Yoon, Yoshihisa Fujisaki, Joo-Won Yoon, and Hiroshi Ishiwara.** The flexible non-volatile memory devices using oxide semiconductors and ferroelectric polymer poly(vinylidene fluoride-trifluoroethylene). [Online] 2011. https://aip.scitation.org/doi/abs/10.1063/1.3608145#.

74. *Effect of composition of poly(3-hydroxybutyrate-co-3-hydroxyhexanoate) on growth of fibroblast and osteoblast.* **Ya-Wu Wang, Fei Yang, Qiong Wu, Yin-chung Cheng, Peter H. F. Yu, Jinchun Chen, Guo-Qiang Chen.** 2005, Biomaterials, Vol. 26, p. 755-761.

75. *Renewable Resource-Based Green Composites from Recycled Cellulose Fiber and Poly(3-hydroxybutyrate-co-3-hydroxyvalerate) Bioplastic.* **Rahul Bhardwaj, Amar K. Mohanty, L. T. Drzal, F. Pourboghrat, M. Misra.** 2006, Biomascromolecules, p. 2044-2051.

76. *Regeneration of Pericardial Tissue on Absorbable Polymer Patches Implanted into the Pericardial Sac: An Immunohistochemical, Ultrastructural and Biochemical Study in the Sheep.* **T. Malm, S. Bowald, A. Bylock, T. Saldeen, C. Busch.** 2009, Scandinavian Journal of Thoracic and Cardiovascular Surgery, Vol. 26, p. 15-21.

77. *A NEW RESORBABLE WRAP-AROUND IMPLANT AS AN ALTERNATIVE NERVE REPAIR TECHNIQUE.* **A. HAZARI, G. JOHANSSON-RUDÉN, K. JUNEMO-BOSTROM, C. LJUNGBERG, G. TERENGHI, C. GREEN, M. WIBERG.** 1999, The Journal of Hand Surgery: British & European Volume, Vol. 24, p. 291-295.

78. *Biodegradable poly-β-hydroxybutyrate scaffold seeded with Schwann cells to promote spinal cord repair.* **Liudmila N. Novikova, Jonas Pettersson, Maria Brohlin, Mikael Wiberg, Lev N. Novikov.** 2008, Biomaterials, Vol. 29, p. 1198-1206.

79. *Electrospun poly(ε-caprolactone)/gelatin nanofibrous scaffolds for nerve tissue engineering.* **Laleh Ghasemi-Mobarakeh, Molamma P. Prabhakaran, Mohammad Morshed, Mohammad-Hossein Nasr-Esfahani, Seeram Ramakrishn.** 2008, Biomaterials, Vol. 29, p. 4532-4539.

80. *Stimulation of Neurite Outgrowth Using an Electrically Conducting Polymer.* **Christine E. Schmidt, Venkatram Prasad Shastri, Joseph P. Vacanti, Robert Langer.** 1997, Proceedings of the National Academy of Sciences , Vol. 94, p. 8948-8953.

81. **J. Hang, L. Kong, J. W. Gu, and T. H. Adair.** VEGF gene expression is upregulated in electrically stimulated rat skeletal muscle. [Online] 1995. https://journals.physiology.org/doi/abs/10.1152/ajpheart.1995.269.5.H1827.

82. *Piezoelectric Scaffolds as Smart Materials for Neural Tissue Engineering.* **Angelika Zaszczynska, Paweł Sajkiewicz, Arkadiusz Gradys.** 2020, Polymers.

83. *Piezoelectric substrates promote neurite growth in rat spinal cord neurons.* **Royo-Gascon N., WiningerM., Scheinbeim J. I., Firestein B. L., Craelius W.** 2013, Ann. Biomed. Eng. , Vol. 41, p. 112-122.

84. *Electrically charged polymeric substrates enhance nerve fibre outgrowth in vitro. .* **Valentini R. F., Vargo T. G., Gardella J. A. Jr., Aebischer P.** 1992, Biomaterials, Vol. 13, p. 183-190.

85. *Piezoelectric guidance channels enhance regeneration in the mouse sciatic nerve after axotomy. .* **Aebischer P., Valentini R. F., Dario P., Domenici C., Galletti P. M.** 1987, Brain Res. , Vol. 436, p. 165-168.

86. *Repair of peripheral nerve defects using a polyvinylidene fluoride channel containing nerve growth factor and collagen gel in adult rats. .* **Delaviz H., Faghihi A., Delshad A. A., Hadi Bahadori M., Mohamadi J., Roozbehi A.** 2011, Cell J., Vol. 13, p. 137-142.

87. *Surface modification of microporous PVDF membranes for neuron culture.* **Young T. H., Chang H. H., Lin D. J., Cheng L. P.** 2010, J. Membr. Sci. , Vol. 350, p. 32–41.

88. *Materials Nanoarchitectonics as Cell Regulators. .* **Ariga K., Jia X., Song J., Hsieh C. T., Hsu S. H.** 2019, ChemNanoMat, Vol. 5, p. 692–702.

89. *Polymeric scaffolds in neural tissue engineering: A review. .* **Ai J., Kiasat-Dolatabadi A., Ebrahimi-Barough S., Ai A., Lotfibakhshaiesh N., Norouzi-Javidan A., Aghayan H. R.** 2014, Arch Neurosci. , Vol. 1, p. 15-20.

90. *Development of three-dimensional piezoelectric polyvinylidene fluoride-graphene oxide scaffold by non-solvent induced phase separation method for nerve tissue engineering.* **Abzan N., Kharaziha M., Labbaf S.** 2019, Mater. Design , Vol. 167.

91. *Concurrent effects of piezoelectricity and hydrostatic pressure on chondrogenic differentiation of stem cells. .* **Khorshidi S., Ansari S., Naghizaden Z., Akbari N., Karkhaneh A., Haghighipour N.** 2019, Mater. Lett. , Vol. 246 , p. 71–75.

92. *The influence of piezoelectric scaffolds on neural differentiation of human neural stem/progenitor cells. .* **Lee Y. S., Arinzeh T. L.** 2012, Tissue Eng. , Vol. 18, p. 2063-2072.

93. *Neurite extension of primary neurons on electrospun piezoelectric scaffolds.* **Lee Y. S., Collins G., Arinzeh T. L.** 2011, Acta Biomater, Vol. 7, p. 3877–3886.

94. *Ultrasound-activated piezoelectric P(VDF-TrFE)/boron nitride nanotube composite films promote differentiation of human SaOS-2 osteoblast-like cells. .* **Genchi G. G., Sinibaldi E., Ceseracciu L., Labardi M., Marino A., Marras S., Ciofani G.** 2018, Nanomedicine, Vol. 14, p. 2421–2432.

95. *Improved nerve regeneration through piezoelectric vinylidenefluoride-trifluoroethylene copolymer guidance channels. .* **Fine E. G., Valentini R. F., Bellamkonda R., Aebischer P.** 1991, Biomaterials, Vol. 12, p. 775-780.

96. *Self-Powered Well-Aligned P (VDF-TrFE) Piezoelectric Nanofiber Nanogenerator for Modulating an Exact Electrical Stimulation and Enhancing the Proliferation of Preosteoblasts.* **Wang A., Hu M., Zhou L., Qiang X.** 2019, Nanomaterials, Vol. 9, p. 349.

97. *Bioelectrochemical control of neural cell development on conducting polymers. .* **Collazos-Castro J. E., Polo J. L., Hernández-Labrado G. R., Padial-Cañete V., García-Rama C.** 2010, Biomaterials, Vol. 31, p. 9244–9255.

98. *Chronic neural recordings using silicon microelectrode arrays electrochemically deposited with a poly (3, 4-ethylenedioxythiophene)(PEDOT) film. .* **Ludwig K. A., Uram J. D., Yang J., Martin D. C., Kipke D. R.** 2006, J. Neural. Eng. , Vol. 59-70, p. 3.

99. *Neural stem cell differentiation by electrical stimulation using across-linkedPEDOTsubstrate: Expanding the use of biocompatible conjugated conductive polymers for neural tissue engineering.* **Pires F., Ferreira Q., Rodrigues C. A., Morgado J., Ferreira F. C.** 2015, Biochim. Biophys. Acta , Vol. 1850, p. 1158–1168.

100. *The effects of poly (3, 4-ethylenedioxythiophene) coating on magnesium degradation and cytocompatibility with human embryonic stem cells for potential neural applications. .* **Sebaa M., Nguyen T. Y., Dhillon S., Garcia S., Liu H.** 2015, J. Biomed. Mater. Res. A , Vol. 103, p. 25-37.

101. *Design of high conductive and piezoelectric poly (3, 4-ethylenedioxythiophene)/chitosan nanofibers for enhancing cellular electrical stimulation. .* **Du L., Li T., Jin F., Wang Y., Li R., Zheng J., Feng Z. Q.** 2020, J. Colloid Interface Sci, Vol. 559, p. 65-75.

102. *Clinical long-term in vivo evaluation of poly (L-lactic acid) porous conduits for peripheral nerve regeneration. .* **Evans G. R., Brandt K., Niederbichler A. D., Chauvin P., Hermann S., Bogle M., Patrick C. W.** 2000, J. Biomater. Sci. Polym. , Vol. 11, p. 869–878 .

103. *Stem cell differentiation on electrospun nanofibrous substrates for vascular tissue engineering. .* **Jia L., Prabhakaran M. P., Qin X., Ramakrishna S.** 2013, Mater. Sci. Eng. C, Vol. 33 , p. 4640–4650.

104. *Fabrication of nano-structured porous PLLA scaffold intended for nerve tissue engineering.* **Yang F., Murugan R., Ramakrishna S., Wang X., Ma Y. X., Wang S.** 2004, Biomaterials, Vol. 25 , p. 1891–1900.

105. *Electrospinning of nano/micro scale poly (L-lactic acid) aligned fibers and their potential in neural tissue engineering. .* **Yang F., Murugan R., Wang S., Ramakrishna S.** 2005, Biomaterials, Vol. 26, p. 2603–2610.

106. *Electrospun nanostructured scaffolds for bone tissue engineering. .* **Prabhakaran M. P., Venugopal J., Ramakrishna S.** 2009, Acta Biomaterials, Vol. 5, p. 2884–2893.

107. *Electrospun conducting polymer nanofibers and electrical stimulation of nerve stem cells. .* **Prabhakaran M. P., Ghasemi-Mobarakeh L., Jin G., Ramakrishna S.** 2011, J. Biosci. Bioeng. , Vol. 112, p. 501–507.

108. *.TheSmartPiezoelectricNanohybridof Poly-(3-hydroxybutyrate-co-3-hydroxyvalerate) and Barium Titanate for Stimulated Cartilage Regeneration. .* **Jacob J., More N., Mounika C., Gondaliya P., Kalia K., Kapusetti G.** 2019, ACS Appl. Bio Mater. , Vol. 2, p. 4922–4931.

109. *Electrospinning of matrigel to deposit a basal lamina-like nanofiber surface. .* **De Guzman R. C., Loeb J. A., VandeVord P. J.** 2010, J. Biomater. Sci. Polym. Ed. , Vol. 21, p. 1081–1101.

110. *Functional synapse formation among rat cortical neurons grown on three-dimensional collagen gels.* **O'Shaughnessy T. J., Lin H. J., Ma W.** 2003, Neurosci. Lett. , Vol. 340, p. 169–172.

111. *Functionalized BaTiO3 enhances piezoelectric effect towards cell response of bone scaffold.* **Shuai C., Liu G., Yang Y., Yang W., He C., Wang G., Peng S.** 2020, Colloids Surf. B. , Vol. 185.

112. *Topographical and Electrical Stimulation of Neuronal Cells through Microwrinkled Conducting Polymer Biointerfaces.* **Alberto Bonisoli, Attilio Marino, Gianni Ciofani, Francesco Greco.** 2017, Macromolecular Bioscience .

113. **Elschner A, Kirchmeyer S, Lovenich W, Merker U, Reuter K.** PEDOT: principles and applications of an intrinsically conductive polymer. [Online] CRC PRess, 2010.

114. **Green, Rylie.** Synthesis and Characterisation ofConducting Polymers. *Conducting polymers for neural interfaces:Impact of physico-chemical properties onbiological performance.* University of New South Wales : s.n., 2009.

115. *Stability of polyp yrrole and poly(3,4_ethylenedioxythiophene) for biosensor application.* **Hitoshi Yamato, Masaki Ohwa, Wolfgang Wernet.** 1995, Journal of Electroanalytical Chemistry , Vol. 397, p. 163-170.

116. *Electrochemical modulation of epithelia formation using conducting polymers. .* **Svennersten K, Bolin MH, Jager EWH, Berggren M, Richter-Dahlfors A.** 2009, Biomaterials, Vol. 30, p. 6257–6264.

117. *CeO2 nanoscale particles: Synthesis, characterization and photocatalytic activity under UVA light irradiation.* **Laouedj Nadjia, Elaziouti Abdelkader, Benhadria Naceur, Bekka Ahmed.** 2018, Journal of Rare Earths, Vol. 36, p. 575-587.

118. **Reyes, Gerardo Pulido.** Biological effects of cerium oxide nanoparticles. Implications at the Bio-Nano interface. 2017.

119. *Oxygen defects and formation of Ce3+ affecting the photocatalytic performance of CeO2 nanoparticles.* **Biswajit Choudhury, Pawan Chetri.** 2014, RSC Advances, Vol. 9.

120. *Gelatin/nanoceria nanocomposite fibers as antioxidant scaffolds for neuronal regeneration.* **Attilio Marino, Chiara Tonda-Turo, Daniele De Pasquale, Francesca Ruini, Giada Genchi, Simone Nitti, Valentina Cappello, Mauro Gemmi, Virgilio Mattoli, Gianluca Ciardelli, Gianni Ciofani.** 2017, Biochimica et Biophysica Acta, Vol. 1861, p. 386-395.

121. **Ilaria Pezzini, Attilio Marino, Serena Del Turo, Chiara Nesti, Stefano Doccini, Valentina Cappello, Mauro Gemmi, Paola Parlanti, Filippo M. Santorelli, Virgilio Mattioli, Gianni Ciofani.** Cerium oxide nanoparticles: the regenerative redox machine in bioenergetic imbalance. *Nanomedicine.* 2016.

122. *The role of cerium redox state in the SOD mimetic activity of nanoceria.* **Heckert EG, Karakoti AS, Seal S, Self WT.** 2008, Biomaterials, Vol. 29, p. 2705-2709.

123. *Catalytic properties and biomedical applications of cerium oxide nanoparticles.* **Carl Walkey, Soumen Das, Sudipta Seal, Joseph Erlichman, Karin Heckman, Lina Ghibelli, Enrico Traversa, James F. McGinnis, William T. Self.** 2015, Environmental Science: Nano.

124. *Synthesis and biomedical applications of nanoceria, a redox active nanoparticle.* **Neelam Thakur, Prasenjit Manna, Joydeep Das.** 2019, Journal of Nanobiotechnology.

125. *Nanoceria as Antioxidant: Synthesis and Biomedical Applications.* **A.S. Karakoti, N.A. Monteiro-Riviere, [...], and S. Seal.** 1989, JOM (Warrendale, Pa).

126. *Effects of Cerium Oxide Nanoparticles on PC12 Neuronal-Like Cells: Proliferation, Differentiation, and Dopamine Secretion.* **Gianni Ciofani, Giada G. Genchi, Ioannis Liakos, Valentina Cappello, Mauro Gemmi, Athanassia Athanassiou, Barbara Mazzolai, et al.** 2013, Pharmaceutical Research, Vol. 30, p. 2133-2145.

127. *Antibody-conjugated PEGylated cerium oxide nanoparticles for specific targeting of Aβ aggregates modulate neuronal survival pathways.* **Cimini A, D'Angelo B, Das S, Gentile R, Benedetti E, Singh V, et al.** 2012, Acta Biomater., Vol. 8, p. 2056–2067.

128. *Neuroprotective mechanisms of cerium oxide nanoparticles in a mouse hippocampal brain slice model of ischemia. .* **Estevez AY, Pritchard S, Harper K, Aston JW, Lynch A, Lucky JJ et al.** 2011, Free Radical Bio Med. , Vol. 51, p. 1155–1163.

129. **Settineri, Luca.** Elements of Additive Manufacturing. Torino : s.n., 2017.

130. **Wheeler, Joseph S.R.** Polymers in Inkjet Printing. [Online] Wiley Online Library, 2015.

131. **Techinstro. [Online] https://www.techinstro.com/ito-coated-on-pet/.**

132. Clevoius P Jet 700 . [Online] 2019. https://www.heraeus.com/media/media/hec/documents_hec/data_sheets_hep/Clevios_P_JET_700.pdf.

133. *Role of ITO and PEDOT:PSS in stability/degradation of polymer: fullerene bulk heterojunctions solar cells.* Mihaela Girtan, M. Rusu. 2010, Solar Energy Materials and Solar Cells , Vol. 94, p. 446-450.

134. Gillis, Joris. Wikipedia. [Online] https://en.wikipedia.org/wiki/Wetting.

135. Henniker Plasma. [Online] https://plasmatreatment.co.uk/henniker-plasma-technology/plasma-surface-technology/plasma-technology-what-is-plasma-treatment/plasma-treatment-explained/.

136. Diener Electronic, Plasma Surface Technology. [Online] https://www.plasma.com/it/?r=1.

137. *Inkjet Printing of Conductive Materials: A Review.* Cummins, G. & Desmulliez, M. P. 2012, Circuit World , Vol. 38, p. 193–213 .

138. *Inkjet Printing—Process and Its Applications. .* Singh, M., Haverinen, H. M., Dhagat, P. & Jabbour, G. E. 2010, Advanced Materials , Vol. 22, p. 673–685 .

139. *Inkjet printing of organic electronics – comparison of deposition techniques and state-of-the-art developments .* Anke Teichler, Jolke Perelaer, Ulrich S. Schubert. 2013, Journal of Materials Chemistry C, Vol. 10.

140. Alpha-Step D-500 Stylus Profiler. [Online] https://www.kla-tencor.com/products/surface-profilers/alphastep-d-500-stylus-profiler.

141. Wikipedia. [Online] https://en.wikipedia.org/wiki/Optical_microscope.

142. Four Point Probe. [Online] Bridge Technology. http://four-point-probes.com/four-point-probe-manual/.

143. Schroder, D. Semiconductor Material and Device Characterization. *isbn: 978-0471-73906-7.*

144. Anuradha, Dr. J. [Online] https://www.slideshare.net/AnuRadha66/cyclic-voltammetry-principle-instrumentation-applications.

145. *A Practical Beginner's Guide to Cyclic Voltammetry.* Noémie Elgrishi, Kelley J. Rountree, Brian D. McCarthy, Eric S. Rountree, Thomas T. Eisenhart,and Jillian L. Dempsey. Journal of Chemical Education.

146. The Human Protein Atlas. [Online] https://www.proteinatlas.org/learn/method/immunocytochemistry.

147. Wikipedia . [Online] https://en.wikipedia.org/wiki/Fluorescence_microscope.

148. Fluorescence in Microscopy | Learn & Share | Leica Microsystems. [Online] https://www.leica-microsystems.com/science-lab/fluorescence-in-microscopy/.

149. B., Dr. Basil. Health and Medicine. [Online] https://www.slideshare.net/brunobasil/fluorometery?next_slideshow=1.

150. *Victor3™ Plate Reader From PerkinElmer.* Kumarasuriyar, Arjuna. 2007, Biocompare.

151. Abcam. [Online] https://www.abcam.com/protocols/introduction-to-flow-cytometry.

152. *CytoFLEX Flow Cytometer Platform.*

153. Libri Texts Chemistry. [Online] 2019. https://chem.libretexts.org/Bookshelves/Analytical_Chemistry/Supplemental_Modules_(Analytical_Chemistry)/Analytical_Sciences_Digital_Library/JASDL/Courseware/Analytical_Electrochemistry%3A_Potentiometry/03_Potentiometric_Theory/04_Reference_Electrodes.

154. *Antioxidant properties of ALD grown nanoceria films with tunable valency.* Ankur Gupta, Tamil S. Sakthivel, Craig J. Neal, Supriya Koul, Sushant Singh, Akihiro Kushima, Sudipta Seal. 2019, Biomaterials Science.

155. Scientific, Thermo. PicoGreen® Assay for dsDNA .

156. Merck. [Online] https://www.sigmaaldrich.com/catalog/product/sial/b2633?lang=it&region=IT&gclid=Cj0KCQiA0ZHwBRCRARIsAK0Tr-quPF1U2WgVpWAaZcyJTNpRlFTI6MG2wR66liupQbf9vapy64Ma_1QaAtOxEALw_wcB.

157. *Electrically charged polymeric substrates enhance nerve fibre outgrowth in vitro. .* Valentini R. F., Vargo T. G., Gardella J. A. Jr., Aebischer, P. p. 1992.

158. *Inkjet printing of viscoelastic polymer inks.* Zhonghui Du, Xinhong Yu, Yanchun Han. 2018, Chinese Chemical Letters, Vol. 29, p. 399-404.

Acknowledgments

Con questo ultimo lavoro giunge ufficialmente al termine il mio percorso universitario. Voglio ringraziare uno ad uno tutte le persone che mi hanno accompagnata in questo percorso formativo ma allo stesso tempo percorso di vita.

Colgo l'occasione innanzitutto di ringraziare il Prof. Gianni Ciofani unitamente alla Prof.ssa Valentina Alice Cauda per aver consentito lo sviluppo di questo progetto di tesi e per avermi dedicato preziosi consigli, professionalità ed estrema disponibilità.

Desidero manifestare profonda gratitudine al Dott. Francesco Greco per avermi accolta nell'Istituto di Fisica dello Stato Solido dell'Università di Tecnologia di Graz (AU). Grazie per avermi guidato sapientemente durante tutto il percorso di tesi e per aver risolto pazientemente ogni dubbio e incertezza. Ringrazio anche Kirill Keller, dottorando presso lo stesso Istituto, per aver speso tempo nell'aiutarmi a svolgere il lavoro nel modo migliore. Tra le meravigliose persone che ho avuto modo di conoscere durante l'esperienza all'estero, voglio ringraziare Erika che mi ha supportata ed aiutata come se ci conoscessimo da sempre.

Un ringraziamento particolare ed importante voglio riservarlo alla Dott.ssa Giada Graziana Genchi, per avermi permesso di completare una parte significativa del progetto presso l'Istituto Italiano di Tecnologia (IIT) di Pontedera. Grazie per la disponibilità e la cortesia avuta nei miei confronti, per l'interesse mostrato verso il mio lavoro, per avermi assistita pazientemente nell'incredibile panorama della biologia.

Dal profondo del mio cuore, ringrazio i miei genitori, a cui dedico questa tesi, senza il cui supporto morale ed economico l'intero percorso universitario non sarebbe stato possibile. Grazie per aver incoraggiato ogni mia scelta, per aver gioito con me per i successi e per aver saputo rendere meno difficili i momenti più bui. Grazie per avermi trasmesso il senso del sacrificio e l'amore per lo studio con un incessante desiderio di conoscenza.

Dedico altresì questo lavoro alla mia luce su questa terra, mia sorella Roberta. Non riuscirò mai a ringraziarti del tutto per il conforto e il sostegno che mi hai sempre assicurato. Grazie per essere sempre al mio fianco, qualsiasi secondo di questa vita. Sei la persona di cui ho più stima in questo mondo. Ogni tua parola, ogni tuo gesto, ogni tuo abbraccio sono stati cardinali in questo percorso. Sei la mia persona, questo racchiude tutto.

Ringrazio tutta la mia famiglia, in particolare i miei nonni, sempre presenti a fornire un abbraccio nei momenti di vicinanza. A loro chiedo scusa per aver sottratto del tempo da passare insieme. Spero che questo piccolo traguardo sia la vostra gioia.

Il Politecnico mi ha dato l'opportunità di conoscere una persona che è diventata essenziale nella mia vita. Desidero ringraziare Francesca, la mia migliore amica. Grazie per avermi sostenuta in questi anni universitari, non solo da un punto di vista didattico ma soprattutto personale. Grazie per aver condiviso e condividere pensieri, emozioni, ansie, paure. Grazie per la tua instancabile vivacità che emani. Grazie per essere entrata semplicemente nella mia quotidianità.

Un ringraziamento particolare va a Nadia e Rossella, amiche lontane ma vicine col cuore. Grazie per aver riposto in me la vostra fiducia, il vostro prezioso tempo e il vostro affetto. Grazie per il costante appoggio che mi date con un singolo messaggio o una rapida chiamata. Da colleghe ad amiche sincere, una fortuna che il Politecnico mi ha regalato.

Grazie ai miei coinquilini, Antonio e Ciccio, per aver fatto parte della mia seconda famiglia a Torino. Grazie per avermi fatto ridere di cuore anche quando ero tutto buio fuori. Grazie per aver inondato le mie giornate di pura allegria con annessa lamentela. Grazie per aver sempre rispettato la mia persona.

Grazie alle mie nuove coinquiline, Simona e Lucia. Aver stabilito in così poco tempo un legame così mi ha aiutato a non demordere in questa ultima corsa contro il tempo.

Ringrazio tutte le persone che in questi anni mi hanno supportata moralmente in questa meravigliosa città, dagli amici della palestra a quelli del venerdì sera. Nonostante il cammino pieno di ostacoli, ci sono state persone che hanno assaporato con me le emozioni di un piccolo tratto.

Grazie a chi ha condiviso con me le fatiche e le gioie del mio percorso di studi, dai banchi della scuola elementare fino all'università. Tra questi, rivolgo un grazie speciale alle mie amiche di sempre, Rosalia ed Elena, che sono una costante nella mia vita e continuano a sostenermi anche da lontano.

Questo percorso mi ha donato tanta vita. Comunque vada, sarà un successo per me.